

POLITECNICO DI TORINO

Department of Chemical Engineering and Materials

Master of Science in Chemical Engineering

Master Thesis

# Development of Catalyst for SCR<sub>o</sub>F Applications



**Supervisor(s):**

Prof. Samir Bensaid

Prof. Fabio Alessandro Deorsola

**Candidate:**

Maria Alejandra Sierra Cano

December 2017

*To my beloved parents and brother*

## **Acknowledgements**

First, I would like to acknowledge my supervisors for giving me the opportunity to do this research project and for all the support. I would like to thank Fabio for always be a kind and willing person, and for all the help during the realization of this work.

Thanks to my parents and brother for always being there for me and gave their unconditionally support in all my decisions and especially during this experience.

Thank you, Cen for all the help, support, and company in these last months. Also for letting me know that delicious Chinese food, that became the best moment of the weekend in the study room. At the end, we didn't have to go to the Po!.

I want to thanks Monica, Maribel and Giancarmine for the company, the laughs, the coffees and for helping me when I needed it. Also, thank you Luca for always look after me and for the help with the italian.

Thank you Estefa for this last two years, so many things happened and we shared a lot of moments that I won't forget. Thank you for always being there.

Finally, I want to express my gratitude to Mariano, Alessandro, Miriam, Tharizi for the company, the help and the coffees in the lab.

Table 1 List of Abbreviations

---

Abbreviation	Meaning
BET	Brunauer, Emmett and Teller method
CDPF	Catalyzed DPF
CRT	Continuous regenerating trap
DeNO <sub>x</sub>	De-nitrification
DOC	Diesel oxidation catalyst
DPF	Diesel particulate filter
FESEM	Field emission scanning electron microscopy
GHSV	Gas hourly space velocity
IF	Inorganic fraction
LNT	Lean NO <sub>x</sub> trap
NO <sub>x</sub>	Nitrogen oxides
NTP	Non-thermal plasma
PM	Particulate matter
SCR	Selective catalytic reduction
SCRoF	SCR on Filter
SCS	Solution combustion synthesis
SOF	Soluble organic fraction
SSA	Specific surface area
TPD	Temperature programmed desorption
TPO	Temperature programmed oxidation
TPR	Temperature programmed reduction
VOC	Volatile organic compounds
W/F	Catalyst weight/Feed flow rate
XPS	X-ray photoelectron spectroscopy
XRD	X-ray powder diffraction

---

Table 2 List of symbols

Symbol	Quantity	Units
Acs	Adsorbate cross sectional area	Å <sup>2</sup> /molecule
BE	Binding energy	eV
C	BET constant	-
d	Distance between adjacent planes of atoms	nm
eV	Electron volts	-
f	Fuel/nitrate molar ratio	-
hν	Photon energy	eV
kE	Kinetic energy	eV
N <sub>A</sub>	Avogadro's number	molecule/mol
n	Amount adsorbed	mol/g
n <sub>m</sub>	Monolayer capacity	mol/g
P	Pressure of the adsorbate	Pa
P <sup>0</sup>	Saturation pressure of the adsorbate	Pa
P/P <sup>0</sup>	Relative pressure	-
Oα	Surface chemisorbed oxygen	-
Oβ	Lattice oxygen	-
S	Specific surface area	m <sup>2</sup> /g
%at	Concentration	%
λ	wavelength of the X-ray beam	nm
φ	Elemental stoichiometric coefficient	-
θ	Incidence angle of the X-ray beam	degrees

# Sommario

## Introduzione

L'inquinamento atmosferico è un problema ambientale e sociale molto importante e per la sua complessità rappresenta una sfida in termini di gestione e mitigazione degli inquinanti nocivi. I composti inquinanti possono essere emessi sia da fonti antropogeniche sia naturali, possono essere emessi direttamente nell'atmosfera (inquinanti primari) o possono essere formati nell'atmosfera da altri gas precursori (inquinanti secondari). Fra i principali inquinanti si possono trovare gli ossidi di azoto ( $\text{NO}_x$ ), ossidi zolfo ( $\text{SO}_x$ ), particolato (PM), CO e composti organici volatili (VOC). Questi composti hanno molti effetti negativi sulla salute, sugli ecosistemi e sul clima.

I principali settori che contribuiscono alle emissioni di inquinanti atmosferici sono il commerciale, trasporto, industriale, energetico, agricolo e dei rifiuti. In particolare, le emissioni da fonti mobili, come automobili e camion, hanno un impatto molto grande sulla qualità dell'aria poiché aumentano considerevolmente i livelli dei gas serra presenti nell'atmosfera. Questo rappresenta un rischio per la salute nelle aree rurali, urbane e industrializzate sia in paesi sviluppati che in quelli in via di sviluppo.

Nel settore automobilistico, i motori Diesel sono ampiamente utilizzati per veicoli ad alte prestazioni e recentemente sono diventati popolari anche per veicoli commerciali leggeri. Questo tipo di motori ha un uso più estensivo rispetto ai motori a benzina a causa di bassi costi operativi, efficienza energetica, elevata durabilità e affidabilità. I motori Diesel offrono anche un minor consumo di carburante ed emettono una minore quantità di  $\text{CO}_2$ . Tuttavia, essi sono associati all'emissione di una notevole quantità di inquinanti presenti nei gas di scarico, inclusi  $\text{NO}_x$ , particolato, CO e idrocarburi incombusti. Fra questi, gli  $\text{NO}_x$  sono quelli presenti nella più alta proporzione (più del 50%), seguiti dal particolato. Il monossido di carbonio e gli idrocarburi sono presenti in concentrazioni molto più basse, poiché nei motori diesel la combustione ha luogo con aria in eccesso.

Il particolato si forma a causa di una combustione incompleta degli idrocarburi nel combustibile e nell'olio lubrificante. Le particelle di particolato sono generalmente sfere con diametro compreso fra 15-40 nm e possono essere divise in tre componenti principali: soot, una frazione organica solubile (SOF) e una -frazione inorganica (IF). Il soot è costituito da un nucleo di

carbonio con tracce di materiale organico ed altri composti adsorbiti e rappresenta più dell'50% del totale delle emissioni di PM.

Siccome il PM è diventato un importante componente dell'inquinamento atmosferico ed è associato a problemi respiratori, malattie cardiovascolari ed alterazioni delle cellule della pelle, la recente legislazione ha introdotto limiti più severi per i veicoli con lo scopo di controllare le emissioni di questo inquinante (per l'Europa il limite stabilito dal 2009 è 0.005 g/km per il PM da veicoli leggeri). Per soddisfare questi standard sono state sviluppate diverse tecnologie di post trattamento, fra le quale la trappola di particolato presente nei gas di scarico attraverso l'utilizzo di filtri antiparticolato diesel (DPF).

I DPF sono in genere realizzati in cordierite o carburo di silicio, hanno una struttura monolitica a nido d'ape con canali ciechi alternati, dove il soot viene rimosso meccanicamente dai gas di scarico. Le pareti del filtro sono progettate con ampie superfici per poter operare con una caduta di pressione accettabile. Ma, con l'accumulo delle particelle di soot nel filtro viene raggiunta una caduta di pressione critica. A questo punto una fase di rigenerazione consente di rimuovere i depositi di soot dal filtro, altrimenti la contropressione può diminuire l'efficienza del motore.

Esistono due tipi di processi di rigenerazione: la rigenerazione attiva e passiva. Nella prima il soot intrappolato viene rimosso periodicamente attraverso un'ossidazione controllata con  $O_2$  a 550°C o temperature più elevate. Post-iniezioni di combustibile o calore sono usati per aumentare la temperatura del DPF. Il calore è fornito da fonti esterne, come riscaldatori o bruciatori a fiamma. Poiché una grande quantità di energia deve essere fornita e le temperature raggiunte nel filtro potrebbero essere così alte da provocare il suo scioglimento, questa tecnica di generazione non è ampiamente utilizzata.

Dall'altra parte, la rigenerazione passiva ha luogo quando la temperatura del gas di scarico è talmente elevata da innescare la combustione del soot accumulato nel filtro, senza l'aggiunta di combustibile o l'uso di calore. Poiché questo materiale brucia a temperature superiori a 600°C mentre la temperatura dei gas di scarico dei motori diesel è quasi sempre nell'intervallo 200-500°C, è necessario l'utilizzo di un catalizzatore per promuovere la combustione del soot. Il Pt è il catalizzatore più ampiamente usato per la sua elevata attività e durata, ma a causa del suo costo si stanno cercando alternative per sostituirlo. I catalizzatori basati su ceria sono uno dei candidati più promettenti per i DPF grazie alla loro eccellente proprietà redox e ai costi minori rispetto ai metalli nobili.

Per quanto riguarda gli ossidi di azoto  $NO_x$  ( $NO + NO_2$ ), questi sono inquinanti primari emessi direttamente dal processo di combustione. Sia  $NO$  che  $NO_2$  sono considerati tossici, ma il biossido di azoto ha un livello di tossicità cinque volte maggiore. Questi composti possono dare origine a nuove specie inquinanti, come l'acido nitrico ( $HNO_3$ ) e acido nitroso ( $HNO_2$ ), che sono responsabili dalle piogge acide. Inoltre, reagendo con altri composti organici in presenza del sole possono produrre smog fotochimico. Il limite stabilito dalla normativa in vigore (Euro 6) è di 0.08 g/km per veicoli leggeri di tipo Diesel.

Fra le tecnologie di post-trattamento per il controllo delle emissioni di  $\text{NO}_x$  in applicazioni mobili si trovano: la decomposizione catalitica diretta, l'intrappolamento di  $\text{NO}_x$  (LNT), la riduzione catalitica selettiva (SCR) e la riduzione assistita con plasma. Inoltre, è possibile utilizzare una strategia di gestione del motore per controllare l'emissione di questi composti chiamata EGR, la quale consiste nel ricircolare una parte dei gas di scarico alla camera di combustione con l'obiettivo di abbassare la temperatura di combustione e in questa maniera ridurre la produzione di  $\text{NO}_x$  nel motore. L'uso di questa strategia però non è sufficiente per soddisfare i recenti limiti stabili per gli  $\text{NO}_x$ .

La riduzione catalitica selettiva (SCR) è una delle tecnologie più promettenti fra quelle menzionate sopra. In questa, un catalizzatore riduce gli  $\text{NO}_x$  a  $\text{N}_2$  e acqua in presenza di un agente riducente, in genere ammoniacca. La particolarità di questa reazione con  $\text{NH}_3$  è che può avvenire in presenza di ossigeno in eccesso, e questo è il motivo per il quale questa tecnologia ha ricevuto molta attenzione per i veicoli a motori diesel. A causa dei problemi pratici e i rischi per la salute legati all'ammoniaca, questa viene fornita al sistema attraverso l'utilizzo di una soluzione acquosa di urea.

Negli ultimi anni i limiti stabiliti per controllare le emissioni di composti presenti nelle emissioni delle macchine sono diventati più severi, costringendo i produttori ad utilizzare sistemi di post-trattamento per i gas di scarico sempre più complessi. A causa di questa crescente complessità, con i relativi costi associati e limitazioni spaziali, è stata proposta un'integrazione di due elementi che fanno parte del classico sistema di controllo delle emissioni per i motori diesel, denominato SCRoF (Selective Catalytic Reduction on Filter), il quale combina le funzionalità della riduzione catalitica selettiva (SCR) per l'abbattimento degli  $\text{NO}_x$  e del filtro per il particolato Diesel (DPF) per l'intrappolamento del soot.

Nel SCRoF, gli  $\text{NO}_x$  sono ridotti in conseguenza dell'aggiunta di  $\text{NH}_3$  mentre il soot si accumula sulle pareti del filtro, il quale è stato impregnato con il catalizzatore di SCR. Anche in questo caso il filtro viene rigenerato utilizzando una strategia passiva (il soot accumulato è continuamente ossidato dal  $\text{NO}_2$ ) oppure una strategia attiva (attraverso l'aumento della temperatura dei gas a monte).

Per implementare con successo un sistema di questo tipo devono essere soddisfatti molti requisiti complessi, per cui l'obiettivo di questa tesi è quello di sviluppare un catalizzatore adeguato per essere utilizzato in questo sistema di post-trattamento dei gas di scarico.

## **Materiali e Metodi**

Sono stati sintetizzati tre catalizzatori a base  $\text{MnO}_x$  utilizzando il metodo SCS, il quale si basa su una reazione di ossidoriduzione esotermica che ha luogo in una soluzione contenente un composto ossidante e un combustibile organico. In questo caso, sono stati usati come ossidanti i nitrati dei metalli di interesse, Mn e Ce, e come combustibile è stata scelta la glicina. Le quantità

di reagenti sono state calcolati come è stato descritto in Deorsola et al. Una volta determinate le quantità giuste, i reagenti sono stati sciolti in 25 mL di acqua distillata. La soluzione è stata agitata a temperatura ambiente per 30 min e poi è stata trasferita in un crogiolo di porcellana ed è stata messa in un forno pre-riscaldato a 600°C per 30 min. I campioni sono stati raccolti, frantumati in un mortaio e infine calcinati per 1 ora a 700°C.

Dopo essere sintetizzati, i tre catalizzatori sono stati caratterizzati per avere una conoscenza più accurata delle loro proprietà e poterle collegare all'attività catalitica. Le tecniche utilizzate per la caratterizzazione sono state: fisisorbimento di azoto, microscopia elettronica a scansione ed emissione di campo (FE-SEM), analisi H<sub>2</sub>-TPR (riduzione a temperatura programmata), NH<sub>3</sub>-TPD (desorbimento a temperatura programmata), diffrazione di raggi-X (XRD) e spettroscopia fotoelettronica a raggi-X (XPS).

Per determinare l'attività catalitica è stata condotta una serie di test per ogni catalizzatore al fine di affrontare alcune reazioni possibilmente coinvolte nel SCR<sub>o</sub>F. In una prima fase sono state studiate individualmente l'ossidazione del soot, l'ossidazione del NO, l'ossidazione di NH<sub>3</sub> e la standard SCR. Successivamente, l'ossidazione dell'ossido nitrico e la standard SCR sono state ripetute in presenza di soot.

I diversi test sono stati condotti in un reattore tubolare a letto fisso di quarzo, il quale è stato riscaldato in un forno tubolare. Si è lavorato con un flusso totale di 500 mL min<sup>-1</sup> con le composizioni riportate nella Tabella 1 e con un'altezza approssimata del letto di 5 mm, con l'obiettivo di avere una GHSV = 50,000 h<sup>-1</sup>. Prima dei test catalitici, il catalizzatore è stato pellettizzato e setacciato ad una frazione di dimensione 250-500 µm per evitare la presenza di bypass e mitigare la caduta di pressione. La temperatura è stata misurata con una termocoppia di tipo K posta all'interno del reattore a contatto con il letto catalitico. Le concentrazioni di NH<sub>3</sub>, NO, NO<sub>2</sub>, N<sub>2</sub>O, CO e CO<sub>2</sub> in uscita sono state monitorate con analizzatori dedicati.

Table 3 Composizione del gas di ingresso nei diversi test.

Reazione	NH <sub>3</sub> (ppm)	NO (ppm)	O <sub>2</sub> (%)	N <sub>2</sub>
Ossidazione soot	0	0	3	Bilancio
Ossidazione NO	0	500	3	Bilancio
Ossidazione NH <sub>3</sub>	500	0	3	Bilancio
Standard SCR	500	500	3	Bilancio
ossidazione NO + soot	0	500	3	Bilancio
Standard SCR + soot	500	500	3	Bilancio

L'ossidazione di NO, l'ossidazione di NH<sub>3</sub> e la standard SCR sono state testate in condizioni isoterme da 150 °C fino a 700 °C con incrementi di 50 °C. Prima di ogni incremento di temperatura, è stato atteso un tempo sufficiente in modo tale che il valore delle concentrazioni fosse stabile. I test in presenza di soot sono stati condotti con la stessa metodologia fino a 400 °C, quindi il riscaldamento è stata condotta linearmente fino a 750 °C con una velocità di

riscaldamento di 3 °C/min. L'ossidazione del soot è stata realizzata con la stessa velocità di riscaldamento nell'intervallo di temperatura 25-750 °C. Per paragonare le attività catalitiche, sono stati calcolati nella reazione SCR i valori di conversione di NO<sub>x</sub> e di NH<sub>3</sub>, e i valori di selettività ad azoto. Per le reazioni in presenza di particolato, la velocità di reazione è stata calcolata e utilizzata per il confronto.

### **Analisi e discussione dei risultati**

- Risultati caratterizzazione fisico-chimica e morfologica

- Fissisorbimento di N<sub>2</sub>:

Nei risultati ottenuti dalla caratterizzazione fatta utilizzando questa tecnica si può notare che i catalizzatori contenenti Ce hanno un'area superficiale specifica più alta, in particolare all'aumentare della percentuale di Ce aumenta la superficie specifica; come si può notare dai valori ottenuti il catalizzatore Ce<sub>0,5</sub>Mn<sub>0,5</sub>O<sub>x</sub> presenta un'area superficiale quasi tre volte più alta rispetto a quella del campione MnO<sub>x</sub>. Inoltre, il volume e il diametro dei pori di questo catalizzatore a base di Ce erano più alti dei rispettivi valori degli altri catalizzatori.

In aggiunta, poiché i valori del diametro dei pori sono contenuti nell'intervallo 2-50 nm, i tre catalizzatori possono essere classificati come materiali mesoporosi, come previsto dalla tendenza osservata nelle isoterme, le cui corrispondono al tipo V secondo la classificazione della IUPAC.

Nelle isoterme si è potuto apprezzare anche che la quantità di azoto adsorbita dal catalizzatore Ce<sub>0,5</sub>Mn<sub>0,5</sub>O<sub>x</sub> è stata molto più alta della quantità adsorbita per gli altri due.

- FESEM:

Nei risultati dell'analisi FESEM è possibile vedere che tutti i catalizzatori sono stati caratterizzati da una struttura spugnosa con la presenza di porosità. Le morfologie dei catalizzatori MnO<sub>x</sub> e Ce<sub>0,25</sub>Mn<sub>0,75</sub>O<sub>x</sub> erano molto simili, con agglomerati di particelle sferiche di diametro inferiore a 100 nm. Il catalizzatore Ce<sub>0,5</sub>Mn<sub>0,5</sub>O<sub>x</sub> ha mostrato una morfologia leggermente diversa, con agglomerati di particelle con forma lamellare, e sembrava di possedere anche una struttura più spugnosa.

- Diffrazione dei raggi-X:

Con questa tecnica è stato possibile determinare le diverse fasi presenti nella struttura cristallina dei catalizzatori. Nel campione MnO<sub>x</sub> quasi tutti i picchi di diffrazione identificati corrispondono alla fase Mn<sub>2</sub>O<sub>3</sub> ed è stato possibile riconoscere solo un picco della fase Mn<sub>3</sub>O<sub>4</sub>.

In entrambi i campioni  $Ce_{0.25}Mn_{0.75}O_x$  e  $Ce_{0.5}Mn_{0.5}O_x$  sono stati identificati picchi di diffrazioni delle fasi  $CeO_2$ ,  $Mn_3O_4$  e  $Mn_2O_3$ , essendo l'ultima fase quella presente nella più piccola proporzione. I pattern di diffrazione di questi due catalizzatori erano molto simili, l'unica differenza notevole era l'intensità dei picchi. Per il campione  $Ce_{0.25}Mn_{0.75}O_x$  i picchi di diffrazione delle fasi  $MnO_x$  erano più intensi dei picchi presenti nel campione  $Ce_{0.5}Mn_{0.5}O_x$ , questo a causa del maggior contenuto di Mn nel campione. Lo stesso è stato evidenziato per i picchi di diffrazione della fase  $CeO_2$ , i quali erano più intensi nel campione  $Ce_{0.5}Mn_{0.5}O_x$ .

Confrontando i pattern di diffrazione dei tre catalizzatori è possibile evidenziare che i picchi del campione  $MnO_x$  erano più stretti e alcuni più intensi rispetto agli altri campioni; questo indica la presenza di una maggiore cristallinità.

– Spettroscopia fotoelettronica a raggi-X (XPS):

Nella regione O 1 si possono distinguere due picchi. In letteratura è riportato che il picco nell'intervallo di energia di legame 529,5-530,0 eV può essere assegnato all'ossigeno  $\beta$  ( $O_\beta$ ) e che l'intervallo 531,0-531,7 eV corrisponde all'ossigeno chemisorbito superficiale (indicato come  $O_\alpha$ ). Tutti i campioni hanno mostrato entrambi i componenti con a circa gli stessi valori di BE.

Per quanto riguarda la concentrazione relativa di  $O_\alpha$  e  $O_\beta$ , la concentrazione di  $O_\alpha$  nel  $MnO_x$  e  $Ce_{0.25}Mn_{0.75}O_x$  è stata molto simile e ha corrisposto a circa la metà della concentrazione di  $O_\beta$ . Nel caso di  $Ce_{0.5}Mn_{0.5}O_x$ , la concentrazione di  $O_\beta$  è stata la più alta tra tutti i catalizzatori, il suo valore è stato quasi il doppio dei valori ottenuti per gli altri.

Gli spettri XPS nella regione Mn 2p hanno mostrato due picchi che potrebbero essere ascritti ai livelli Mn  $2p_{3/2}$  e Mn  $2p_{1/2}$ . Secondo la letteratura, l'energia di legame agli intervalli 640.4-640.8 eV, 641.5-642.0 eV e 642.5-643.8 eV è assegnata rispettivamente a  $Mn^{2+}$ ,  $Mn^{3+}$  e  $Mn^{4+}$ . In tutti i campioni è stata apprezzata la presenza di picchi corrispondenti alle tre specie citate prima in quasi le stesse posizioni. Tutti i catalizzatori hanno mostrato un contenuto simile di  $Mn^{4+}$ , essendo più alta la quantità presente nel catalizzatore  $Ce_{0.25}Mn_{0.75}O_x$ , per il quale il rapporto  $Mn^{4+}/Mn^{3+}$  era 0.64. Questa grande quantità potrebbe essere correlata ad un incremento nel comportamento ossidativo. In questo catalizzatore, la quantità di  $Mn^{2+}$  e  $Mn^{3+}$  presente è stata simile. Nel caso di  $MnO_x$  come per  $Ce_{0.5}Mn_{0.5}O_x$ ,  $Mn^{3+}$  è stata la specie nella quantità più alta seguita da  $Mn^{2+}$ , ma per il secondo catalizzatore la quantità di  $Mn^{2+}$  è stata considerevolmente inferiore alla quantità di  $Mn^{3+}$ , essendo la specie nella più piccola quantità.

Per gli spettri nella regione Ce 3d sono stati evidenziati picchi multipli corrispondenti a Ce  $3d_{3/2}$  e Ce  $3d_{5/2}$ . I risultati ottenuti per entrambi i catalizzatori sono stati molto simili, con quantità simili di Ce (III) e Ce (IV), essendo l'ultima la specie presente nella proporzione più elevata.

– H<sub>2</sub>-TPR:

Nei risultati ottenuti, è possibile vedere che la riduzione dei catalizzatori a base di Ce è iniziata nello stesso intervallo di temperatura, ma per il catalizzatore Ce<sub>0.25</sub>Mn<sub>0.75</sub>O<sub>x</sub> è stato ottenuto solo un picco (a 141 ° C) attribuito alla riduzione della fase MnO<sub>2</sub> amorfa. Nel caso di Ce<sub>0.5</sub>Mn<sub>0.5</sub>O<sub>x</sub> sono stati osservati tre picchi di riduzione, il primo a bassa temperatura (170 ° C) corrispondente alla riduzione della fase MnO<sub>2</sub> amorfa, il secondo a 334 ° C è attribuito alla riduzione di altri MnO<sub>x</sub> presenti e la terza a 521 ° C rappresenta la riduzione di Mn<sub>3</sub>O<sub>4</sub>. D'altra parte, la riduzione del catalizzatore MnO<sub>x</sub> è iniziata a temperature più elevate, in questo caso sono stati identificati due picchi di intensità maggiore rispetto ai picchi ottenuti per i catalizzatori a base di Ce. Il primo a 453 ° C corrispondeva alla riduzione di MnO<sub>2</sub> e il secondo a 526 ° C è attribuito alla riduzione di Mn<sub>3</sub>O<sub>4</sub>.

– NH<sub>3</sub>-TPD:

Nei risultati ottenuti si è evidenziato che tutti e tre catalizzatori presentavano soltanto un picco di desorbimento più o meno alla stessa temperatura, fra 100°C e 200°C. Siccome i picchi sono stati localizzati sotto i 300°C, i siti acidi dei catalizzatori sono stati classificati come di tipo Brønsted, secondo quello riportato in letteratura.

L'intensità del picco osservato per il catalizzatore MnO<sub>x</sub> era molto piccola, indicando la sua scarsa capacità di adsorbimento. Nel caso del catalizzatore Ce<sub>0.25</sub>Mn<sub>0.75</sub>O<sub>x</sub> il picco era più alto, ma la sua intensità era ancora piccola rispetto al picco ottenuto per il campione Ce<sub>0.5</sub>Mn<sub>0.5</sub>O<sub>x</sub>, il quale ha mostrato le migliori caratteristiche acide.

In quanto riguarda la quantità totale di ammoniaca adsorbita, il valore ottenuto per i catalizzatori Ce<sub>0.25</sub>Mn<sub>0.75</sub>O<sub>x</sub> e MnO<sub>x</sub> era molto simile ma rappresentava meno della metà della capacità di adsorbimento del catalizzatore Ce<sub>0.5</sub>Mn<sub>0.5</sub>O<sub>x</sub>. Inoltre, per i tre catalizzatori, la quantità fisicamente adsorbita e conseguentemente facilmente desorbita a temperatura ambiente era superiore a quella chimicamente adsorbita.

• Risultati test catalitici

– Ossidazione del NO:

Nel test di ossidazione del NO, per tutti e tre i catalizzatori a basse temperature, come descritto dalla reazione di equilibrio, la formazione di NO<sub>2</sub> è stata favorita, solo da una certa temperatura (per i catalizzatori MnO<sub>x</sub> e Ce<sub>0.5</sub>Mn<sub>0.5</sub>O<sub>x</sub> 300°C e per il catalizzatore Ce<sub>0.25</sub>Mn<sub>0.75</sub>O<sub>x</sub> 350°C) l'equilibrio si è spostato verso la produzione di NO. La differenza (più nota) fra i profili ottenuti con e senza soot è stata intorno a 350°C, dove la concentrazione di NO<sub>2</sub> era maggiore in assenza di soot. Ciò indica che una parte del NO<sub>2</sub> è stata utilizzata nell'ossidazione del soot.

Facendo un confronto fra la conversione di NO con e senza soot si è verificata una diminuzione dei valori di conversione in presenza di soot. Questa diminuzione è stata dovuta al fatto che la concentrazione di NO è aumentata poiché è stato prodotto nella reazione fra NO<sub>2</sub> e soot. Siccome la conversione di NO è diminuita di più per il catalizzatore Ce<sub>0.25</sub>Mn<sub>0.75</sub>O<sub>x</sub> che per gli altri, questo catalizzatore è stato quello in cui c'è stato più NO<sub>2</sub> consumato anche nella reazione di ossidazione del soot.

– Ossidazione del NH<sub>3</sub>:

Tutti i catalizzatori testati hanno mostrato un'elevata attività nella reazione di ossidazione dell'ammoniaca dato che la temperatura in cui la conversione è del 50% era inferiore a 200°C ed è stata raggiunta una conversione quasi completa a 250°C. Comunque, l'attività a temperature più basse era molto scarsa, con conversioni del 20% e 10% per i catalizzatori Ce<sub>0.25</sub>Mn<sub>0.75</sub>O<sub>x</sub> e MnO<sub>x</sub> rispettivamente, i risultati sono migliorati un po' per il catalizzatore Ce<sub>0.5</sub>Mn<sub>0.5</sub>O<sub>x</sub>, con una conversione sopra il 40%.

Sebbene siano state raggiunte alte conversioni con i catalizzatori, la selettività verso la reazione desiderata (equazione 3.8) è stata molto scarsa, come si può vedere nei profili di concentrazione, dove la quantità di azoto presente era inferiore rispetto agli altri composti prodotti.

Paragonando i risultati ottenuti con i catalizzatori MnO<sub>x</sub> e Ce<sub>0.25</sub>Mn<sub>0.75</sub>O<sub>x</sub>, l'aggiunta di Ce in quella proporzione non ha migliorato l'attività del catalizzatore per questa reazione specifica, invece la quantità di sottoprodotti formati era più alta. D'altra parte, l'uso di Mn e Ce in proporzioni uguali ha aumentato la conversione di NH<sub>3</sub>, anche se c'è stata una maggiore formazione di N<sub>2</sub>O, è stato comunque possibile ottenere conversioni superiori al 90% da 200°C, mentre con gli altri catalizzatori la conversione era leggermente superiore al 60%.

– Standard SCR:

Nella prova fatta in assenza di soot, per tutti e tre catalizzatori la conversione era circa del 100% a 250°C. Per il catalizzatore MnO<sub>x</sub> la conversione era molto bassa a 150°C ma è aumentata rapidamente con l'aumentare della temperatura. Una tendenza simile è stata ottenuta con il catalizzatore Ce<sub>0.25</sub>Mn<sub>0.75</sub>O<sub>x</sub> ma i valori erano leggermente più alti. Invece, con il catalizzatore Ce<sub>0.5</sub>Mn<sub>0.5</sub>O<sub>x</sub> sono state raggiunte le maggiori conversioni.

Le conversioni di NO<sub>x</sub> più alte sono state raggiunte con il catalizzatore Ce<sub>0.25</sub>Mn<sub>0.75</sub>O<sub>x</sub>, 96% a 200°C e 86% a 250°C, mentre il catalizzatore MnO<sub>x</sub> è stato quello con la minore attività. A 200°C la conversione degli NO<sub>x</sub> per tutti e tre catalizzatori ha raggiunto il suo valore massimo, dopo questa temperatura la conversione è caduta, diminuendo in modo più pronunciato per il catalizzatore MnO<sub>x</sub>, diventando zero a 300°C. I catalizzatori Ce<sub>0.25</sub>Mn<sub>0.75</sub>O<sub>x</sub> e Ce<sub>0.5</sub>Mn<sub>0.5</sub>O<sub>x</sub> hanno raggiunto una conversione nulla a 350°C e 400°C

rispettivamente. Quest'ultimo è stato il catalizzatore con l'intervallo di conversione più alto.

Rispetto alle selettività durante la formazione di  $N_2$ , i catalizzatori non sono stati molto selettivi, come si può vedere nella notevole formazione di sottoprodotti. In generale, il catalizzatore  $MnO_x$  è stato quello più selettivo. Il catalizzatore  $Ce_{0.25}Mn_{0.75}O_x$  solo ha avuto un solo valore di selettività diverso da zero a  $150^\circ C$ , e anche a questa temperatura il valore era molto basso. Il catalizzatore  $Ce_{0.5}Mn_{0.5}O_x$  ha presentato un valore massimo di selettività a  $150^\circ C$ , 81%, dopo dopodiché il valore è diminuito fino a zero a  $400^\circ C$ .

Dai risultati ottenuti con i tre catalizzatori è possibile affermare che la reazione di SCR non è stata quella principale, reazioni indesiderate come la riduzione incompleta di  $NO$  e l'ossidazione di  $NH_3$  hanno avuto un ruolo importante e dopo  $200^\circ C$  sono diventate predominanti. I valori più alti di conversione degli  $NO_x$  sono stati ottenuti per il catalizzatore  $Ce_{0.25}Mn_{0.75}O_x$ , però la sua scarsa selettività permette di concludere che la presenza di  $Ce$  in quella proporzione non rappresenta un miglioramento rispetto al  $MnO_x$ , anche se l'attività catalitica era maggiore.

Nel test fatto in presenza di soot è stato ottenuto per il catalizzatore  $Ce_{0.25}Mn_{0.75}O_x$  un aumento nell'attività catalitica a basse temperature, come evidenziato nei valori più alti di conversione di  $NH_3$  e  $NO_x$ . In particolare, è stato evidenziato un aumento della concentrazione di azoto a  $150^\circ C$ , ma anche la concentrazione di  $N_2O$  è aumentata e lo ha fatto in una proporzione maggiore. Questo significa che l'aumento dei valori di conversione è stato probabilmente dovuto al fatto che l' $NO$  e l'ammoniaca sono stati consumati in reazioni indesiderate, come l'ossidazione di  $NH_3$  e la riduzione incompleta del  $NO$ , e non nella standard SCR. Inoltre, dopo  $200^\circ C$  il catalizzatore è stato influenzato in maniera negativa dalla presenza di soot, come si vede nella diminuzione della conversione di  $NO_x$ .

D'altra parte, nel caso del catalizzatore  $Ce_{0.5}Mn_{0.5}O_x$  il miglioramento della performance di SCR è stato considerevolmente più alto, principalmente a  $150^\circ C$  dove c'è stato un aumento di circa 80 ppm nella quantità di  $N_2$  prodotta rispetto al caso in cui non c'era presenza di soot, per il  $N_2O$  l'aumento è stato solo di circa 50 ppm, questo dimostra che la reazione di SCR è stata prevalente rispetto alle altre reazioni indesiderate. Tuttavia, la diminuzione nella conversione degli  $NO_x$  a partire da  $250^\circ C$  indica che l'attività di SCR ha patito la presenza di soot. Inoltre, poiché la concentrazione massima di  $NO_2$  (corrispondente a  $350^\circ C$ ) è stata inferiore di quando non c'era soot nel sistema, una parte di questo composto è stata probabilmente consumata nella reazione di ossidazione del soot o nella reazione fast-SCR, aumentando allo stesso tempo la concentrazione di  $N_2$ .

Per il catalizzatore  $MnO_x$ , a differenza degli altri catalizzatori, in presenza di soot si è verificato un aumento delle conversioni di  $NH_3$  e  $NO_x$  dopo  $200^\circ C$ . In particolare, i valori più alti di conversione di  $NO_x$  potrebbero essere dovuti al fatto che anche il  $NO_2$  è stata consumata nella reazione fast-SCR, ciò spiega l'aumento della quantità di  $N_2$  prodotta. Inoltre, principalmente nell'intervallo di temperatura da  $300^\circ C$  a  $400^\circ C$ , è possibile che

solo una piccola parte del  $\text{NO}_2$  disponibile abbia partecipato alla reazione di combustione del soot, producendo una minore quantità di  $\text{NO}$  e in tal modo riducendo la generazione di  $\text{NO}_x$ .

Sia per il catalizzatore  $\text{MnO}_x$  che per  $\text{Ce}_{0.5}\text{Mn}_{0.5}\text{O}_x$  è stato evidenziato un aumento della concentrazione di  $\text{N}_2$  in presenza di soot nell'intero intervallo di temperatura. Dai profili di concentrazione è possibile affermare che questo aumento è stato più probabilmente dovuto ad un aumento dell'ossidazione di  $\text{NH}_3$  in  $\text{N}_2$ , la quale potrebbe essere stata potenziata dalla presenza di soot, come riportato in letteratura.

Infine, anche in presenza di un aumento delle conversioni, la presenza di soot non ha avuto alcuna influenza nell'intervallo di temperatura in cui si è verificato un effettivo abbattimento degli  $\text{NO}_x$ .

– Ossidazione del soot:

Come si può vedere nei risultati ottenuti per l'ossidazione del soot, è stata raggiunta una conversione completa con pochi gradi di differenza per tutti i catalizzatori. Per i catalizzatori con Ce, una conversione del 100% è stata ottenuta all'incirca la stessa temperatura ( $660^\circ\text{C}$ ). Con il catalizzatore  $\text{MnO}_x$  l'intera conversione del soot è stata ottenuta in un intervallo di temperatura di  $100^\circ\text{C}$ , e come è stato evidenziato nel profilo di concentrazione, la  $\text{CO}_2$  ha raggiunto un valore maggiore, ma è necessaria una temperatura più alta per innescare la reazione. Inoltre, il soot è stato convertito a una velocità maggiore con il catalizzatore  $\text{Ce}_{0.5}\text{Mn}_{0.5}\text{O}_x$ , seguito da  $\text{Ce}_{0.25}\text{Mn}_{0.75}\text{O}_x$  e  $\text{MnO}_x$ , come si può vedere nelle valori corrispondenti alla temperatura dov'è stata raggiunta una conversione del 50% :  $550^\circ\text{C}$ ,  $570^\circ\text{C}$  e  $600^\circ\text{C}$ , rispettivamente. Nel test non catalitico, questa temperatura è stata di circa  $640^\circ\text{C}$  e la conversione completa è stata raggiunta a temperatura più elevata rispetto ai test catalitici.

In generale, i risultati ottenuti con i catalizzatori a base di Ce sono stati molto simili, sia l'intensità che la temperatura del picco avevano dei valori molto vicini. In confronto con il catalizzatore  $\text{MnO}_x$ , con la presenza di Ce si è verificato uno spostamento verso temperature più basse per il picco di  $\text{CO}_2$ , anche la combustione è iniziata prima, nel caso del catalizzatore  $\text{Ce}_{0.5}\text{Mn}_{0.5}\text{O}_x$ , e si è svolta ad una velocità maggiore, mentre con il catalizzatore  $\text{MnO}_x$  è stata ottenuta una conversione completa in un intervallo di temperatura più ristretto e anche se il picco aveva più intensità, la temperatura è stata anche più alta. Per i catalizzatori con Ce c'è stata una produzione minore di  $\text{CO}_2$  e il range di temperatura necessario per finire la reazione è stato più ampio.

Tenendo conto dei risultati ottenuti nel test non catalitico, è chiaro che la diminuzione della temperatura del picco della  $\text{CO}_2$  non è stata molto rappresentativa con l'utilizzo dei catalizzatori, ma è stato possibile ottenere una notevole selettività verso la produzione di  $\text{CO}_2$ , date le piccolissime quantità di  $\text{CO}$  prodotto.

Per quanto riguarda i test di ossidazione di NO e standard SCR fatti in presenza di soot, è stato osservato uno spostamento verso valori più bassi nella temperatura a cui la velocità di reazione era massima in presenza di  $\text{NO}_x$  e  $\text{NH}_3$ . Inoltre, il soot è stato consumato a una velocità minore quando questi composti erano presenti nel sistema, questo a causa del fatto che diverse reazioni in parallelo hanno luogo e competono per l'uso di  $\text{O}_2$  e  $\text{NO}_2$ .

Per il catalizzatore  $\text{MnO}_x$ , l'ossidazione del soot in presenza di  $\text{NO}_x$  è cominciata a una temperatura inferiore, quasi  $200^\circ\text{C}$ , rispetto al caso base (cioè l'ossidazione del soot con la sola presenza di ossigeno), e ha raggiunto un valore massimo di circa  $500^\circ\text{C}$ , temperatura alla quale è iniziata l'ossidazione del soot con ossigeno. Nel caso della SCR, l'ossidazione del soot è cominciata alla stessa temperatura dell'ossidazione di NO, ma la velocità di reazione era minore, per questo la temperatura dove è stata raggiunta la velocità massima era maggiore. Questa diminuzione della velocità di reazione è stata dovuta al fatto che una parte del  $\text{NO}_2$  disponibile per l'ossidazione del soot è stata utilizzata nella reazione fast-SCR.

Nel caso del catalizzatore  $\text{Ce}_{0.25}\text{Mn}_{0.75}\text{O}_x$ , diversamente dagli altri catalizzatori, l'ossidazione del soot ha cominciato e ha raggiunto una velocità di reazione massima a una temperatura inferiore nel test SCR + soot (a circa  $450^\circ\text{C}$ ), il che significa che la maggior parte dell' $\text{NO}_2$  disponibile è stata utilizzata per l'ossidazione del soot e non nella reazione fast-SCR. Nel test di ossidazione dell'NO in presenza di soot, la reazione è iniziata a circa  $300^\circ\text{C}$ , come per gli altri catalizzatori, la velocità massima è stata raggiunta a  $500^\circ\text{C}$  e il suo valore era molto simile a quello ottenuto per il test SCR. In entrambi i casi, si osserva un altro piccolo picco intorno a  $670^\circ\text{C}$ , corrisponde all'ossidazione del soot con l'ossigeno.

Per il catalizzatore  $\text{Ce}_{0.5}\text{Mn}_{0.5}\text{O}_x$ , la reazione in presenza degli  $\text{NO}_x$  ha avuto luogo a una velocità più bassa, ciò indica che l'ossidazione del soot è stata in qualche modo inibita e il percorso di reazione preferito del  $\text{NO}_2$  era quello fornito dall'equilibrio con il NO. Nonostante questo, l'ossidazione del soot è iniziata a una temperatura inferiore e la velocità di reazione ha raggiunto un massimo più velocemente rispetto al caso base. È possibile apprezzare anche un piccolo picco intorno a  $600^\circ\text{C}$  a causa della reazione di ossidazione con  $\text{O}_2$ . D'altra parte, nel test SCR eseguito in presenza di soot, le velocità di reazione sono state più elevate rispetto al caso dell'ossidazione di NO, ma erano ancora inferiori rispetto al caso base. L'ossidazione della soot è iniziata approssimativamente  $150^\circ\text{C}$  prima e il consumo massimo di soot è stato apprezzato a circa  $470^\circ\text{C}$ .

## **Conclusioni**

L'obiettivo principale di questa tesi è stato quello di sviluppare catalizzatori per applicazioni SCR<sub>oF</sub>. Per ottenere ciò, tre diversi catalizzatori sono stati sintetizzati utilizzando il metodo SCS. Dopo essere stati sintetizzati, questi catalizzatori sono stati caratterizzati utilizzando diverse tecniche con lo scopo di avere una migliore comprensione di alcune delle loro proprietà fisiche e chimiche e di come queste potrebbero influenzare le loro prestazioni nelle reazioni di interesse.

Successivamente, sono stati condotti una serie di test per capire meglio tutte le reazioni che potrebbero essere coinvolte nel SCRof e per determinare l'adeguatezza dei catalizzatori per questo tipo di applicazione.

Tutti i catalizzatori hanno mostrato un'elevata attività nella reazione di ossidazione dell'ammoniaca, raggiungendo una conversione quasi completa a 250 ° C. Tuttavia, la selettività verso la formazione di azoto è stata molto scarsa e quindi si è formata un'alta quantità di sottoprodotti, in particolare la presenza di Ce ha favorito la formazione di N<sub>2</sub>O mentre per il catalizzatore di MnO<sub>x</sub> si è prodotta una quantità apprezzabile di NO<sub>2</sub>.

Nell'ossidazione NO, rispetto all'ossidazione dell'ammoniaca, l'attività è stata più bassa con una conversione massima del 60%. Tra tutti i catalizzatori, MnO<sub>x</sub> è stato quello con un'attività minore. Inoltre, si è apprezzato che a partire da 300 ° C, per il caso dei catalizzatori MnO<sub>x</sub> e Ce<sub>0,5</sub>Mn<sub>0,5</sub>O<sub>x</sub>, e da 350 ° C per Ce<sub>0,25</sub>Mn<sub>0,75</sub>O<sub>x</sub>, l'equilibrio favoriva la formazione di NO.

Per quanto riguarda la reazione SCR, i catalizzatori non hanno esibito le migliori prestazioni perché anche se sono state raggiunte elevate conversioni di ammoniaca, i catalizzatori hanno mostrato una scarsa selettività, come riflesso nell'elevata quantità di sottoprodotti formati. Inoltre, solo a basse temperature è stato possibile ottenere un'elevata attività di DeNO<sub>x</sub>, con conversioni di NO<sub>x</sub> fino al 96%, ma dopo 200 ° C i valori sono diminuiti costantemente fino a raggiungere un valore pari a zero nell'intervallo di temperatura tra 300 ° C e 400 ° C.

Nell'ossidazione del soot, sebbene con l'uso di catalizzatori la diminuzione della temperatura del picco di CO<sub>2</sub> non è stata molto rappresentativa rispetto al test non catalitico, è stato possibile ottenere una notevole selettività verso la formazione di CO<sub>2</sub>.

Nei test eseguiti in presenza di soot è stata osservata una diminuzione della concentrazione di NO<sub>2</sub> nell'intervallo di temperatura tra 300 ° C e 400 ° C, stando a indicare che una parte del NO<sub>2</sub> è stata utilizzata nella reazione di ossidazione del soot. Questo è stato effettivamente confermato nei risultati ottenuti per la velocità di reazione del soot in funzione della temperatura, dove è stata evidenziata attività di combustione del soot a temperature più basse rispetto al test di ossidazione del soot fatto in presenza di O<sub>2</sub>. Per il catalizzatore MnO<sub>x</sub>, la velocità di reazione è stata molto bassa nel caso del test SCR, il che significa che il NO<sub>2</sub> è stata preferibilmente consumata nella reazione fast-SCR, mentre per il catalizzatore Ce<sub>0,5</sub>Mn<sub>0,5</sub>O<sub>x</sub> i valori di velocità di reazione più bassi sono stati ottenuti per il test di ossidazione del NO, indicando in questo caso che il percorso di reazione preferito del NO<sub>2</sub> è stato quello della sua decomposizione. Al contrario, per Ce<sub>0,25</sub>Mn<sub>0,75</sub>O<sub>x</sub> sono state ottenute le più alte velocità di reazione sia per i test di ossidazione SCR che NO, evidenziando un elevato consumo di NO<sub>2</sub> nella rigenerazione del soot.

Anche la presenza di soot ha avuto una certa influenza sulle prestazioni della SCR. Si è verificato un aumento dell'attività catalitica, come riflesso nei maggiori valori di conversione di NH<sub>3</sub> e NO<sub>x</sub> ottenuti. Comunque, nel caso dei catalizzatori a base di Ce, dopo 200 ° C c'è stata una perdita nell'attività DeNO<sub>x</sub>. È stato inoltre osservato un aumento della selettività N<sub>2</sub>, poiché la quantità di N<sub>2</sub> prodotta aumentava mentre la produzione di NO<sub>2</sub> diminuiva, ma dai profili

di concentrazione è possibile affermare che questo aumento della concentrazione di  $N_2$  è stato probabilmente dovuto ad un aumento della quantità di ammoniaca ossidata in  $N_2$ , aumentata in qualche modo dalla presenza di soot.

Tra i tre catalizzatori sintetizzati e testati, il  $Ce_{0.5}Mn_{0.5}O_x$  è stato il catalizzatore con la maggiore attività catalitica. Questo è stato attribuito alla composizione superficiale, caratterizzata da una maggiore quantità di ossigeno labile superficiale e una notevole quantità di  $Mn^{4+}$ . A quest'ultimo è ascritta la grande capacità adsorbente dell'ammoniaca evidenziata. Anche la sua superficie specifica è stata considerevolmente più alta.

Inoltre, alcune delle proprietà fisico-chimiche dei catalizzatori  $MnO_x$  e  $Ce_{0.25}Mn_{0.75}O_x$  sono state simili a causa dell'elevato contenuto di Mn in quest'ultimo. Tuttavia, la presenza di Ce e la diversa composizione superficiale, hanno portato ad un aumento dell'attività catalitica, ma in alcuni casi questa crescita ha comportato una considerevole diminuzione della selettività.

# Contents

<b>List of Figures</b>	<b>xxi</b>
<b>List of Tables</b>	<b>xxiii</b>
<b>1 Introduction</b>	<b>1</b>
1.1 Air pollution . . . . .	1
1.2 Soot abatement . . . . .	5
1.2.1 Diesel Particulate Filter . . . . .	6
1.2.1.1 Active regeneration . . . . .	7
1.2.1.2 Passive regeneration . . . . .	7
1.2.1.3 Soot oxidation catalyst performance . . . . .	8
1.3 NO <sub>x</sub> removal . . . . .	10
1.3.1 Direct decomposition of NO . . . . .	10
1.3.2 Lean NO <sub>x</sub> trap . . . . .	11
1.3.3 Plasma-assisted abatement . . . . .	14
1.3.4 Selective catalytic reduction . . . . .	14
1.4 Typical diesel emission control system . . . . .	18
1.5 SCR on Filter (SCRoF) . . . . .	19
1.6 Motivation . . . . .	20
<b>2 Experimental section</b>	<b>22</b>
2.1 Catalysts preparation . . . . .	22
2.2 Catalysts characterization . . . . .	23
2.2.1 N <sub>2</sub> physisorption . . . . .	24

---

2.2.2	Field Emission Scanning Electron Microscopy (FESEM) . . . . .	27
2.2.3	X-ray Powder Diffraction (XRD) . . . . .	28
2.2.4	X-ray Photoelectron Spectroscopy (XPS) analysis . . . . .	29
2.2.5	H <sub>2</sub> -TPR (Temperature Programmed Reduction) analysis . . . . .	29
2.2.6	Temperature Programmed Desorption (NH <sub>3</sub> -TPD) . . . . .	31
2.3	Catalytic activity measurements . . . . .	32
<b>3</b>	<b>Results and discussion</b>	<b>36</b>
3.1	Catalyst characterization . . . . .	36
3.1.1	N <sub>2</sub> physisorption . . . . .	36
3.1.2	FESEM . . . . .	38
3.1.3	XRD . . . . .	39
3.1.4	X-ray Photoelectron Spectroscopy (XPS) analysis . . . . .	40
3.1.5	H <sub>2</sub> -TPR analysis . . . . .	43
3.1.6	Temperature Programmed Desorption (NH <sub>3</sub> -TPD) . . . . .	45
3.2	Catalytic activity measurements . . . . .	46
3.2.1	NO oxidation . . . . .	46
3.2.2	NH <sub>3</sub> oxidation . . . . .	49
3.2.3	Standard SCR . . . . .	52
3.2.4	Standard SCR in soot presence . . . . .	57
3.2.5	Soot oxidation . . . . .	64
<b>4</b>	<b>Conclusions</b>	<b>69</b>
	<b>References</b>	<b>71</b>

# List of Figures

1.1	Air pollutants sources . . . . .	2
1.2	Composition of diesel exhaust gas . . . . .	3
1.3	Comparisons between NO <sub>x</sub> standards and real-world emissions . . . . .	5
1.4	Diesel Particulate Filter . . . . .	6
1.5	CRT operation . . . . .	8
1.6	LNT operating principle and variations of NO <sub>x</sub> concentration . . . . .	12
1.7	LNT/CDPF system . . . . .	13
1.8	Scheme of plasma-assisted catalysts . . . . .	14
1.9	SCR system . . . . .	15
1.10	Operating temperature windows for different SCR catalysts . . . . .	17
1.11	Typical diesel emission control system . . . . .	18
1.12	Diesel oxidation catalyst . . . . .	19
1.13	SCRoF operating principle . . . . .	20
2.1	Synthesized catalysts, (a) MnO <sub>x</sub> , (b) Ce <sub>0.25</sub> Mn <sub>0.75</sub> O <sub>x</sub> , (c) Ce <sub>0.5</sub> Mn <sub>0.5</sub> O <sub>x</sub> . . . . .	23
2.2	Isotherms IUPAC classification . . . . .	24
2.3	Pore shapes according to the hysteresis loop . . . . .	25
2.4	BET instrument . . . . .	27
2.5	FESEM instrument . . . . .	28
2.6	TPR instrument . . . . .	31
2.7	laboratory installation for the experiments . . . . .	32
2.8	Laboratory Equipment . . . . .	34
3.1	Adsorption-desorption isotherms . . . . .	37

3.2	FESEM micrographs . . . . .	39
3.3	XRD patterns, of samples (a) $\text{MnO}_x$ (b) $\text{Ce}_{0.25}\text{Mn}_{0.75}\text{O}_x$ and (c) $\text{Ce}_{0.5}\text{Mn}_{0.5}\text{O}_x$ .	40
3.4	XP Spectra in the Mn 2p and O 1s core level regions, of samples (a) $\text{Ce}_{0.25}\text{Mn}_{0.75}\text{O}_x$ , (b) $\text{Ce}_{0.5}\text{Mn}_{0.5}\text{O}_x$ and (c) $\text{MnO}_x$ . . . . .	42
3.5	XP Spectra in the Ce 3d core level region, of samples (a) $\text{Ce}_{0.25}\text{Mn}_{0.75}\text{O}_x$ , (b) $\text{Ce}_{0.5}\text{Mn}_{0.5}\text{O}_x$ . . . . .	43
3.6	TPR curves of samples $\text{MnO}_x$ (a), $\text{Ce}_{0.25}\text{Mn}_{0.75}\text{O}_x$ (b) and $\text{Ce}_{0.5}\text{Mn}_{0.5}\text{O}_x$ (c). .	44
3.7	$\text{NH}_3$ -TPD curves . . . . .	45
3.8	NO oxidation $\text{MnO}_x$ . . . . .	47
3.9	NO oxidation $\text{Ce}_{0.25}\text{Mn}_{0.75}\text{O}_x$ . . . . .	47
3.10	NO oxidation $\text{Ce}_{0.5}\text{Mn}_{0.5}\text{O}_x$ . . . . .	48
3.11	NO conversion . . . . .	48
3.12	$\text{NH}_3$ Oxidation . . . . .	50
3.13	$\text{NH}_3$ conversion . . . . .	51
3.14	Standard SCR . . . . .	54
3.15	Standard SCR: $\text{NH}_3$ and $\text{NO}_x$ conversion, $\text{N}_2$ selectivity . . . . .	56
3.16	Standard SCR + soot: $\text{NH}_3$ and $\text{NO}_x$ conversion, $\text{N}_2$ selectivity . . . . .	58
3.17	Standard SCR $\text{MnO}_x$ catalyst . . . . .	59
3.18	Standard SCR $\text{MnO}_x$ catalyst with and without soot: (a) $\text{N}_2$ selectivity, (b) $\text{NH}_3$ and $\text{NO}_x$ conversion. . . . .	60
3.19	Standard SCR $\text{Ce}_{0.25}\text{Mn}_{0.75}\text{O}_x$ catalyst . . . . .	61
3.20	Standard SCR $\text{Ce}_{0.25}\text{Mn}_{0.75}\text{O}_x$ catalyst with and without soot: (a) $\text{N}_2$ selectivity, (b) $\text{NH}_3$ and $\text{NO}_x$ conversion. . . . .	61
3.21	Standard SCR $\text{Ce}_{0.5}\text{Mn}_{0.5}\text{O}_x$ catalyst . . . . .	62
3.22	Standard SCR $\text{Ce}_{0.5}\text{Mn}_{0.5}\text{O}_x$ catalyst with and without soot: (a) $\text{N}_2$ selectivity, (b) $\text{NH}_3$ and $\text{NO}_x$ conversion. . . . .	63
3.23	Soot Oxidation . . . . .	64
3.24	Soot conversion . . . . .	65
3.25	Soot reaction rate . . . . .	67

# List of Tables

1	List of Abbreviations . . . . .	iv
2	List of symbols . . . . .	v
3	Composizione del gas di ingresso nei diversi test. . . . .	ix
1.1	Euro standards for passenger cars, $\text{g km}^{-1}$ . . . . .	4
2.1	Gas composition during the experiments . . . . .	33
3.1	Specific surface area, pore diameter and pore volume . . . . .	38
3.2	Binding Energy values (BE) and chemical composition (% at) . . . . .	41
3.3	Quantity of $\text{H}_2$ consumed . . . . .	44
3.4	Amounts of $\text{NH}_3$ adsorbed . . . . .	46

# Chapter 1

## Introduction

### 1.1 Air pollution

Air pollution is a very important environmental and social issue and due to its complexity represents a challenge in terms of management and mitigation of noxious pollutants. Air pollutants can be emitted from both anthropogenic and natural sources; they can be emitted directly to the atmosphere (primary pollutants) or can be formed in the atmosphere from other precursor gases (secondary pollutants). Some of the current regulated pollutants are nitrogen oxides, sulfur oxides, particulate matter (PM), CO and volatile organic compounds (VOC). These compounds have a lot of negative effects on health, ecosystems, the built environment and the climate. Besides, because they may be transported or formed over long distances, they may even affect large areas. [1]

PM is emitted directly to the atmosphere (primary PM) but can also be formed (secondary PM). The gases  $\text{NH}_3$ ,  $\text{SO}_2$  and  $\text{NO}_x$  react in the atmosphere to form ammonium ( $\text{NH}_4^+$ ), sulphate ( $\text{SO}_4^{2-}$ ) and nitrate ( $\text{NO}_3^-$ ) compounds, which can form new particles in the air or condense onto the pre-existing ones and form what it is called the secondary inorganic aerosols. On the other hand, primary PM originates from natural and anthropogenic sources. Natural sources include sea salt, naturally suspended dust, pollen and volcanic ash. In the anthropogenic sources fuel combustion in thermal power generation, waste incineration, domestic heating for households and fuel combustion for vehicles are included.[1]

Sulfur dioxide ( $\text{SO}_2$ ) and CO are both products of combustion.  $\text{SO}_2$  is emitted from the combustion of fuels containing sulfur. The main anthropogenic emissions derive from stationary power generation, industry and commercial, institutional and household fuel combustion. The biggest natural source of  $\text{SO}_2$  are volcanoes. Meanwhile, CO is emitted as a result of the incomplete combustion of fossil fuels and biofuels.[1]

The major source of  $\text{NO}_x$  are combustion processes. The transport sector is responsible for 50% of the global anthropogenic emissions, the reminder originates from stationary sources,

such as power plants, internal combustion engines, industrial boilers, waste incinerators, process heaters and gas turbines[2]. They can be produced from natural sources as well, such as nitrogen fixation by lightning, volcanic activity, oxidation of ammonia in the troposphere, inflow of NO from the stratosphere and ammonia oxidation from proteins decomposition [3]. Most NO<sub>2</sub> is formed in situ by the oxidation NO, which represents the majority of NO<sub>x</sub> emissions.

As it could be appreciated in the sources of the different pollutants, the main sectors that contribute to emissions of air pollutants are transport, commercial, institutional and households sector, industry, energy, agriculture and waste [1]. As it is illustrated in Fig. 1.1, energy is by far the largest source of air pollution from human activity. They are originated from the combustion of fossil fuels and bioenergy, also from coal extraction and other forms of mining and industrial activities, the processing of coal, oil refining natural gas transportation, as well as non-exhaust emissions from the transports sector, such as tyre and brake wear, and road abrasion. The emissions of key pollutants as SO<sub>2</sub>, NO<sub>x</sub> and primary PM are almost completely attributable to energy production and use.[4]

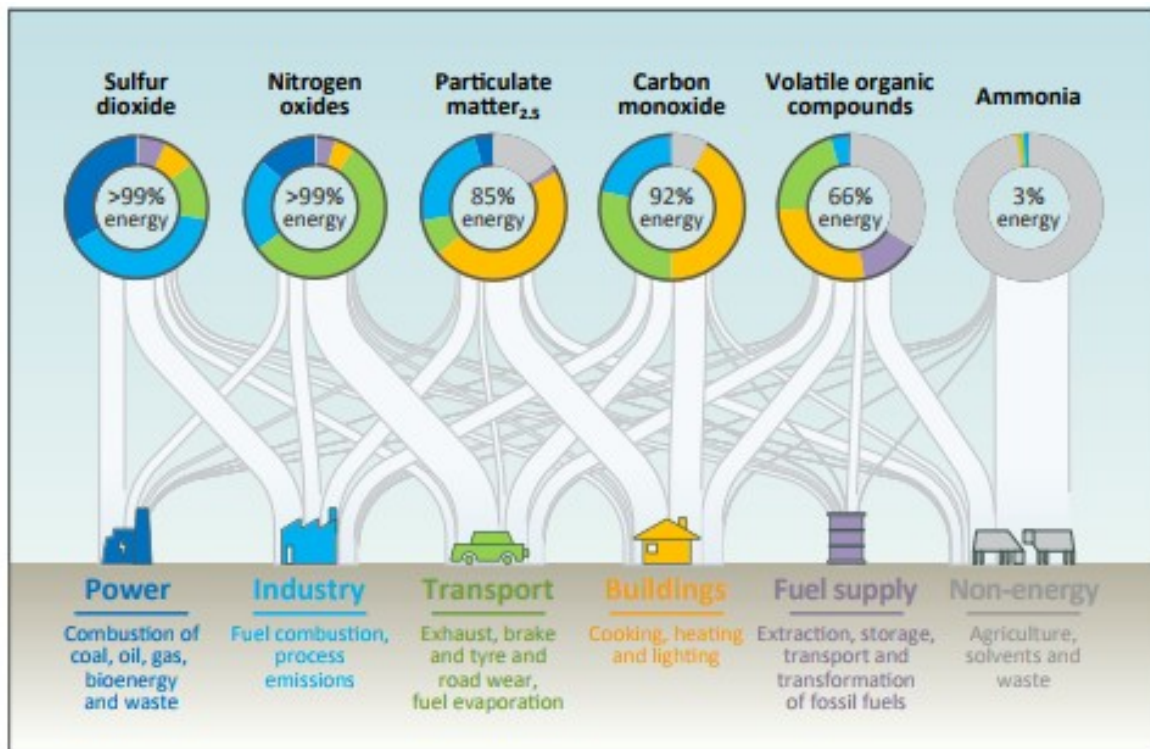


Fig. 1.1 Air pollutants sources

In particular, air pollution from mobile sources, such as cars and trucks, contributes to a great extent to air quality since they add considerably to the levels of greenhouse gases in the atmosphere, causing health risks in rural, urban and industrialized areas in both developed and developing countries. About 60 million are produced every year, 700 million cars are used worldwide and it is expected that the vehicle population increases to almost 1300 million by 2030 [5, 6].

In the automotive field, Diesel engines are extensively used for high duty vehicles and more recently they have become popular for light duty vehicles and passenger cars as well. This type of engines has an extensive usage in comparison to gasoline engines due to its low-operating cost, energy efficiency, high durability and reliability. Diesel engines also provides a better fuel economy and produce lower CO<sub>2</sub> emissions. They are used for a wide range of applications such as vehicles, locomotives, ships, working machines, cranes and power generators. However, they are associated with the emission of a considerable amount of pollutants in the exhaust gases, including NO<sub>x</sub>, particulate matter (PM), CO and hydrocarbons(HC) [7, 8].

In the Fig. 1.2 an approximate composition of diesel exhaust gas is represented. The pollutants represent less than 1% of the diesel exhaust gas, being NO<sub>x</sub> the one present in the highest proportion (more than 50%) followed by PM. Because in the diesel engine the combustion takes place with an excess of air, the concentration of CO and HC is minimal. Besides, it is possible to find SO<sub>2</sub> in the exhaust gases depending on the specifications and quality of the fuel.[5]

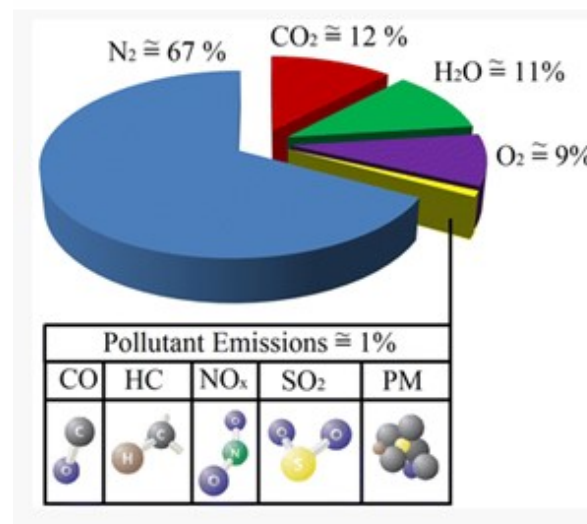


Fig. 1.2 Composition of diesel exhaust gas

The adverse effects of diesel emissions on health and environment have forced governments to establish legislations to control these emissions. Europe has developed Euro standards to limit the maximum amount emitted by both diesel and petrol engines, they were introduced in 1992 and have been modified since then. [5, 9]

Table 1.1 shows the most important regulations defined for passenger cars with diesel engines, from Euro 1 (1992) until the most recent Euro 6 (2014). The limits are defined in g/km. Previous regulations limited HC and NO<sub>x</sub> together, later individual limits were established.

Table 1.1 Euro standards for passenger cars, g km<sup>-1</sup>

<b>Euro Standard</b>	<b>Date</b>	<b>CO</b>	<b>HC</b>	<b>HC + NO<sub>x</sub></b>	<b>NO<sub>x</sub></b>	<b>PM</b>
Euro 1	07.1992	2.72	-	0.97	-	0.14
Euro 2	01.1996	1.00	-	0.70	-	0.08
Euro 3	01.2000	0.64	-	0.56	0.50	0.05
Euro 4	01.2005	0.50	-	0.30	0.25	0.025
Euro 5	09.2009	0.50	-	0.23	0.18	0.005
Euro 6	09.2014	0.50	-	0.17	0.08	0.005

As the regulations have become more stringent with the years, the vehicle manufactures have been forced to work on reducing pollutant emission. For the first regulations, actions such as engine modifications, electronic controlled fuel injections systems and improvements in the fuel properties were enough to achieve the limits, but at some point, it was necessary to use aftertreatment emission control systems to meet the standards. [5]

For certain pollutants, such as NO<sub>x</sub> and CO<sub>2</sub>, there is a wide difference between official emission measurements and the average real-world driving emissions. This gap has increased in recent years, counteracting the effect of the more stringent regulations. The amount of fuel used by cars on the road, and therefore also the CO<sub>2</sub> emissions, was in 2014 40% higher than the official measurements. [1]

The differences for the NO<sub>x</sub> emissions are even higher, especially for diesel vehicles, where the average real-world emissions can be more than four times or higher than those measured in the laboratory. An evidence of this is illustrated in Fig. 1.3, where it is possible to see that real-world emission from petrol cars in the EU have decreased since 2000, according to the increasingly stringent emissions limits. In contrary, NO<sub>x</sub> emissions from diesel cars have not improved much, which means that the reductions have not been as large as planned by the legislation. Until the Euro 6 regulations, this kind of cars were allowed to emit three times as much NO<sub>x</sub> as petrol cars. [1]

The discrepancy between the real world and test-cycle emissions affects the ability of the countries to comply with the limit and target values set by the legislations. For this reason, two initiatives are planned to ensure a better consistency: changing the official test procedure to one more representative of real-world emissions and introducing a procedure for measuring the real driving emissions of vehicles on the road. Also, it is planned a a stricter approval and market surveillance of motor vehicles. [1]

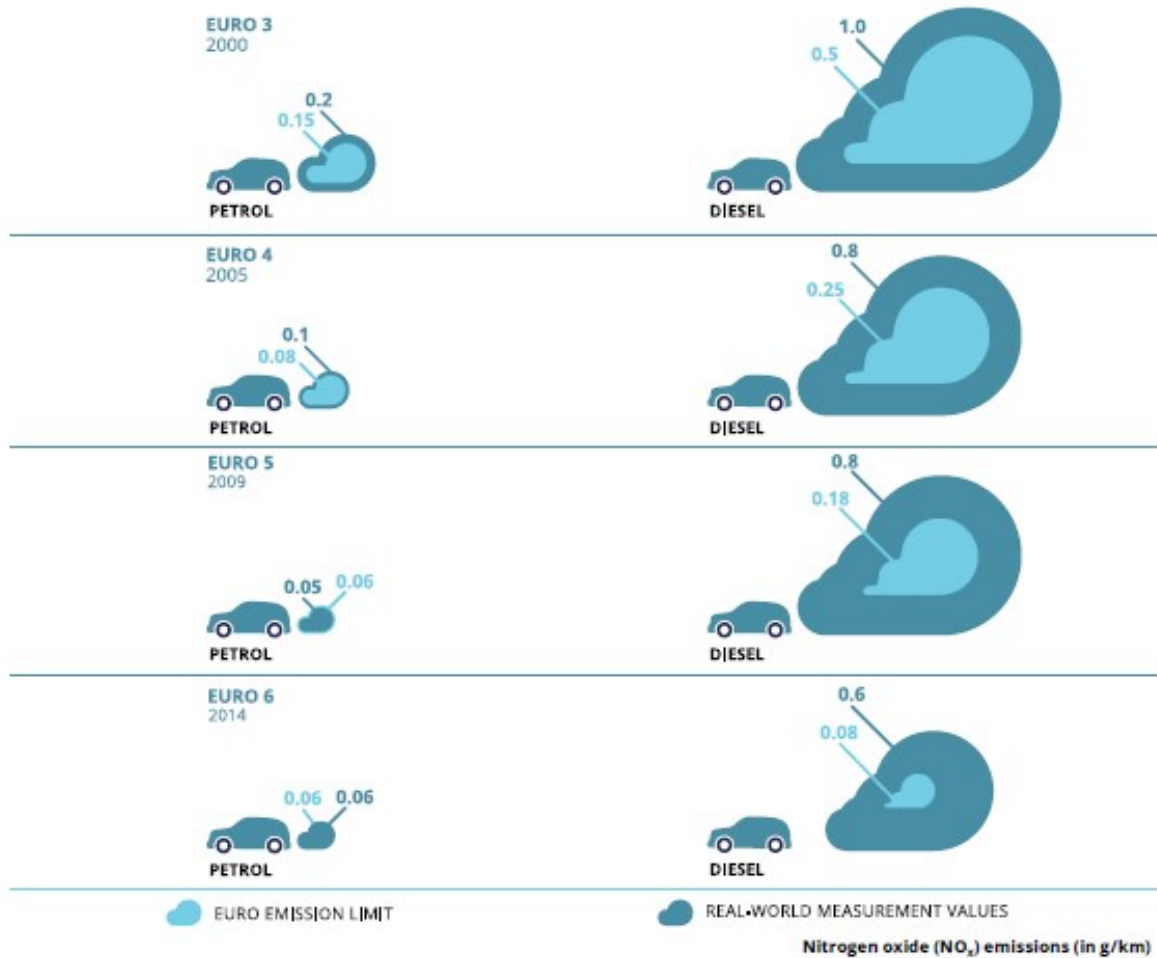


Fig. 1.3 Comparisons between NO<sub>x</sub> standards and real-world emissions

## 1.2 Soot abatement

Particulate matters are formed because of an incomplete combustion of the hydrocarbons in the fuel and lube oil. They are typically spheres with diameters of about 15-40 nm and can be divided into three main components: soot, soluble organic fraction (SOF) and inorganic fraction (IF). Soot is made of a carbon nucleus with trace amounts of inorganic material and other adsorbed compounds and constituted more than 50% of the total PM emissions. SOF consists of heavy hydrocarbons adsorbed or condensed on the soot and can come from the lubricating oil, unburned fuel and other compounds formed during combustion. [5]

Since PM has become a major constituent of air pollution and is associated with respiratory problems, cardiovascular diseases and skin cell alterations, the recent legislation has introduced more strict limits for vehicles to control the PM emissions, for example the limit established for Europe is 0.005 g/km for PM from passenger cars and light vehicles with Diesel or GDI engines since 2009. To satisfy these standards different after-treatment technologies have been

developed, among them the trap of particulates from exhaust gases by Diesel particulate filters (DPFs). [10, 11]

### 1.2.1 Diesel Particulate Filter

DPFs are usually made of cordierite ( $2\text{MgO}\cdot 2\text{Al}_2\text{O}_3\cdot 5\text{SiO}_2$ ) or silicon carbide (SiC) honeycomb structure monoliths with the channels blocked at alternate ends where soot is separated by mechanical filtration from the exhaust gases. This filter consists of a series of parallel mostly square channels. The thickness of the channel walls is generally 300-400  $\mu\text{m}$  and its size is specified by the cell density (typical value: 100-300 cpsi) [5]. Filtration efficiency varies in the range 70-95%. Higher values, exceeding 95% are reported in literature for the solid particulate fraction, which includes elemental carbon and metal ash. Nevertheless, much lower efficiencies values have been reported for the soluble organic fraction (SOF) of the particulate [12]. In Fig. 1.4 there is a representation of a DPF and its operating principle [13].

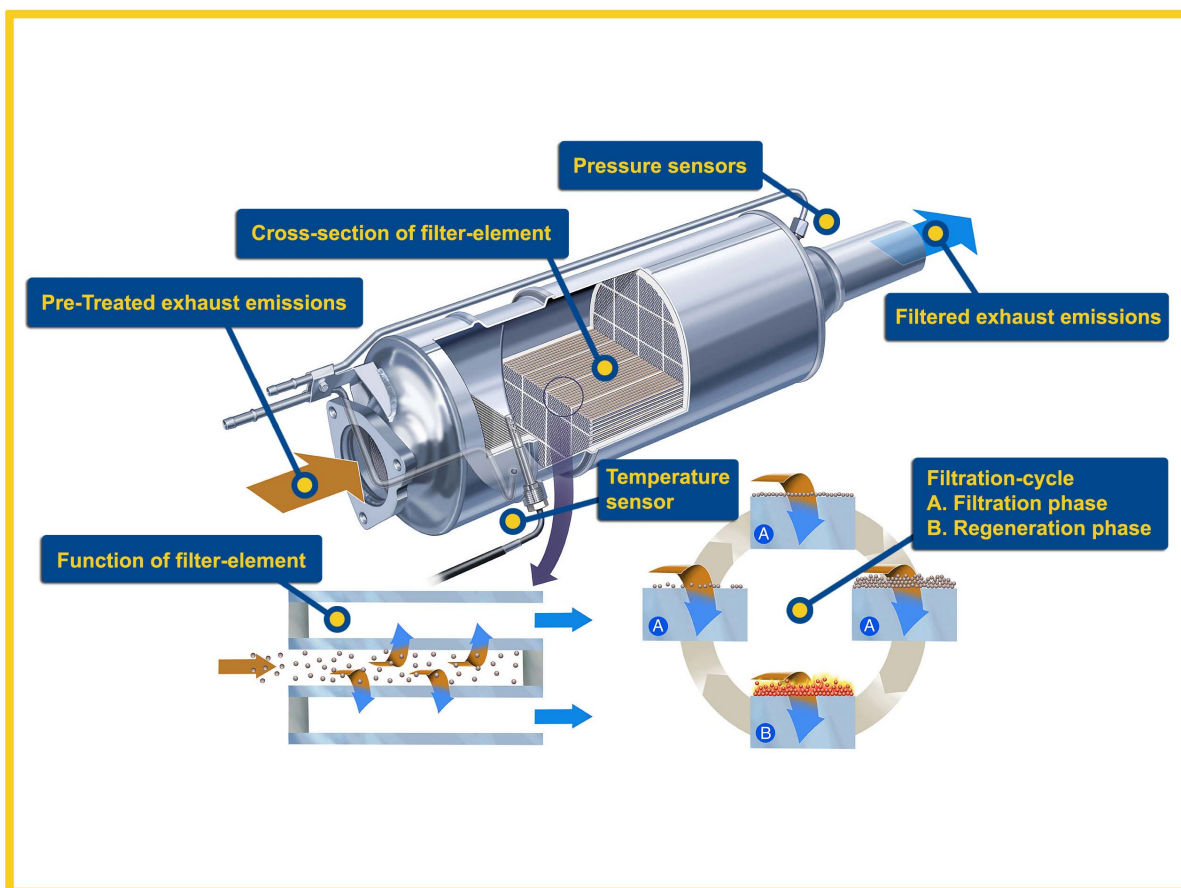


Fig. 1.4 Diesel Particulate Filter

The filter walls are designed with large surface areas to operate with an acceptable pressure drop. However, as the soot particles accumulate in the filter a critical pressure drop is reached. At this point a regeneration step allows to remove the soot deposits from the filter otherwise

the backpressure can decrease the engine efficiency [5, 7]. The frequency of regeneration is determined by factors such as the duty cycle of the engine, PM emission rate and filter technology. There are two types of regeneration processes: the active and passive regeneration. [5, 14]

### 1.2.1.1 Active regeneration

In the active regeneration, the trapped soot is removed periodically through a controlled oxidation with  $O_2$  at  $550^\circ C$  or higher temperatures. Fuel post-injections or heat are used to raise the DPF temperature. The heat is provided by outside sources, such as an electric heater or a flame-based burner. This process takes place once the soot loading in the filter reaches a certain limit (around 45%) indicated by pressure drop across the filter. Because a large amount of energy needs to be supplied and the temperatures reached in the filter could be as high as its melting point, this regeneration technique is not widely used. [5, 14]

The use of microwave heating allows to have a significantly lower soot ignition temperature due to the instantaneous penetration of microwaves into the filter body and the selective adsorption of microwaves by the soot layer. For this reason, it is considered promising and suitable for soot combustion, especially in SiC DPFs. [15]

The PSA system by Peugeot-Citr en Soci t  d'Automobiles developed a system that relies on an active regeneration strategy, which key component is a Ce-fuel additive that leads to the formation of  $CeO_2$  particles well embedded into the particulate structure, maximizing the soot-catalyst contact. In the presence of high-pressure drops, the fuel injection increases the exhaust gas temperature, initiating the burning of the soot and regenerating in this way the filter. The presence of  $CeO_2$  lowers the ignition temperature with the benefit of post-injected fuel savings. Besides, since the sulfur content in the fuel has fell in the last decade, the residual Cerium ash after the regeneration could be an active soot oxidation catalyst, in the form of Cerium oxide, Cerium nitrate and Cerium carbonate instead of Cerium sulfate, which is toxic lungs and mucus membranes. [11]

### 1.2.1.2 Passive regeneration

Passive regeneration occurs when the exhaust gas temperatures are high enough to initiate the combustion of the soot accumulated in the filter, without the addition of fuel or the use of heat [14]. Since this material burns at temperatures above  $600^\circ C$  while diesel exhaust gases temperature most of the time is in the  $200^\circ C$ - $500^\circ C$  range, it is necessary to use a catalyst to promote the soot combustion. Pt is the most widely used catalyst for its high activity and durability, but due to its high cost many researchers are looking for substitute materials [5, 10].

Ceria-based catalysts are one of the most promising candidates for DPFs due to their excellent redox properties and the minor costs compared with the noble metals. Besides, the activity and the stability of Ceria can be improved by the addition of dopants or the addition of different

elements to the crystal lattice. The thermal stability is one of the most important factors since the temperature inside the filter can increase even until 1000 °C due to the exothermicity of the soot combustion reaction. [11]

MnO<sub>x</sub>-CeO<sub>2</sub> oxides can exhibit an excellent catalytic activity for soot oxidation in O<sub>2</sub> and NO<sub>2</sub> assisted conditions, this is attributed to the synergetic effect between the MnO<sub>x</sub> and the CeO<sub>2</sub> and the strong redox ability obtained because the incorporation of Mn<sup>x+</sup> into CeO<sub>2</sub> promote the oxygen mobility and storage capacity, improving the availability of surface active oxygen [16]. It has been also reported that the Mn based catalysts are efficient in the oxidation of soot, CO, NO and some hydrocarbons. [7]

In the temperature range between 200°C and 450°C, the presence of NO<sub>2</sub> promotes the continuous oxidation of the deposited soot. This is the operating principle of the continuously regenerating trap (CRT), which uses NO<sub>2</sub> to oxidize soot within relatively low temperatures over a DPF [5]. In Fig. 1.5 there is a representation of how the CRT works. First, the NO<sub>2</sub> concentration in the exhaust stream is increased from 5-15% to 50% of total NO<sub>x</sub> by the diesel oxidation catalyst (DOC). Then, the NO<sub>2</sub> amount is enough to consume the soot along with the participation of O<sub>2</sub> [17].

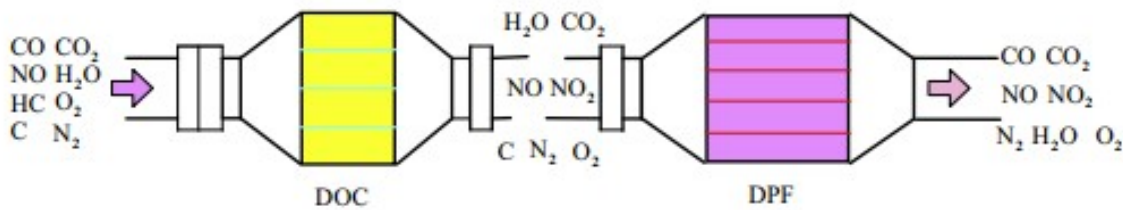


Fig. 1.5 CRT operation

In diesel passenger cars, because the NO<sub>x</sub>/soot ratio is insufficient an additional active regeneration is required. Thereby, common strategies involve the post-injection of fuel producing the emission of large amounts of hydrocarbons and CO, that are oxidized in the DOC increasing the upstream temperature of the filter, initiating soot combustion. [18]

Alternatively, it is possible to use catalyzed DPFs (CDPF) where the catalyst used in the DOC is placed on the filter. In this system, there is not any aftertreatment systems upstream the DPF, all the reactions occur in the CDPF and the oxidation temperature of soot can also be decreased. The efficiency of this system is related to the tight proximity of soot and catalyst, while under practical conditions the loose contact is generally predominant. [5, 7]

### 1.2.1.3 Soot oxidation catalyst performance

The catalytic performance of the soot oxidation catalyst can be affected by different factors such as the contact between soot and catalyst, the reaction atmosphere and the flow rate of the reaction gas. [10, 11]

Gases like NO, NO<sub>2</sub>, SO<sub>2</sub>, CO<sub>2</sub>, CO, HCs, H<sub>2</sub>O and O<sub>2</sub> could be present in the engine exhaust, among them oxygen is considered as the principal gas to oxidize diesel soot. The NO is important too, since it has a beneficial effect on the catalyst activity as it forms NO<sub>2</sub>, which is a strong oxidant and can react with soot efficiently at about 350 °C reducing the soot oxidation temperature. As it was mentioned before, the flow rate of the reaction gas may also have some influence. A high flow rate could increase the mole of oxidizing gases per unit time and mass of the soot benefiting in this way the soot oxidation, but if there is NO present high flow rates may reduce the reaction time for the NO oxidation and hereby the quantity available of NO<sub>2</sub> leading to the presence of NO<sub>2</sub>-soot incomplete reactions. [10]

The other factor that influences the catalyst performance is the contact of the soot with the catalyst due to the nature of the reaction where the catalytic activity is related to the interaction between the two solids and the gas. In laboratory studies there are two main contact modes, loose and tight. A loose contact condition is obtained by mixing the soot with the catalyst with a spatula for 1 or 2 minutes. Some studies have shown that the contact between the catalyst and soot in a DPF is similar as the one obtained using this method. On the other hand, the tight contact condition can be accomplished in a mortar or through a ball milling to obtain an intimate contact between the soot and the catalyst. Generally, this contact mode gives a more efficient oxidation thanks to the greater contact points between soot and catalyst particles. Also, it is useful to study the intrinsic activities and stabilities without masking the results with the mass and energy transfer limitations. [10, 11]

Regarding the catalyst-soot contact mode, it is important to note that it can be influence by the particle size and the mass ratio of the soot/catalyst. Particles with small dimensions have a high surface area, which leads to a good contact with the soot [10]. Additionally, an increase in the soot/catalyst ratio beyond a certain value will result only in an increase of the oxidation temperature since there is no catalyst available to meet the soot particles. Because of this, it is not recommended to use soot/catalyst ratios above 1/5 otherwise negative effects will be observed on the catalytic activity. [11]

At laboratory scale, a catalyst screening can be carry out using temperature programmed oxidation/combustion experiments (TPO/TPC). In this kind of test, a model soot and the catalyst are loaded into a tubular quartz reactor in an atmosphere containing oxygen and then heated at a constant rate. The CO<sub>2</sub> concentration in the outlet gas is usually measured and the CO<sub>2</sub>-peak temperature is used as an index of the catalytic activity along with other parameters like the light-off temperature (temperature at which 50% conversion is reached) and the onset temperature (the temperature corresponding to 10% conversion). The catalytic activity can be determined as well by a thermogravimetric analysis, using mass spectrometer or gas chromatograph detectors.[11]

The available model soot samples and the real soot can be very different both in the micro structure and reactivity. The amount and the type of ashes can change since real soot includes into its structure the metals that diesel fuels and lubricating oil contain. Also, real soot has a variable number of adsorbed hydrocarbons (SOF) and due to the presence of this compounds

the soot combustion generally occurs at lower temperatures than those of model soot samples. The real soot properties are also influenced by the type and age of the engine or its operating conditions. [18]

The use of a model soot as a substitute of diesel soot in the catalyst activity studies is convenient because the absence of SOF in its composition allows to obtain conservative results. It is possible to get a difference of tens to hundreds of Celsius degrees between soot oxidation temperatures of real and model soot. [11]

### 1.3 NO<sub>x</sub> removal

Nitrogen oxides NO<sub>x</sub> (NO +NO<sub>2</sub>) are primary pollutants emitted directly from the combustion process. Both NO and NO<sub>2</sub> are considered toxic, but nitrogen dioxide has a level of toxicity five times greater. They can give origin to new pollutant species, such as nitric acid (HNO<sub>3</sub>) and nitrous acid (HNO<sub>2</sub>), which are responsible for acid rains. Also, by reacting with other organic compounds in the presence of sunlight can produce photochemical smog. [5, 8]

The amount of NO<sub>x</sub> produced is a function of the maximum temperature in the cylinder, oxygen concentration and residence time. Among various types of vehicles, diesel engines are the principal contributors, they are responsible for approximately 85% of the total NO<sub>x</sub> emissions from mobile sources, mainly in the form of NO. Specifically, in comparison with gasoline engines, a diesel engine need higher temperatures because they work with a compression-ignition mechanism. [5]

Among the aftertreatment technologies for the control of NO<sub>x</sub> emissions in mobile applications are: direct catalytic decomposition, lean NO<sub>x</sub> trap (LNT), selective catalytic reduction (SCR), and plasma-assisted abatement [6]. Also, a common engine management strategy to control NO<sub>x</sub> emissions is Exhaust Gas Recirculation (EGR). In this strategy a fraction of the exhaust gas is recirculated to the combustion chamber with the purpose of reduce the combustion temperature and the production of the engine-out NO<sub>x</sub>. There are different approaches, the high-pressure EGR where the exhaust gas is extracted from upstream of the turbine and the low-pressure EGR, where the exhaust gas is drawn from after the DPF instead. The two approaches can be combined. This strategy is more effective at low engine loads and there is a maximum applicable exhaust recirculation rate depending on the engine load. There is an economic limit too related to the fuel cost and the use of this strategy alone is not enough to meet the recent NO<sub>x</sub> regulations. [6, 19]

#### 1.3.1 Direct decomposition of NO

In the direct decomposition of NO, as the exhaust flows over a solid catalyst the NO is split into its elements, according to the reaction:



This reaction has received attention in the field of environmental catalyst, since it is favored below 1000°C and it is not required to use reducing agents. The principal concern is to find a material active and oxidation-resistance. With this aim many materials have been investigated including noble metals, metal oxides, perovskites and zeolites.

The catalytic activity of the metal oxides towards the NO decomposition is lower than that of noble metals, for this reason the operating temperature must be kept at high values (up to 1000°C), which can lead to catalyst sintering. However, the inhibiting effect of oxygen is lower for metal oxides than for noble metals, which can be easily oxidized and hence are not very active in the presence of oxygen. The perovskites exhibit high thermal stability and are more resistant to the presence of oxygen, but the main disadvantage is the high temperature required to achieve a high NO decompositions activity. Also, their low surface areas and pore volumes are other drawbacks. Finally, the zeolites are not the best candidates due to their low hydrothermal stability and low SO<sub>2</sub> resistance.

Due to the operating temperatures of these catalysts are usually higher than those required for the catalytic reduction of NO, the direct decomposition of NO is not very interesting to be used in aftertreatment exhaust devices. [6]

### 1.3.2 Lean NO<sub>x</sub> trap

Lean NO<sub>x</sub> traps are also known as NO<sub>x</sub> adsorber catalyst (NAC), DeNO<sub>x</sub> traps (DNT), NO<sub>x</sub> storage catalyst, NO<sub>x</sub> storage/reduction (NSR) catalysts or simply NO<sub>x</sub> traps.

In this system the NO<sub>x</sub> are adsorbed during lean engine operation. When the adsorber capacity is saturated, the system is regenerated in a period of rich engine operation during which NO<sub>x</sub> are catalytically reduced to N<sub>2</sub>. A representation of the operating principle is in Fig.1.6. [6, 9, 19]

Since the rich mode of operation is not possible in the diesel engines, it is necessary to make periodic fuel injections. The quantity of fuel and the frequency of the injections, as well as the storage capacity of the materials, are the parameters than need to be optimized to compensate the use of additional fuel required for this technology. [6]

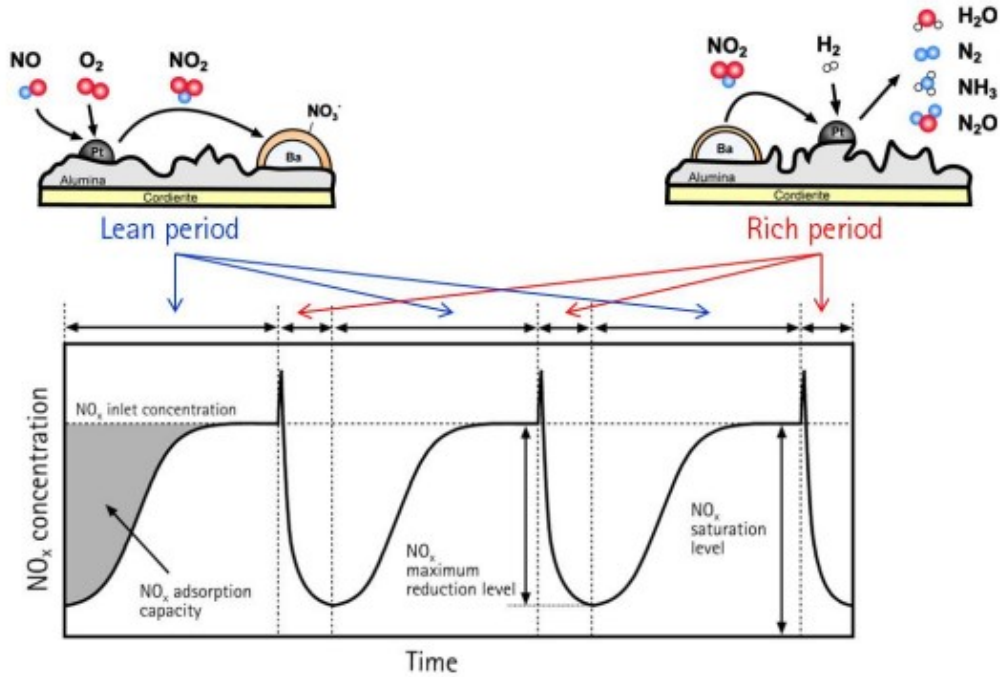
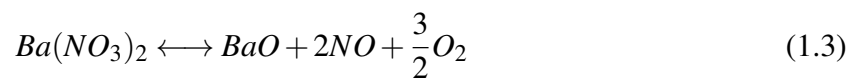


Fig. 1.6 LNT operating principle and variations of  $\text{NO}_x$  concentration

LNT combine three active components: an oxidation catalyst like platinum (Pt), an adsorbent such as barium or other oxides, and a reduction catalyst such as rhodium (Rh)[19]. Since the exhaust is rich in NO but traps are more effective toward  $\text{NO}_2$  entrapment, before  $\text{NO}_x$  adsorption there is an NO oxidation to  $\text{NO}_2$  step. This is carried out by an oxidation catalyst, that should be able to operate at the low exhaust temperatures of light-duty diesel engines, the reaction that takes place is:



The  $\text{NO}_2$  formed on the solid surface is trapped on an adsorbent ( $\text{BaO}$ ) in the form of a chemically stable nitrate ( $\text{Ba}(\text{NO}_3)_2$ ). The adsorption capacity of an  $\text{NO}_x$  trap depends on the accessibility of the  $\text{BaO}$  sites. During the regeneration process, the oxygen concentration decays to almost zero, and in this way the reductant conditions for NO abatement are achieved. First, the decompositions of the ( $\text{Ba}(\text{NO}_3)_2$ ) takes place and it is possible to recover the  $\text{BaO}$  active phase (equation 1.3). As a result, NO is released and a suitable amount of fuel has to be dosed to reduce it.



NO reduction is achieved by means of a reducing catalyst. When the engine is switched to a fuel-rich condition, HC, CO and  $\text{H}_2$  react with NO to form  $\text{N}_2$ ,  $\text{CO}_2$  and  $\text{H}_2\text{O}$ , according to equations 1.4 and 1.5.



The operating temperature of the NO<sub>x</sub> traps has a lower limit, determined by the Pt activity towards the NO oxidation and the NO<sub>x</sub> release and reduction in the regeneration step. The upper limit is related to the stability of the NO<sub>3</sub> species, which could be decomposed at high temperatures.

Additionally, the presence of parasitic reactions that lead to the formation of undesired products, such as NH<sub>3</sub>, N<sub>2</sub>O and H<sub>2</sub>S, reduces the NO<sub>x</sub> trap efficiency and makes necessary the control of secondary emissions. [6]

Some of the advantages of this technology are that it is not necessary an additional dosing reductant device, unlike for the SCR, this makes installation cost lower; also, LNT has a wide operating temperature range depending on the type of NO<sub>x</sub> adsorber material used. However, an LNT has some problems: the NO<sub>x</sub> storage capacity is limited and needs to be regenerated periodically with the addition of fuel, expensive precious metals are used as catalysts, and because NO<sub>x</sub> adsorbers also adsorb sulfur oxides, that can compete with NO<sub>2</sub> in the formation of barium salts, fuels with a very low sulfur content are required. [19, 20]

In the look for more efficient exhaust aftertreatment systems, an integration of the LNT and CDPF has been proposed as an alternative for the simultaneous reduction of NO<sub>x</sub> and PM. Some studies have revealed that LNT (2Pt2Ba5Co)/CDPF system improve the NO<sub>x</sub> performance and can improve the PM oxidation rate compared to the DPF. A scheme of the system is represented in Fig.1.7. [20]

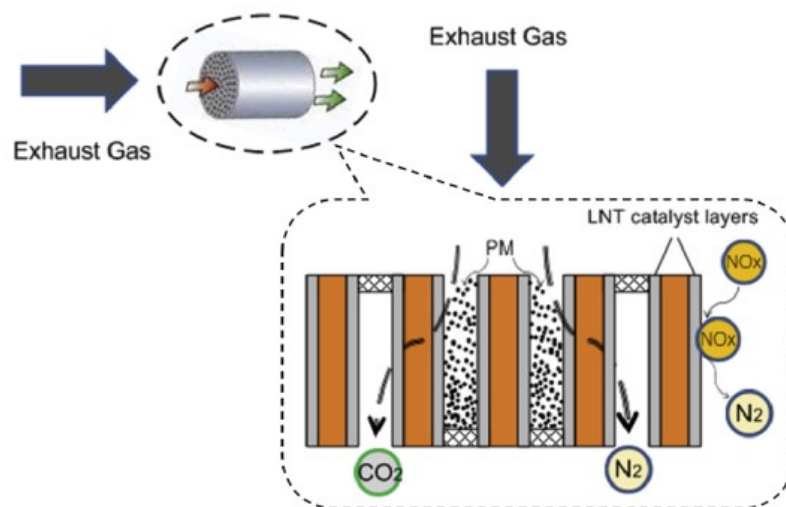


Fig. 1.7 LNT/CDPF system

### 1.3.3 Plasma-assisted abatement

Non-Thermal plasma (NTP) discharges have been investigated to reduce  $\text{NO}_x$  and PM emissions in diesel exhaust. It is generated using electrical excitation to induce thermodynamically unstable  $\text{NO}_x$  species, which decompose into  $\text{N}_2$  and  $\text{O}_2$ . In automotive applications, the reduction of  $\text{NO}_x$  is preferred but the oxidative  $\text{NO}_x$  reactions dominate the subsequent kinetics, converting the  $\text{NO}$  to  $\text{NO}_2$  and  $\text{HNO}_3$  through reactions with plasma-produced oxygen. Because other kinds of byproducts can be formed as well, the selectivity is an important drawback of this method added to the large power requirement[6].

The combination of plasma with solid catalysts, known as ‘plasma-assisted catalysts’ or ‘plasma catalysts’, has been suggested for  $\text{NO}_x$  reduction. The reducing capability of some catalysts is considerably enhanced when  $\text{NO}_x$  is present as  $\text{NO}_2$ . In this way, the NTP technology may significantly improve catalyst selectivity and removal efficiency. Besides, the presence of water vapor and oxygen promotes the  $\text{NO}$  removal rate, because of synergistic phenomena on the catalyst surface. In Fig. 1.8 it is represented a scheme of this system[6].

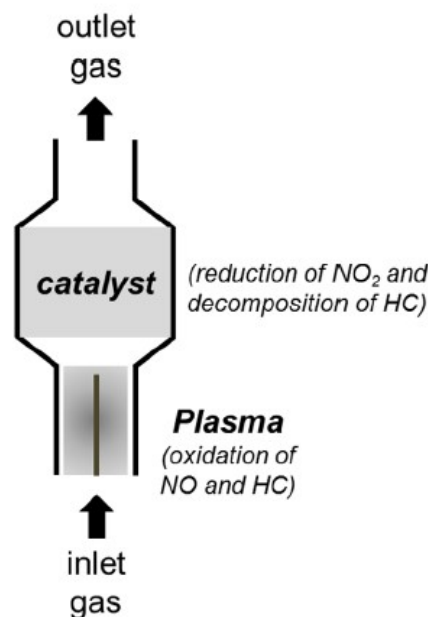


Fig. 1.8 Scheme of plasma-assisted catalysts

### 1.3.4 Selective catalytic reduction

In the SCR (Fig. 1.9) a catalyst reduces  $\text{NO}_x$  to  $\text{N}_2$  and water in the presence of ammonia. The singularity of this reaction with  $\text{NH}_3$  is that it can occur in presence of  $\text{O}_2$  in excess, and that is the reason why this technology has received a lot of attention for diesel engine vehicles [5, 20].

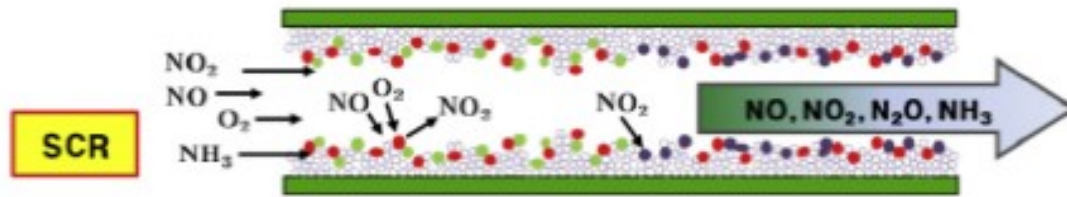
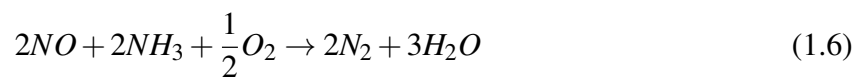
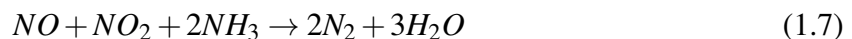


Fig. 1.9 SCR system

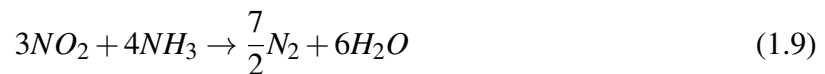
NH<sub>3</sub>-SCR occurs via three types of reaction paths depending on the NO<sub>2</sub> fraction present. The so-called standard SCR is described by equation 1.6:



When NO<sub>2</sub> is contained in the feed, an equimolar NO-NO<sub>2</sub> reaction (fast SCR) takes place at considerably higher rate than the standard SCR:

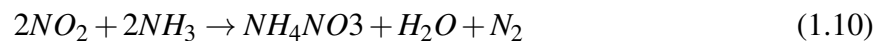


If NO<sub>2</sub> is present in a higher quantity than NO (NO<sub>2</sub>/NO > 1), the NO<sub>2</sub> reacts also via alternative NO<sub>2</sub> SCR routes:



The NO<sub>2</sub> SCR reactions are slower than the fast SCR reaction (equation 1.7) above 200°C [21].

These reactions are inhibited by water, which can be present in the exhaust gases. Also, particular temperature conditions (100°C-200°C) could lead to the formation of NH<sub>4</sub>NO<sub>3</sub>, which is explosive and deposits in the cavities of the catalytic material, causing its deactivation. An equimolar consumption of ammonia and NO<sub>2</sub> at this temperature range indicates the formation of NH<sub>4</sub>NO<sub>3</sub>, according to the reaction[6, 8]:



Due to the health and practical problems associated with ammonia (NH<sub>3</sub> is a toxic gas that has to be stored under pressure) it is provided from an aqueous solution of urea, obtained by mixing 33% (mass) urea and 67% (mass) of pure water. The solution of urea is injected into the exhaust gases, where as a result of the water vaporization, the solid particles of urea begin to melt and thermolysis takes place, as described by equation 1.11:



Successively, the isocyanic acid (HNCO) reacts with water in a hydrolysis reaction (equation 1.12), where more NH<sub>3</sub> is produced.



The whole decomposition process takes places at about 200°C and can be described by the global reaction (equation 1.13):



Thermolysis and hydrolysis reactions are faster than SCR reactions and their efficiency depends in great measure on exhaust gas temperature [5].

Urea has been selected as the best ammonia source because of its low toxicity, safety, availability and low cost. However, some part of the urea solutions has freezing temperatures (-11°C) that are not acceptable for winter conditions in cold climates. So, it has been proposed the use of ammonium formate (HCO<sub>2</sub>NH<sub>4</sub>) for SCR applications in cold climates, though it has a lower NH<sub>3</sub> content. Another alternative is to use solid urea rather than aqueous solutions [6].

The ammonia (or urea) can be introduced either in the exhausted gases or in a flux of the reductant gas. NO<sub>x</sub> conversion efficiencies up to 98% can be reached using this technology.

There are some limitations related to the catalyst, at low-load driving conditions there is small NO<sub>x</sub> conversion when a vanadium catalyst is used, also catalysts as cooper-zeolite are sensitive to fuel sulfur content. It is required process a precise control of the ammonia injection rate, due to the fact that an insufficient injection may result in low NO<sub>x</sub> conversions, while an elevate injection rate results in an ammonia splip, which can cause the release of ammonia to the atmosphere. Other limitation is the exhaust temperatures, the decomposition of urea into ammonia requires a temperature of at least 180°C but for light-duty vehicles the exhaust temperature during urban driving conditions is usually bellow 200 °C. Besides, for the urea is required an additional distribution infrastructure, injections systems, on board-storage and heating [3, 19]. Although the limitations mentioned above for the SCR system, it is one of the most promising technologies for controlling NO<sub>x</sub> emissions with acceptable efficiency over a wide range of temperatures [22].

The main aspect of the SCR technology is the catalyst. The first SCR technology developed was based on a Pt-containing catalyst, but NO<sub>x</sub> reduction over the Pt surface is only effective until 250°C (Fig. 1.10). Poor selectivity towards N<sub>2</sub> is observed because at temperatures between 225°C and 250°C the oxidation of NH<sub>3</sub> to NO and H<sub>2</sub>O becomes dominant. Also, Pt catalyzes the reduction of NO<sub>x</sub> to N<sub>2</sub>O, a powerful greenhouse gas. Pt has the benefit of have a good SO<sub>2</sub> resistance and possesses good thermal stability, but it may favor the formation of SO<sub>3</sub> [6].

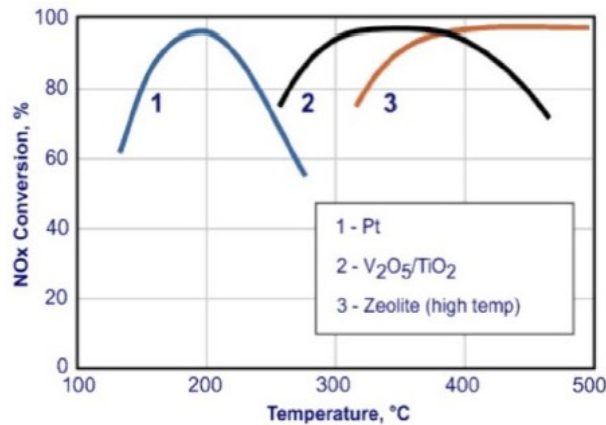


Fig. 1.10 Operating temperature windows for different SCR catalysts

Vanadium oxide catalysts have a good performance in a wider and upper temperature range, from 260°C up to 450°C. V<sub>2</sub>O<sub>5</sub>/WO<sub>3</sub> and V<sub>2</sub>O<sub>5</sub>/MoO<sub>3</sub> are the two of commercial catalysts that have been widely applied in both stationary and mobile areas. These catalysts show excellent performances in the 340°C – 400°C range but have several disadvantages, such as toxicity, high activity for oxidizing SO<sub>2</sub> and a limited reaction temperature range [23].

Zeolitic materials have a temperature range of application between 300°C and 450°C. For light duty diesel applications, the catalyst consists of Cu or Fe and zeolite, as Fe-beta and Cu-chabazite. The last one exhibits an excellent low temperature activity, a broad temperature window of activity and stability at high temperatures [6, 24].

In the last years, manganese oxide-based catalyst has been studied because of they are versatile, eco-compatible, contain diverse labile oxygen atoms and are considerably active in low temperature SCR [15]. Also, a MnO<sub>x</sub>-CeO<sub>x</sub> catalyst has been studied due to its non-toxicity and outstanding activity between 100°C-200°C [23].

As an alternative to the use of ammonia, it is possible to employ hydrocarbons as reductant agents, in the HC-SCR process. Also known as DeNO<sub>x</sub> or lean-NO<sub>x</sub> process. In this approach, the hydrocarbons can be oxidized by the oxygen present in the NO<sub>x</sub>, according to the reaction:



There are other paths involved in the NO reduction too, that lead to the formation of undesired products as N<sub>2</sub>O. Another important thing to consider is that because the HC-SCR reaction proceeds competitively with the combustion reaction of hydrocarbons, the selectivity to N<sub>2</sub> is the parameter that determines how feasible is this process. Also, since in order to reach a 80% NO<sub>x</sub> conversion it is necessary to have a certain excess of hydrocarbons and that surplus is not usually present in diesel exhaust gases, hydrocarbons or diesel fuel have to be added to the diesel exhaust gases. There are two main ways of HC enrichment: low or high pressure injection of diesel fuel ahead the catalyst ('active DeNO<sub>x</sub>') and utilization of unburned HC directly from the engine exhaust gas ('passive DeNO<sub>x</sub>') [6].

In diesel engines, the primary font of HC is diesel fuel, but it is possible to inject other HCs such as ethanol, acetone and propanol, into the exhaust stream to help in the reduction of  $\text{NO}_x$ . Regarding the catalyst,  $\text{Ag-Al}_2\text{O}_3$  is the most promising catalyst for this application [5].

It is possible to use the lean  $\text{NO}_x$  trap and the SCR together by placing a SCR unit is downstream of the LNT, this allows higher  $\text{NO}_x$  conversion efficiencies but the costs and the complexity are more elevated [19].

## 1.4 Typical diesel emission control system

In Fig. 1.11 is schematized the disposition of the components in a classical exhaust-gas aftertreatment system for a diesel engine. The first element is the diesel oxidation catalyst (DOC), followed by the DPF and the SCR, discussed before. In addition to these, other main components of the system are the urea delivery system, that includes the storage tank (DEF tank) and some sensors, the heated delivery line, the pump, the dosing module (injector and mixer) and the control system [25].

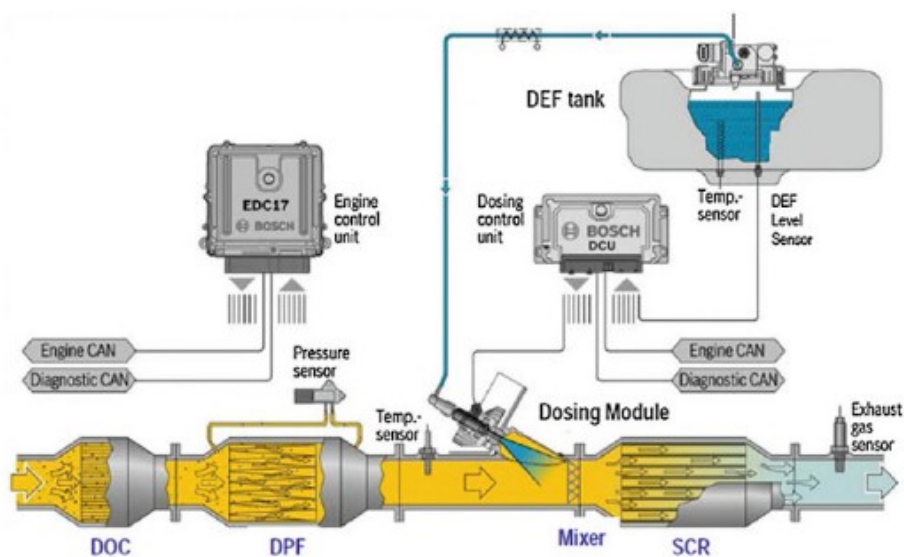


Fig. 1.11 Typical diesel emission control system

The DOC has as a main function oxidize hydrocarbons and carbon monoxide present in the exhaust gas to carbon dioxide and water. The heat generated by this reaction can be used to raise the exhaust- gas temperature downstream of the DOC, this temperature increase favors the DPF regeneration. A representation of this is showed in Fig. 1.12 [5].

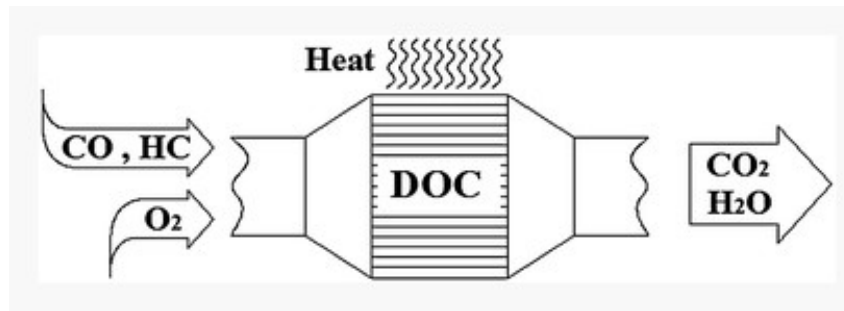


Fig. 1.12 Diesel oxidation catalyst

Another role of the DOC is to oxidize NO to NO<sub>2</sub>, which can be used to continuously oxidize the soot retained on the DPF and for increase the SCR efficiency by enhancing the fast SCR reactions, specially at low temperatures [25].

DOC consists of a monolith honeycomb substrate coated with precious metal particles of Pt and Pd supported on high surface inorganic oxides such as aluminum oxide (Al<sub>2</sub>O<sub>3</sub>), cerium oxide (CeO<sub>2</sub>) and zirconium oxide (ZrO<sub>2</sub>) [24, 25].

Urea injection quality and mixing and complex and represent significant parameters on conversion efficiency. Some studies have shown that the urea injection can affect conversion efficiency up to 10% [5]. Additionally, the molar ratio of ammonia to NO<sub>x</sub> is set below one (sub-stoichiometric conditions) to minimize ammonia slip. Typical SCR process operates with an oxidation catalyst, such as V<sub>2</sub>O<sub>5</sub>-WO<sub>3</sub>/TiO<sub>2</sub>, downstream from the SCR to prevent the unreacted ammonia from leaving the reactor. This oxidation catalyst could also favor the oxidation of CO and HC, if they are present [6].

## 1.5 SCR on Filter (SCRoF)

As it could be seen before, the removal of NO<sub>x</sub> and particulate matter for diesel exhaust is performed by two separate devices, but the increasing complexity and costs of the catalytic systems required to meet the strict emission standards has pointed out the necessity decrease the number of aftertreatment components. Another concern is that with the efforts to improve the thermal efficiency of diesel engines, due to the lower exhaust temperatures expected it is going to be necessary to move aftertreatment component as the SCR closer to the engine to maintain their performance level. Based on the above, a possible approach is an integration of the diesel particulate filter and the SCR system in a single component called SCR on Filter (SCRoF) [26]

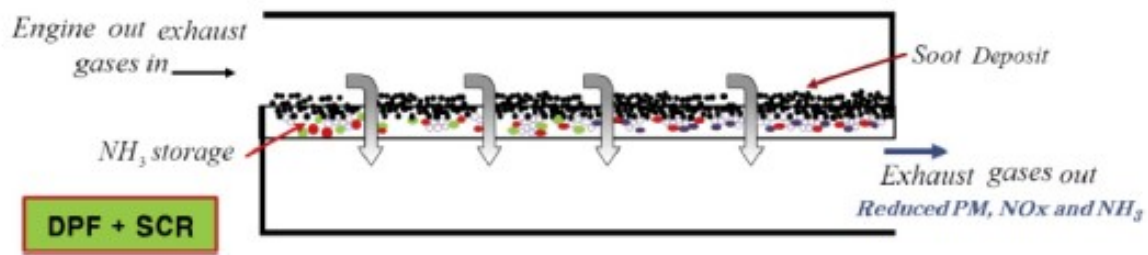


Fig. 1.13 SCRoF operating principle

In Fig. 1.13 is represented the operating principle of the SCRoF, where the porous walls of the filter are impregnated with the SCR catalyst [20]. In this system, the  $\text{NO}_x$  are reduced as a result of the addition of  $\text{NH}_3$  while soot accumulates on the filter walls, that is regenerated by passive regeneration (the soot accumulated is continuously oxidized by  $\text{NO}_2$ ) or active regeneration (through the increase of the upstream gas temperature in the DOC up to the soot combustion temperature). In particular, the SCRoF can benefit from the simultaneous SCR reaction and the filter passive regeneration. At determinate temperature and  $\text{NO}_2$  concentration, the  $\text{NO}_2$  assisted soot oxidation is promoted, which converts the  $\text{NO}_2$  in  $\text{NO}$  reducing its content in the fuel gas, meanwhile, the SCR reaction completes the  $\text{NO}$  and  $\text{NO}_2$  reduction to  $\text{N}_2$  [27].

There are some technological challenges related to the combination of the de- $\text{NO}_x$  and PM abatement functionalities, mainly related to the interactions between the SCR and soot chemistries that can result in a SCRoF performance lower than that of the individual devices. Also, the impact on the mass-transfer characteristics by the presence of soot can affect in a negative way the de- $\text{NO}_x$  efficiency. To minimize the impacts of this factors, the catalytic material and the coating process are very important [26, 28].

Another factor to take into account is the filter porosity since it is desirable to introduce the highest possible quantity of catalyst in the pores of the filter but there are limits established by the maximum pressure loss a filter component can have [22]. In addition, it is necessary to prevent thermal damage of the SCR-coating and the SDPF-monolith [28].

## 1.6 Motivation

The environmental and health problems related to the vehicle emissions have forced to established legislations to limit the amounts of contaminants emitted. With the increase in the use of vehicles specially diesel engines, the policies have become stricter with the pass of time forcing the manufactures to use more complex aftertreatment systems. Due to this increasing complexity, the associated cost and the space limitations, an integrated system of the aftertreatment elements, as the SCRoF, has been proposed as an alternative to solve these difficulties.

To implement this system successfully there are a lot of factors to consider. Specially, the performance should be higher than the corresponding to the individual devices, because of this the catalyst choice is very important.

The aim of this thesis is to develop catalysts that can meet all the requirements to be used in the SCRoF exhaust aftertreatment system. To do this, three catalysts were synthesized and characterized to have a better understanding of their properties and how they are related to the catalytic activity. Finally, a series of tests were carried out with the purpose of determine the catalytic activity and to study the interactions between the SRC and soot chemistries.

# Chapter 2

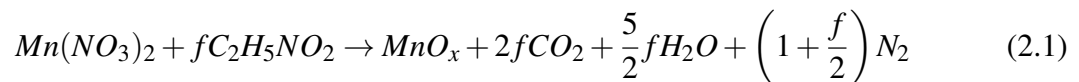
## Experimental section

### 2.1 Catalysts preparation

The catalysts were synthesized by Solution Combustion Synthesis (SCS). This method is based on exothermic redox reaction that is initiated under heating at the ignition temperature and becomes self-sustaining within a certain interval of time, resulting in a powder as a final product. It makes use of salts, such as nitrates, metal sulfates and carbonates, as oxidants and fuels, such as glycine, sucrose, urea, or other water soluble carbohydrates, as reducing agents. One of the advantages of this method is that it allows to rapidly produce fine and homogeneous powders with a less consume of energy, since most of the heat required for the synthesis is proportionated by the reaction itself [29, 30].

The characteristics of the resulting powders, such as crystalline and amorphous structure, crystalline size, surface area, purity and particle agglomeration, have a high dependency on the nature of the fuel, the fuel-oxidant ratio and other parameters of the process [29].

For the  $MnO_x$  catalyst, manganese (II) nitrate tetrahydrate ( $Mn(NO_3)_2 \cdot 4H_2O$ ) and glycine ( $C_2H_5NO_2$ ) were used as reactants. As described by Deorsola et al.[31] the amounts of both reagents were determined according to the following equation:



where  $x$  is half the oxidation number of Mn and  $f$  is the fuel/nitrate molar ratio. To determine the theoretical value of it is used an additional quantity, the “elemental stoichiometric coefficient”  $\phi$ , that can be calculated for the considered reaction as:

$$\phi = \frac{f[2x4_{(C)} + 5x1_{(H)} + 2x - 2(O) + 0(N)]}{- [2x_{(Mn)} + 2(0_{(N)} + 3x - 2(O))]} = \frac{9f}{12 - 2x} \quad (2.2)$$

$\phi$  is equal to 1 for stoichiometric conditions,  $\phi < 1$  in sub-stoichiometric conditions and  $\phi > 1$  in over-stoichiometric conditions. In this case,  $\phi$  was considered as 0.5.

The  $\text{Ce}_{0.5}\text{Mn}_{0.5}\text{O}_x$  and  $\text{Ce}_{0.25}\text{Mn}_{0.75}\text{O}_x$  catalysts were prepared using  $\text{Ce}(\text{NO}_3)_2 \cdot 6\text{H}_2\text{O}$ , manganese (II) nitrate tetra-hydrate ( $\text{Mn}(\text{NO}_3)_2 \cdot 4\text{H}_2\text{O}$ ) and glycine ( $\text{C}_2\text{H}_5\text{NO}_2$ ) as reactants. The amounts of the reagents were calculated as described before with  $\phi = 2$ .

For the synthesis of the different catalysts, the reagents were dissolved in 25 mL of distilled water and stirred at room temperature for 30 min. The solution was then transferred into a porcelain crucible and put in a preheated oven at  $600^\circ\text{C}$  for 30 min. The samples were collected, crushed in mortar and finally calcined for 1h at  $700^\circ\text{C}$ . Fig.2.1 shows the three catalysts synthesized.

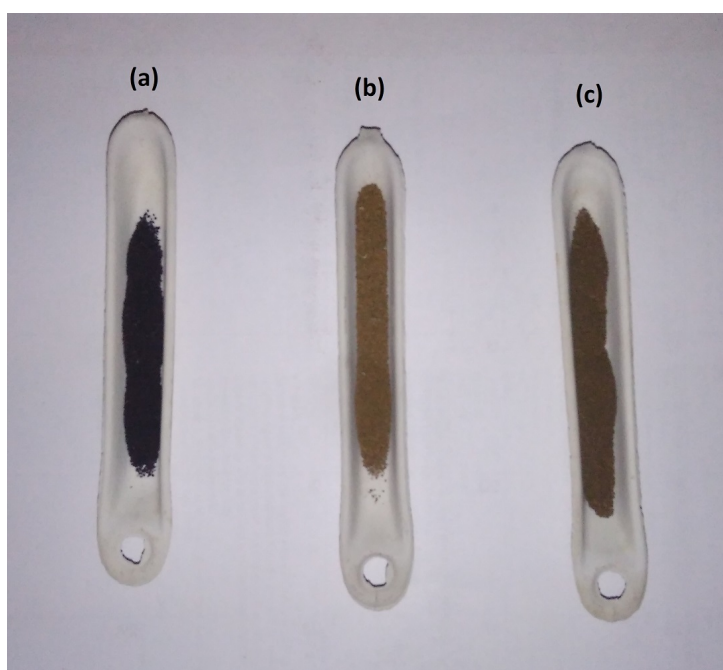


Fig. 2.1 Synthesized catalysts, (a)  $\text{MnO}_x$ , (b)  $\text{Ce}_{0.25}\text{Mn}_{0.75}\text{O}_x$ , (c)  $\text{Ce}_{0.5}\text{Mn}_{0.5}\text{O}_x$

## 2.2 Catalysts characterization

Some of the physico-chemical properties of the synthesized catalysts were studied by different characterization techniques, such as  $\text{N}_2$  adsorption at  $-196^\circ\text{C}$ , Field Emission Scanning Electron Microscopy (FESEM), X-ray Powder Diffraction (XRD), X-ray Photoelectron Spectroscopy (XPS),  $\text{H}_2$ -Temperature Programmed Reduction ( $\text{H}_2$ -TPR) and Temperature Programmed Desorption of  $\text{NH}_3$  ( $\text{NH}_3$ -TPD).

### 2.2.1 N<sub>2</sub> physisorption

The term physisorption or physical adsorption is used to describe the phenomenon of gas molecules adhering to a surface without the formation of a chemical bond at a pressure less than the vapor pressure. Between the molecules of adsorbate and the surface there is only a weak Van der Waals attraction. Unlike the chemisorption, where there is a chemical bond formation, physical adsorption takes place on all surfaces and can form multiple layers under proper conditions. Also, since it is only a weak bond, physical adsorption can be easily reversed and the enthalpy values usually do not exceed 80 kJ/mol [32, 33].

In an adsorption experiment it is possible to determine the adsorption isotherm, which is obtained by measuring the amount of gas adsorbed across a wide range of relative pressure at constant temperature. Desorption isotherms can be obtained as well, through the measurement of gas removed as pressure is reduced. Analyses of physical adsorption isotherm data gives information of the total surface area, total pore volume and pore size distribution [33].

Nitrogen is generally employed as the probe molecule. It is exposed to the solid surface in a liquid state (i.e. 77 K). The surface area is evaluated from the measured monolayer capacity and knowledge of the cross-sectional area of the probe molecule. For the case of nitrogen, the cross-sectional area is taken as 16.2 Å<sup>2</sup>/molecule [32, 33].

There are six types of isotherms according to the IUPAC classification where most of the isotherms can be grouped (Fig. 2.2).

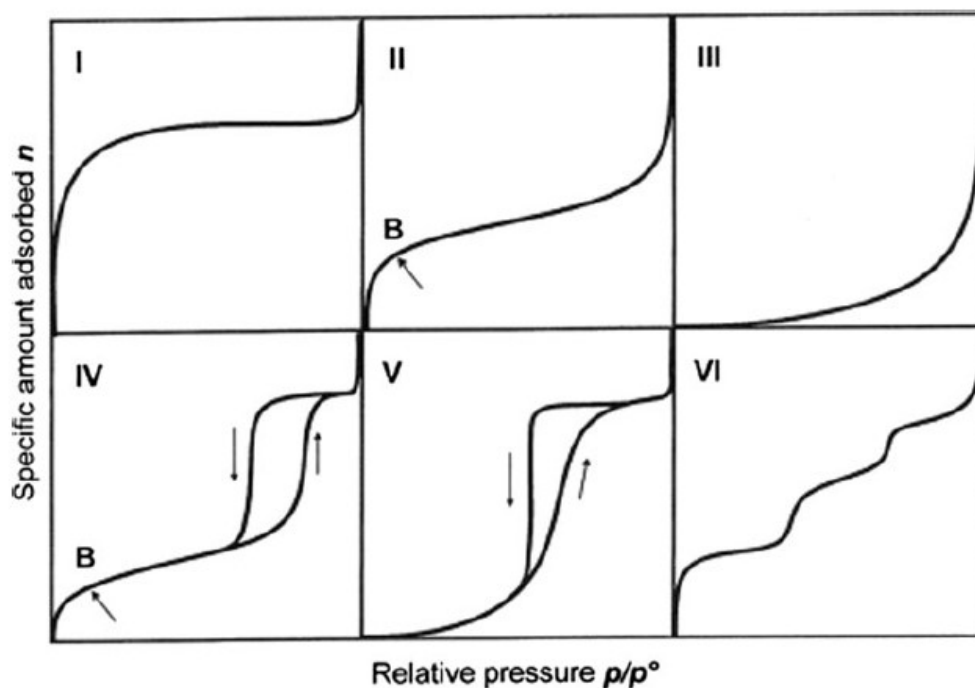


Fig. 2.2 Isotherms IUPAC classification

- Type I: Microporous materials (< 2 nm), whose pores once filled with the adsorbate, leave little or no external surface to further adsorption (e.g. zeolite and activated carbon).
- Type II: Nonporous materials or materials with diameters exceeding micropores (>50 nm). Inflection point(B) occurs near the completion of the first adsorbed monolayer (e.g. nonporous alumina and silica).
- Type III: Nonporous materials and materials where the adsorbate interaction with an adsorbed layer is greater than the interaction with the adsorbent surface (e.g. graphite/water).
- Type IV: Mesoporous materials (2-50 nm). Initial part follows the same path as the type II. At higher pressures there is an increased uptake of adsorbate as pores become filled. The difference between the adsorption and desorption paths indicates the presence of hysteresis (e.g. Mesoporous alumina and silica).
- Type V: Porous materials (2-50 nm) that have weak interaction between adsorbate and adsorbent (similar to type III). There is hysteresis (e.g. activated carbon / water).
- Type VI: Homogeneous surface material. There is a step for each filling layer (e.g. graphite/Kr and NaCl/Kr) [32, 33].

The adsorption hysteresis can be classified as well and there is also a correlation between the shape of the hysteresis loop and the texture of a mesoporous material, for example it is related with the pore size distribution, pore geometry and connectivity. Five types of hysteresis loops were identified and related with different pore shapes by De Boer (Fig.2.3). Type A corresponds to cylindrical pores or agglomerates of approximately uniform spheres; type B is related to slit-shaped pores; type C and D are ascribed to wedge-shaped pores, and type E is produced by pores with a bottle neck geometry [34, 35].

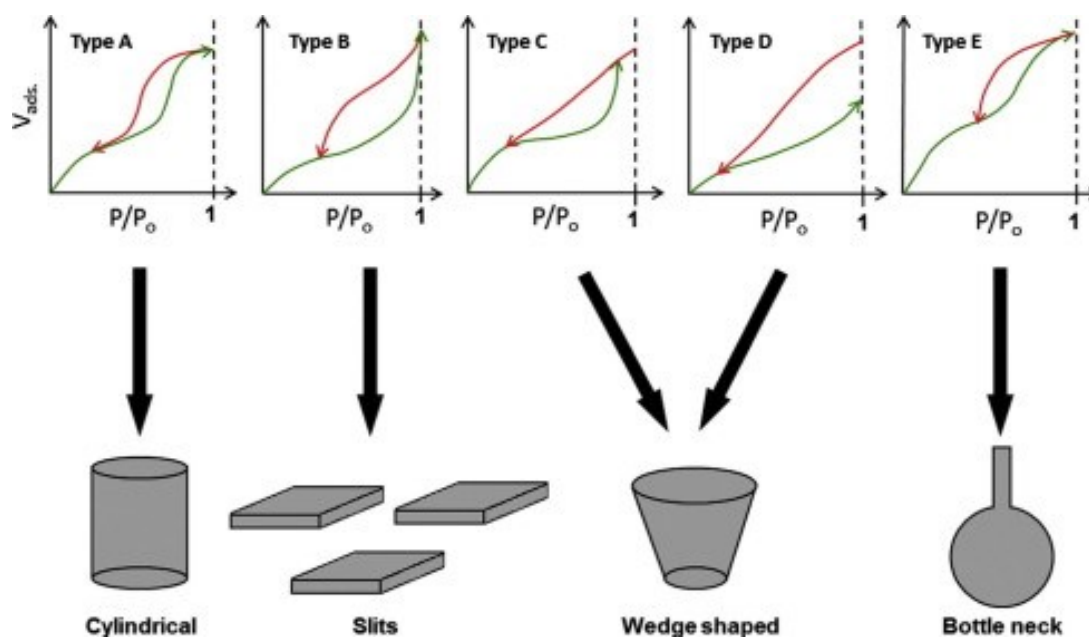


Fig. 2.3 Pore shapes according to the hysteresis loop

Several models have been developed for the use of the experimental data. Each one based in different assumptions that may affect the model's validity for a certain surface. One of them is the Langmuir theory, that is used for ideal localized monolayer adsorption (isotherm type I). The most widely used is the Brunauer, Emmett and Teller (BET) and its modifications including the Brunauer, Deming, Deming and Teller (BDDT). The assumptions use to derive the BET isotherm are:

- The molecules in the gas behave ideally.
- Multiple nitrogen molecules can be adsorbed to each site.
- Each adsorbed molecule provides a site for the adsorption of a molecule in the layer above it (multilayer adsorption).
- All sites on the surface are equivalent.
- There are no adsorbate-adsorbate interactions.
- The adsorbed molecules are immobile.
- Nitrogen in the second and higher layers is assumed to be liquid.

In the evaluation of the surface area from physisorption data by the BET method involves two stages. The first stage is to construct the BET plot and determine the value of the monolayer capacity,  $n_m$ . In the second stage, the specific surface area is calculated. The BET equation expressed in the linear form is:

$$\frac{p/p^o}{n(1-p/p^o)} = \frac{1}{n_m C} + \frac{(C-1)}{n_m C} \left( \frac{p}{p^o} \right) \quad (2.3)$$

Where  $n$  is the amount adsorbed,  $(p/p^o)$  the relative pressure,  $n_m$  is the monolayer capacity and  $C$  is the BET constant.

The specific surface area can be calculated with the following equation:

$$S = n_m N_A A_{CS} \quad (2.4)$$

Where  $N_A$  is the Avogadro's number and  $A_{CS}$  is the adsorbate cross sectional area[33, 34, 36].

The  $N_2$  physisorption was conducted at  $-196$  °C using a Micrometrics Tristar II instrument (Fig. 2.4). First, the samples were degassed at  $150$ °C to remove any surface contamination. The specific surface area was determinate using the Brunauer-Emmett-Teller (BET) method, pore total volume was measured at  $p/p^o=0.99$  and the pore size distribution was calculated using the BJH method.



Fig. 2.4 BET instrument

### 2.2.2 Field Emission Scanning Electron Microscopy (FESEM)

FESEM is a non-destructive technique that reveals detailed information about the morphology and the composition of natural and manufactured materials. It uses electrons to illuminate a sample, instead of visible light as in optical microscopy. Since the wavelength of electrons is smaller than that of visible light, scanning electron microscopes are able of imaging at much higher magnification in comparison with light microscopes. Besides, the FESEM can be classified as a high vacuum instrument (with less than  $1 \times 10^{-7}$  Pa in the gun zone). The vacuum allows the electron movement along the column without scattering and helps prevent discharges inside the gun zone as well [37–39].

There are two classes of electron emission sources: thermionic emitter and field emitter. The emitter type is the main difference between the scanning electron microscope (SEM) and the FESEM. Thermionic emitters use electrical current to heat up the filament, which is usually made of tungsten (W) or lanthanum hexaboride ( $\text{LaB}_6$ ). This kind of source has relative low brightness, evaporation of cathode material and thermal drift during operation. On the other hand, a field emission gun (FEG), also called cold cathode field emitter, does not heat the filament, the emission is reached instead by placing the filament in an electrical potential gradient. With this kind of emitter, it is possible to avoid the problems present when a thermionic emitter is used. FESEM uses a Field Emission Gun, producing a cleaner image, less electrostatic distortions and spatial resolution less than 2 nm (3 or 6 times better than SEM) [37].

Once the electrons are liberated from the field emission source, they are accelerated in a high electrical field gradient. With the high vacuum column, with which the instrument is equipped, these electrons (primary electrons) are focused and deflected by electronic lenses to produce

a scan beam that bombards the object. As a result, secondary electrons are emitted from the object. These electrons are caught by a detector that produces an electronic signal. Their angle and velocity are related to the surface structure of the object [38].

The morphology of the different samples was studied with this technique on a Zeiss Merlin microscope equipped with a GEMINI II column (Fig. 2.5).



Fig. 2.5 FESEM instrument

### 2.2.3 X-ray Powder Diffraction (XRD)

XRD is an analytical technique used for phase identification of crystalline materials and can also provide information on unit cell dimensions. X-ray diffractometers consist of three basic elements: an X-ray tube, a sample holder and an X-ray detector. The wavelength of these X-ray is characteristic of that target [40].

X-ray are generated in a cathode ray tube by heating a filament to produce electrons. These electrons are accelerated through the application of a high voltage, typically 15-60 kV. When the electrons hit a determinate target material (Cu, Fe, Mo,Cr), X-rays are produced. These X-rays are collimated and directed into the sample (powder). As the sample and detector are rotated, the intensity of the reflected X-rays is recorded. When the geometry of the incident X-rays satisfies the Bragg equation (equation 2.5), there is a constructive interference and a peak in intensity occurs, whose height is proportional to the number of grains in a preferred orientation.

$$2d \sin \theta = n\lambda \quad (2.5)$$

Where  $d$  is the distance between adjacent planes of atoms, the integer  $n$  is the order of the diffracted beam,  $\lambda$  and  $\theta$  are the wavelength and angle of incidence of the X-ray beam, respectively [40, 41].

The X-ray spectra generated by this technique provide a structural fingerprint, that can be compared with standard reference patterns to make a properly interpretation[42].

In this case, the XRD analysis was made on a Panalytical X'Pert Pro Diffractometer using Cu-K $\alpha$  radiation. The diffractogram was recorded from 10° to 70° (2 $\theta$  mode) with a step =0.01 and a time of 240s per step. Finally, XRD peaks were identified using the JCPDS database.

#### 2.2.4 X-ray Photoelectron Spectroscopy (XPS) analysis

X-ray photoelectron spectroscopy, also known as electron spectroscopy for chemical analysis (ESCA), is a technique which analyzes the elements constituting the sample surface, its composition, and chemical bonding state. XPS is a special form of the photoemission process that uses X-ray photons (most frequently magnesium and aluminum k-alpha X-rays) to irradiate the sample surface. The kinetic energy of the electrons emitted, called photoelectrons, is measured. The typical photon sources employed generate photoelectrons with kinetic energies in the range of tens to hundreds of electron volts (eV). Kinetic energy is the factor that determines the depth from which the electron can escape into a vacuum where they can be measured [43, 44].

In an XPS experiment, a survey scan is conducted that covers a kinetic energy of a few eV to approximately 1000 eV. In this range, all elements have one or more distinctive photoelectron characteristics that allow the identification. Information both quantitative and qualitative is provided.

The XPS data are reported as binding energy, but because the kinetic energy is the measured experiment parameter, it is necessary to calculate it:

$$\text{Binding energy}(BE) = \text{photon energy}(h\nu) - \text{kinetic energy}(KE) \quad (2.6)$$

Where the binding energy is the net energy required to decompose a molecule, an atom, or a nucleus into its components.

Another characteristic of the XPS is its ability to distinguish different chemical states. For example, with this technique can provide information that differentiates between aluminum metal and aluminum oxide. it is possible also to determine the oxidation state of most metals [44].

This characterization was performed on a XPS PHI 5000 Versa probe apparatus. The XP spectra were recorded with a pass energy of 20 eV, a resolution of 1.1 eV, and a step of 0.2 eV.

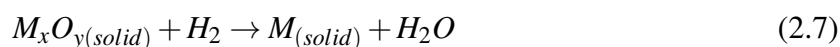
#### 2.2.5 H<sub>2</sub>-TPR (Temperature Programmed Reduction) analysis

Temperature programmed reduction (TPR) is used for the characterization of metal oxides, mixed metal oxides, and metal oxides dispersed on a support. In general, temperature-programmed methods are some of the best and quickest methods to fingerprint a metal oxide or a supported

metal catalyst. Specially, TPR is a very sensitive technique for the determination of a catalyst condition, specifically when a new catalyst preparation is used or the catalyst is being modified [45].

This characterization technique can be used for quantitative and qualitative analysis. It gives information about the redox properties of materials, the heterogeneity of the reducible surface, the temperature range of consumption and the total consumption of the reducing agent, and valence states of metal atoms in zeolites and metal oxides. Also, this method allows to identify the supported precursor phases and their interaction with the support, and characterize complex systems, as bimetallic or doped catalyst, with the objective of determine the role of the second component and establish if there is alloy formation or promotion effects [45–47].

In the TPR, the catalyst is exposed to a flow of dilute reductant gas mixture, such as H<sub>2</sub>/Ar, while the temperature is linearly increased. The reduction rate is monitored through the analysis of the change in composition of the reactive mixture at the reactor exit. This is often done using a thermal conductive sensor, that allows to compare the thermal conductivity of the gas before and after the reactor. It is possible to include too a gas chromatograph or a mass spectroscope to measure the composition of the gas at the exit of the reactor. In the obtained profile, the peak maxima are an indication of the reducibility of the metal oxide phase. The reaction between the metal oxide and the hydrogen is represented by the reaction:



TPR results are highly influenced by the programmed heating rate, H<sub>2</sub> concentration in the flowing gas stream and the flow rate. The particle size is an important experimental too; in fact, for bulk oxides as the particle size increases it is expected an increase in  $T_{max}$  [45–47].

H<sub>2</sub>-TPR analysis was carried out on a TPD/R/O 1100 ThermoQuest instrument (Fig.2.6). First, the 50 mg powder samples were pre-treated with inert gas, to eliminate any contaminant present in the catalyst. The TPR section was performed in the 50-850°C temperature range at a heating rate of 10°/min under constant flow (20 mL/min) of 5% H<sub>2</sub>/Ar mixture.



Fig. 2.6 TPR instrument

### 2.2.6 Temperature Programmed Desorption (NH<sub>3</sub>-TPD)

Temperature programmed desorption is a classic method to determine the amount and the strength of adsorbed species on a solid sample based on its desorption temperature. Especially, it is widely used for characterizing the acid sites on oxide surface. In a TPD experiment, a gas or vapor (adsorbate) is adsorbed on the catalyst material (adsorbent). Then, the sample is vacuumed or flushed to remove excess adsorbate, in this way only the adsorbed species remain on the sample. Finally, the sample is heated linearly in an inert gas flow to remove the adsorbed species and the outlet gas is monitored on-line with either a temperature conductivity detector (TCD), a mass spectrometer (MS) or a Fourier-transform infrared (FTIR) analyzer [48, 49].

The interaction of acid sites and basic probe molecules is often studied to distinguish between Brønsted (B) and Lewis (L) type sites and to determine their amounts and strength, which is very important to understand and predict the performance of a catalyst. There are three types of molecular probes commonly used for characterizing acid sites: ammonia, non-reactive vapors, such as pyridine and *t*-butyl; and reactive probes as propyl amines [49, 50].

With the NH<sub>3</sub>-TPD method is possible to determine the concentration of sites with similar strengths and the average adsorption heat or activation energy of NH<sub>3</sub> desorption. Often the temperature of maximum desorption rate (the temperature of a TPD peak) is used as an approximate measure of the acid strength of the adsorption sites. This method is widely used due to its simplicity and because the small ammonia molecular size allows it to penetrate into all pores of the solid where larger molecules only have access to large micropores and mesopores [49, 50].

One of the limitations of this method is that it can distinguish sites by adsorption strength only, but not L- from B-type sites. Also, desorption can take place simultaneously from sites of different types resulting in overlapping TPD peaks [50].

The temperature programmed desorption was conducted on a fixed-bed quartz tube reactor. Before TPD measurement, 200 mg sample was pretreated with a constant flow of  $N_2$  (100 mL/min) at a heating rate of  $10^\circ\text{C min}^{-1}$  from room temperature up to  $500^\circ\text{C}$ , then the temperature was kept at this value for 30 min. After cooling until  $100^\circ\text{C}$ , the  $NH_3$  adsorption was carried out by flowing a gas mixture of 2000 ppm  $NH_3$  and  $N_2$  balance until saturation. To remove the loosely bonded  $NH_3$ ,  $N_2$  (400 mL/min) was flushed at  $25^\circ\text{C}$  for 1h. Finally, to desorb the strongly bonded  $NH_3$  a temperature- programmed desorption was performed with a heating rate of  $5^\circ\text{C min}^{-1}$  up to  $600^\circ\text{C}$ . The temperature was monitored by a K-type thermocouple placed inside the tube reactor.  $NH_3$  concentrations were measured by a ND-IR Uras gas analyzer (ABB Spa).

## 2.3 Catalytic activity measurements

A series of tests were carried out to have a better understanding of all the reactions that could be involved in the SCRoF. First, the individual reactions (soot oxidation,  $NH_3$  oxidation, NO oxidation and standard SCR) were studied, after another set of reactions was performed with the presence of soot.



Fig. 2.7 laboratory installation for the experiments

All the tests were conducted in a fixed bed tubular quartz reactor (inner diameter = 11.8 mm) heated by an electric furnace. It was used a total flow rate of  $500\text{ mL min}^{-1}$  with the composition reported in Table 2.1 and a fixed bed height of approximately 5 mm ( $GHSV = 50,000\text{ h}^{-1}$ ).

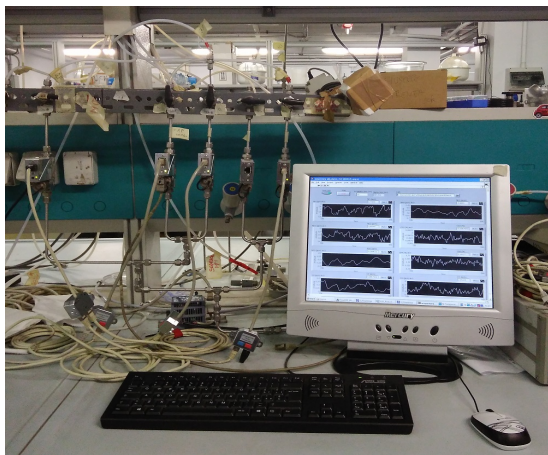
Table 2.1 Gas composition during the experiments

Reaction	NH <sub>3</sub> (ppm)	NO (ppm)	O <sub>2</sub> (%)	N <sub>2</sub>
Soot oxidation	0	0	3	Balance
NO oxidation	0	500	3	Balance
NH <sub>3</sub> oxidation	500	0	3	Balance
Standard SCR	500	500	3	Balance
NO oxidation + soot	0	500	3	Balance
Standard SCR + soot	500	500	3	Balance

The gases were dosed by using independent mass flow controllers. The temperature was monitored by a K-type thermocouple placed inside the tube reactor, NH<sub>3</sub> concentrations were measured by a ND-IR Uras gas analyzer (ABB Spa), NO and NO<sub>2</sub> concentrations were analyzed by a NO/NO<sub>2</sub> UV Limas gas analyzer (ABB Spa) and the CO and CO<sub>2</sub> concentrations by a Non Dispersive IR-Analyzer. Finally, the data acquisition was made with LabView. In fig.2.8 it is possible to see the various equipment used.

For the experiments with soot, the catalyst and synthetic soot were mixed (mass ratio of 20/1, W/F = 56 g s/cm<sup>3</sup>) with a spatula for 2 min, according to the loose contact methodology. In the experiments without soot, it was used a catalyst sample of 500 mg (W/F= 60 g/s cm<sup>3</sup>) to maintain the same gas hourly space velocity. The catalyst was previously pelletized and sieved to a size fraction of 125-250 μm to prevent bypass and mitigate the pressure drop.

The NO oxidation, NH<sub>3</sub> oxidation and standard SCR tests were carried out under isothermal conditions in the 150°C-700°C temperature range with steps of 50°C, the temperature was only increased when the concentration reached a stable value. On the other hand, the tests with soot presence were performed under isothermal conditions from 150°C- 400°C, following the same methodology mentioned before, and then with a heating rate of 3 °C/min until 750°C, while for the soot oxidation the temperature was ramped up from 25°C to 750°C with the same heating rate.



(a) Mass Flow controllers



(b) Analyzers



(c) Furnace



(d) Tubular quartz reactor

Fig. 2.8 Laboratory Equipment

Finally, the NO, NO<sub>x</sub> and NH<sub>3</sub> conversions, and the N<sub>2</sub> selectivity were calculated according to the following equations:

$$NO_x \text{ conversion}(\%) = \left( \frac{[NO_x]_{in} - [NO_x]_{out}}{[NO_x]_{in}} \right) \times 100 \quad (2.8)$$

$$NO \text{ conversion}(\%) = \left( \frac{[NO]_{in} - [NO]_{out}}{[NO]_{in}} \right) \times 100 \quad (2.9)$$

$$NH_3 \text{ conversion}(\%) = \left( \frac{[NH_3]_{in} - [NH_3]_{out}}{[NH_3]_{in}} \right) \times 100 \quad (2.10)$$

$$N_2 \text{ selectivity}(\%) = \left( 1 - \frac{2[N_2O]_{out}}{[NH_3]_{in} + [NO_x]_{in}} \right) \times 100 \quad (2.11)$$

# Chapter 3

## Results and discussion

### 3.1 Catalyst characterization

In this section are reported the obtained results with the different characterization techniques used. Through this characterization was possible to have a better understanding of some physical and chemical properties of the catalysts and how they could affect their performance in the reactions of interest.

#### 3.1.1 N<sub>2</sub> physisorption

Fig. 3.1. Shows the N<sub>2</sub> adsorption-desorption isotherm for the three catalysts. All the isotherms correspond to the Type V according to the IUPAC classification, characteristic of mesoporous materials. The Ce<sub>0.25</sub>Mn<sub>0.75</sub>O<sub>x</sub> and MnO<sub>x</sub> catalysts had isotherms very similar, with the presence of a small hysteresis loop, which is associated with the capillary condensation in mesoporous and can limit the uptake at high relative pressures as well. For the first catalyst, the amount adsorbed was higher but the difference was not that representative as for the case of Ce<sub>0.5</sub>Mn<sub>0.5</sub>O<sub>x</sub>, whose quantity adsorbed was almost twice the quantity adsorbed with MnO<sub>x</sub>. Also, for Ce<sub>0.5</sub>Mn<sub>0.5</sub>O<sub>x</sub> the hysteresis loop was bigger.

The trend of the hysteresis loop is related to the pore geometry. According to the classification established by De Boer, the adsorption hysteresis exhibited by all the catalysts is very similar to the type A, which is generally associated with a cylindrical shape.

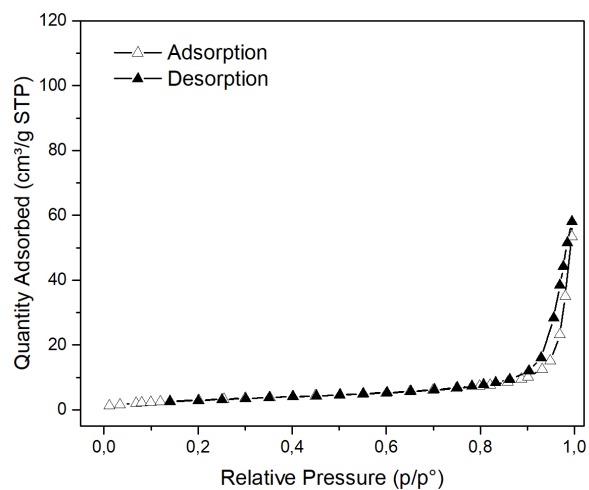
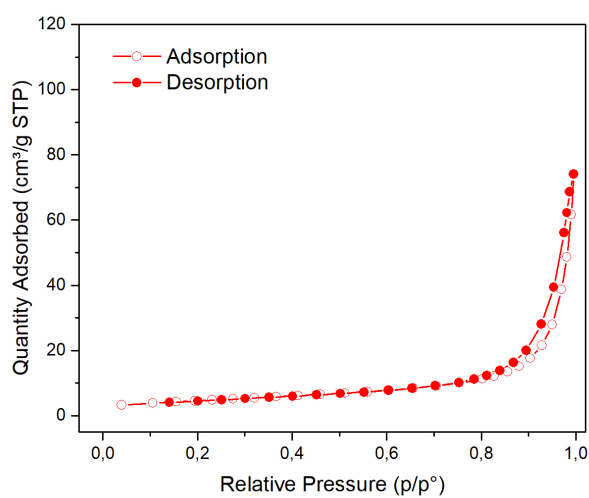
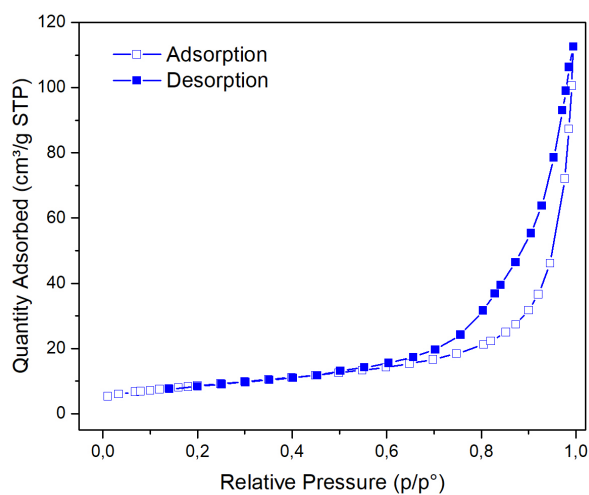
(a)  $\text{MnO}_x$ (b)  $\text{Ce}_{0.25}\text{Mn}_{0.75}\text{O}_x$ (c)  $\text{Ce}_{0.5}\text{Mn}_{0.5}\text{O}_x$ 

Fig. 3.1 Adsorption-desorption isotherms

The results obtained for the BET surface area, pore diameter and pore volume are reported in Table 3.1.

Table 3.1 Specific surface area, pore diameter and pore volume

Parameters	MnO <sub>x</sub>	Ce <sub>0.25</sub> Mn <sub>0.75</sub> O <sub>x</sub>	Ce <sub>0.5</sub> Mn <sub>0.5</sub> O <sub>x</sub>
Specific surface area (m <sup>2</sup> /g)	10	16	30
Pore volume (cm <sup>3</sup> /g)	0.036	0.060	0.11
Pore diameter (nm)	12	14	14

The catalysts containing Ce have higher SSA values, specifically increasing the Ce percentage increases the specific surface area as it can be seen in the value obtained for Ce<sub>0.5</sub>Mn<sub>0.5</sub>O<sub>x</sub>, which was almost three times the corresponding value to MnO<sub>x</sub>. Also, the pore volume and diameter of this Ce-based catalyst were higher than the respective values of the other catalysts. For the pore volume the differences between the results were remarkable while for the pore diameter the values were very similar, particularly the Ce<sub>0.25</sub>Mn<sub>0.75</sub>O<sub>x</sub> and Ce<sub>0.5</sub>Mn<sub>0.5</sub>O<sub>x</sub> catalysts have porous of almost the same diameter. Moreover, since the pore diameter values are inside the range 2-50 nm, the three catalysts can be classified as mesoporous materials, as it was expected from the trend observed in the isotherms.

### 3.1.2 FESEM

In the FESEM results (Fig. 3.2) it is possible to see that all the catalysts were characterized by a spongy structure with the presence of porosities. The morphologies of the MnO<sub>x</sub> and Ce<sub>0.25</sub>Mn<sub>0.75</sub>O<sub>x</sub> catalysts were very similar, with spherical particles of diameter below 100 nm forming large agglomerates. The Ce<sub>0.5</sub>Mn<sub>0.5</sub>O<sub>x</sub> showed a morphology slightly different, with agglomerates of particles with laminar shapes, and seems to have a spongier structure as well.

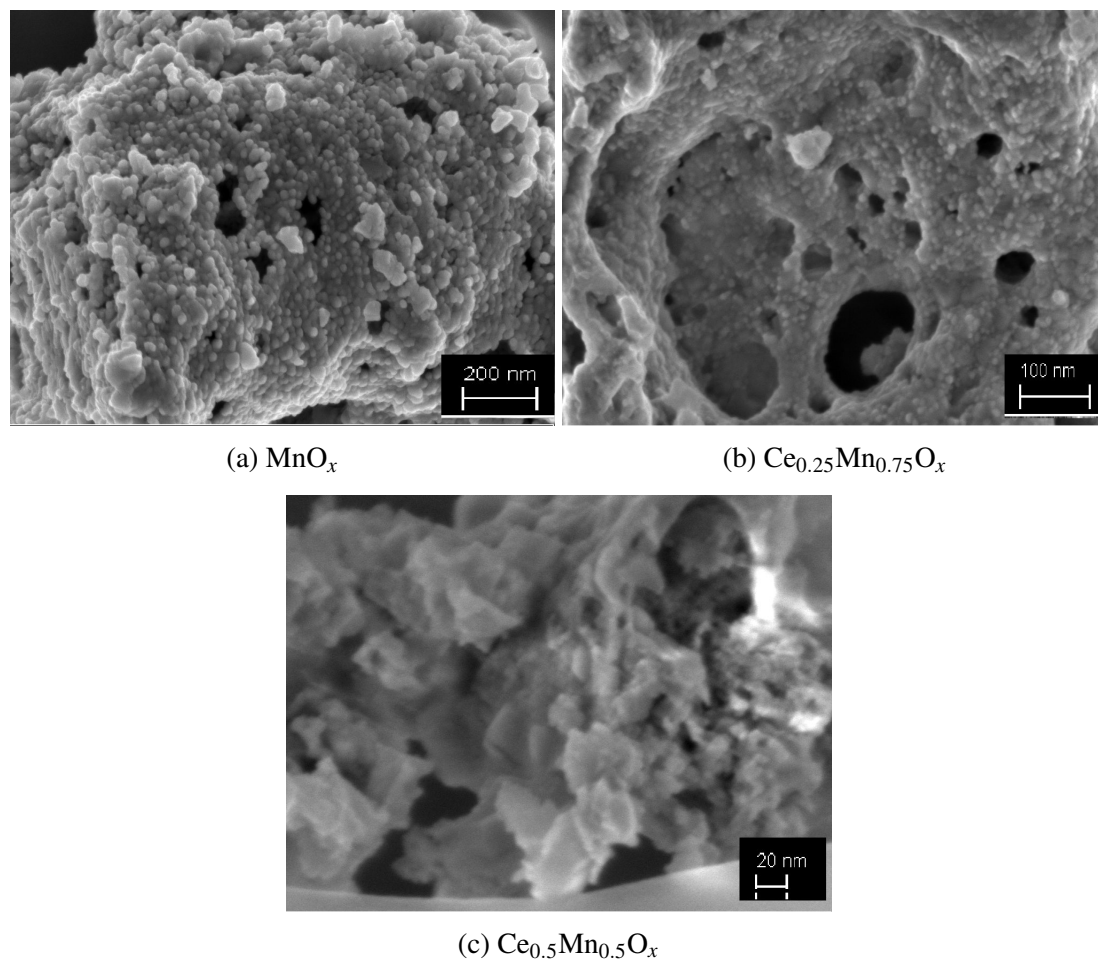


Fig. 3.2 FESEM micrographs

### 3.1.3 XRD

In Fig.3.3 are reported the XRD patterns of the three catalysts synthesized. In MnO<sub>x</sub> sample almost all the diffraction peaks identified correspond to the Mn<sub>2</sub>O<sub>3</sub>, it was possible to recognize only one peak of the Mn<sub>3</sub>O<sub>4</sub> phase ( $2\theta=37,98^\circ$ ). The most intense peak ( $2\theta=32,98^\circ$ ) is characteristic of the Mn<sub>2</sub>O<sub>3</sub> phase.

In both Ce<sub>0.25</sub>Mn<sub>0.75</sub>O<sub>x</sub> and Ce<sub>0.5</sub>Mn<sub>0.5</sub>O<sub>x</sub> patterns, diffraction peaks of CeO<sub>2</sub>, Mn<sub>3</sub>O<sub>4</sub> and Mn<sub>2</sub>O<sub>3</sub> phases were identified, being the last one the phase present in the smallest proportion. The peaks with the highest intensity ( $2\theta=28,55^\circ$ ,  $47,48^\circ$ ,  $56,33^\circ$ ) are characteristic of the CeO<sub>2</sub> phase. As for the MnO<sub>x</sub> sample, there was a peak at about  $32,98^\circ$ , typical of the Mn<sub>2</sub>O<sub>3</sub> phase, but with a lower intensity. Besides, for both Ce-based catalysts the patterns were very similar, the only difference was the intensity of the peaks. For the Ce<sub>0.25</sub>Mn<sub>0.75</sub>O<sub>x</sub> the diffraction peaks of the MnO<sub>x</sub> phases were more intense in comparison with the peaks present in the Ce<sub>0.5</sub>Mn<sub>0.5</sub>O<sub>x</sub> pattern, this due to the higher Mn content in the sample. The same was evidenced for the diffraction peaks of the CeO<sub>2</sub> phase, they were more intense in the Ce<sub>0.5</sub>Mn<sub>0.5</sub>O<sub>x</sub> sample.

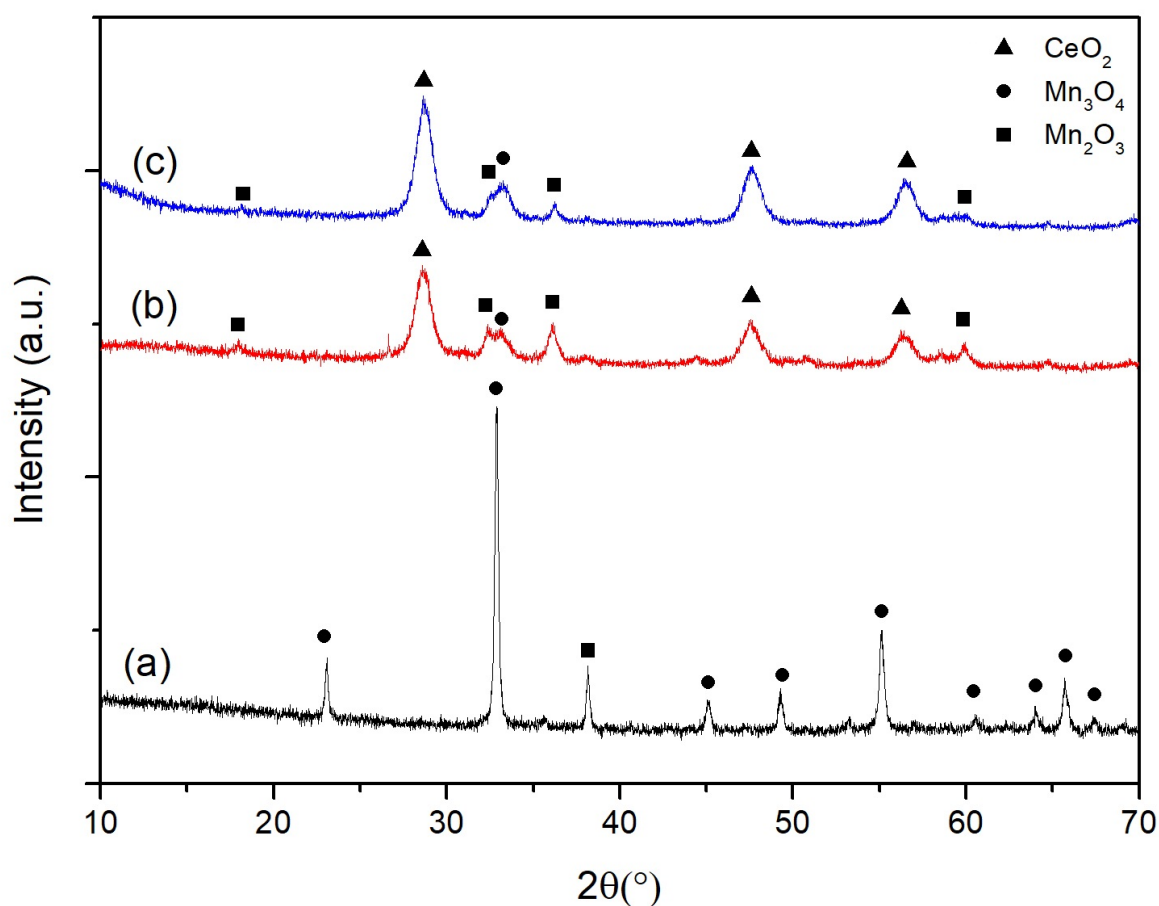


Fig. 3.3 XRD patterns, of samples (a)  $\text{MnO}_x$  (b)  $\text{Ce}_{0.25}\text{Mn}_{0.75}\text{O}_x$  and (c)  $\text{Ce}_{0.5}\text{Mn}_{0.5}\text{O}_x$

Comparing the three patterns it is possible to see that the peaks of the  $\text{MnO}_x$  sample were sharper and some of them more intense than for the other samples, indicating the presence of a higher crystallinity.

### 3.1.4 X-ray Photoelectron Spectroscopy (XPS) analysis

The XPS spectra of Mn 2p, Ce 3d and O 1s are shown in figure x. The binding energy of each component and the relative percentages of Mn, Ce and O atoms are reported in Table 3.2.

In the O 1s can be distinguished two peaks. In the case of  $\text{Ce}_{0.5}\text{Mn}_{0.5}\text{O}_x$  the peak corresponding to a higher binding energy had a much lower intensity than the other one, for the  $\text{MnO}_x$  this peak was a little more intense while in the case of the  $\text{Ce}_{0.25}\text{Mn}_{0.75}\text{O}_x$  the intensity of the peak was much higher than for the other two catalysts, but it did not have a defined shape. In literature is reported that the peak in the 529.5 - 530.0 eV range can be assigned to lattice oxygen  $\text{O}^{2-}$  (denoted as  $\text{O}_\beta$ ) and that in the 531.0 - 531.7 eV range corresponds to surface chemisorbed oxygen  $\text{O}^-$  or  $\text{O}_2^{2-}$  (denoted as  $\text{O}_\alpha$ ). The latter possesses a higher mobility, which results in a higher activity in the catalytic processes, particularly its concentration is very significant in SCR of  $\text{NO}_x$  because a high concentration of  $\text{O}_\alpha$  species favors the formation of  $-\text{NH}_2$  species that react

with NO to form N<sub>2</sub> [23, 31]. All the samples showed both components at more or less the same BE values. Regarding the relative concentration of O<sub>α</sub> and O<sub>β</sub>, the concentration of O<sub>α</sub> in the MnO<sub>x</sub> and Ce<sub>0.25</sub>Mn<sub>0.75</sub>O<sub>x</sub> was very similar and corresponded to approximately half of the concentration of O<sub>β</sub>. In the case of Ce<sub>0.5</sub>Mn<sub>0.5</sub>O<sub>x</sub>, the concentration of O<sub>α</sub> was the highest among all the catalysts, its value was almost twice the values obtained for the others.

Table 3.2 Binding Energy values (BE) and chemical composition (% at)

Surface Species	Values	MnO <sub>x</sub>	Ce <sub>0.25</sub> Mn <sub>0.75</sub> O <sub>x</sub>	Ce <sub>0.5</sub> Mn <sub>0.5</sub> O <sub>x</sub>
O <sub>β</sub>	BE (eV)	529.73	529.08	529.25
	% at	61.92	68.68	33.7
O <sub>α</sub>	BE (eV)	531.11	531	530.57
	% at	38.08	31.32	66.3
O <sub>α</sub> /O <sub>β</sub>		0.61	0.46	1.97
Mn <sup>2+</sup>	BE (eV)	640.8	640.4	640.4
	% at	22.82	35.84	8.6
Mn <sup>3+</sup>	BE (eV)	641.91	641.76	641.5
	% at	56.35	39.09	71.38
Mn <sup>4+</sup>	BE (eV)	643.59	643.65	643.58
	% at	20.38	25.07	20.03
Mn <sup>4+</sup> /Mn <sup>3+</sup>		0.37	0.64	0.46
Ce(III)	% at		25.88	27.6
Ce(IV)	% at		74.12	72.39
Ce(III)/(Ce(III)+Ce(IV))			0.26	0.28

The XP spectra in the Mn 2p region showed two peaks that could be ascribed to the Mn 2p<sub>3/2</sub> and Mn 2p<sub>1/2</sub> core levels. According to literature, the binding energy at 640.4 - 640.8 eV, 641.5 - 642.0 eV and 642.5 - 643.8 eV ranges are assigned to Mn<sup>2+</sup>, Mn<sup>3+</sup> and Mn<sup>4+</sup>, respectively. In all the samples was appreciated the presence of peaks corresponding to the three species mentioned before at almost the same positions. All the catalysts showed a similar content of Mn<sup>4+</sup>, being higher the amount present in Ce<sub>0.25</sub>Mn<sub>0.75</sub>O<sub>x</sub>, for which the Mn<sup>4+</sup>/Mn<sup>3+</sup> ratio was 0.64. This large amount could be related to an increased oxidizing behavior. In this catalyst, the amount of Mn<sup>2+</sup> and Mn<sup>3+</sup> species were similar. In the case of MnO<sub>x</sub> as for Ce<sub>0.5</sub>Mn<sub>0.5</sub>O<sub>x</sub>, the Mn<sup>3+</sup> was the species in the highest quantity followed by Mn<sup>2+</sup>, but in the Ce-containing catalyst the amount of Mn<sup>2+</sup> was considerably less than the amount of Mn<sup>3+</sup>, being the species in the smallest quantity.

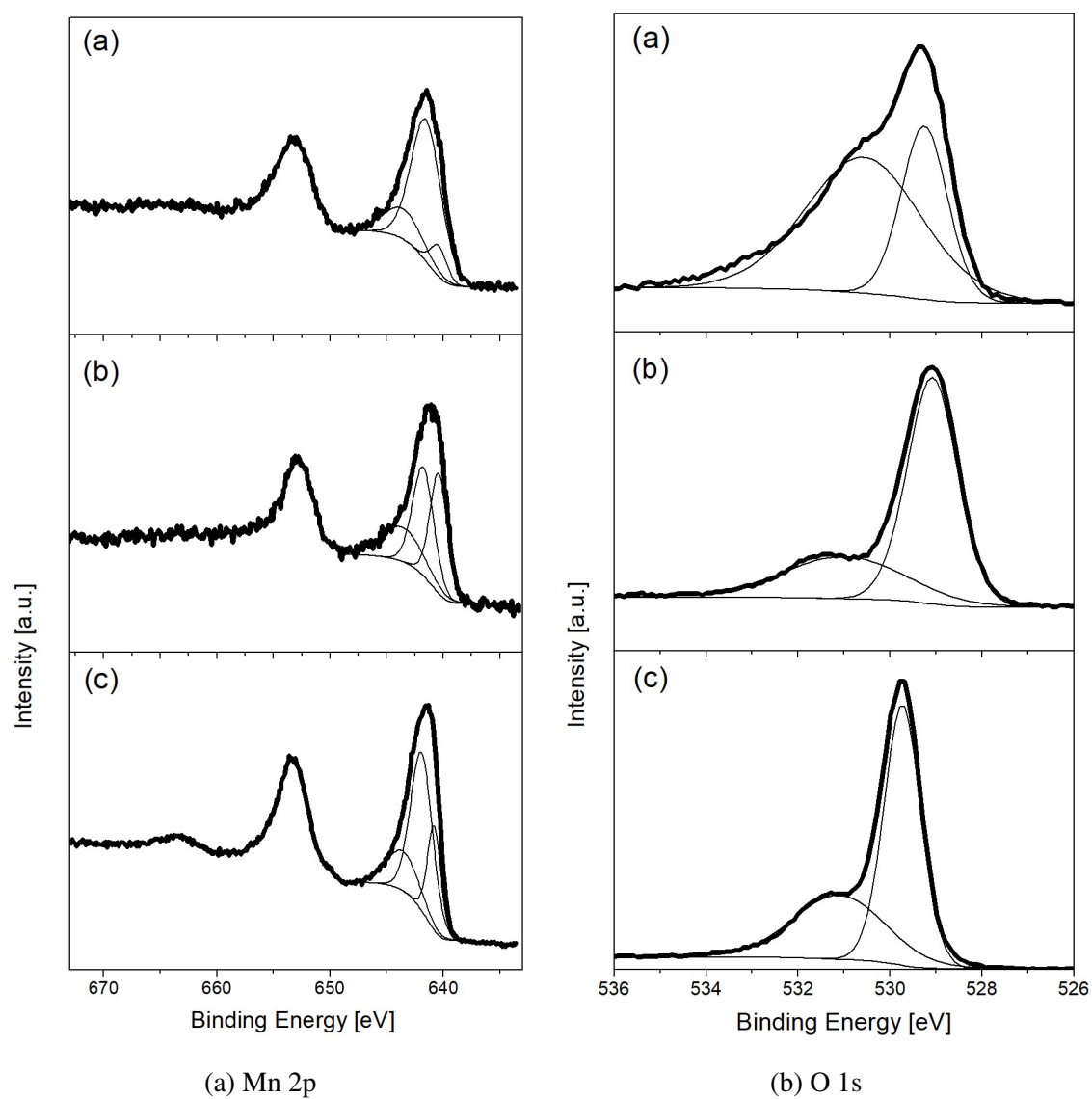


Fig. 3.4 XPS Spectra in the Mn 2p and O 1s core level regions, of samples (a)  $\text{Ce}_{0.25}\text{Mn}_{0.75}\text{O}_x$ , (b)  $\text{Ce}_{0.5}\text{Mn}_{0.5}\text{O}_x$  and (c)  $\text{MnO}_x$

For the XPS spectra in the Ce 3d region were evidenced multiple peaks corresponding to the Ce  $3d_{3/2}$  and Ce  $3d_{5/2}$ . The results obtained for both catalysts were very similar, with similar amounts of Ce (III) and Ce (IV), being the last one the species present in the highest proportion.

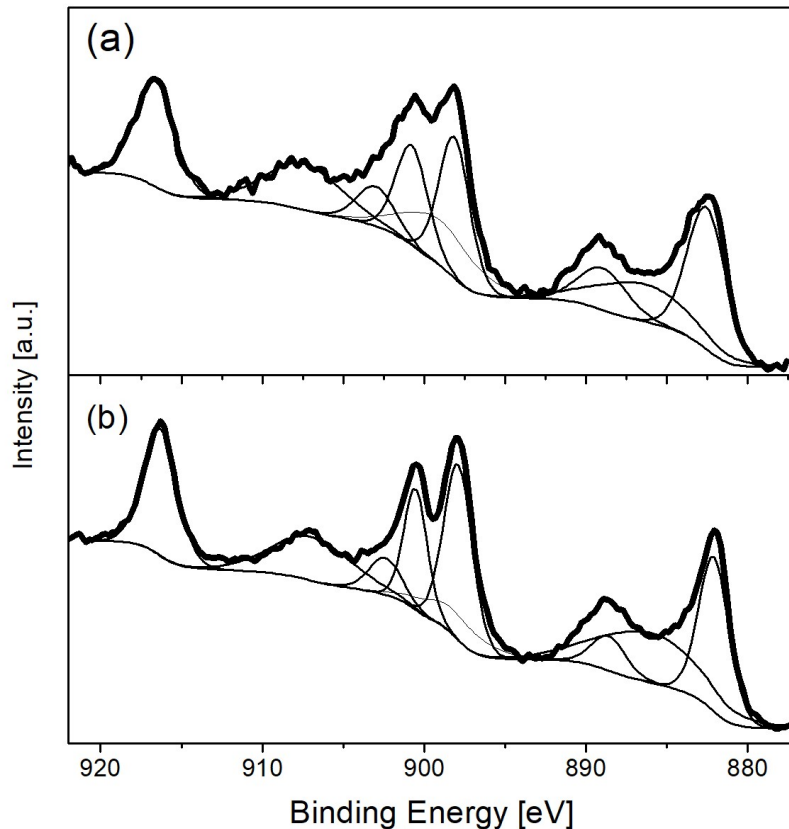


Fig. 3.5 XPS Spectra in the Ce 3d core level region, of samples (a)  $\text{Ce}_{0.25}\text{Mn}_{0.75}\text{O}_x$ , (b)  $\text{Ce}_{0.5}\text{Mn}_{0.5}\text{O}_x$

### 3.1.5 $\text{H}_2$ -TPR analysis

The  $\text{H}_2$ -TPR was performed to characterize the redox properties of the catalysts, which are required in the  $\text{NH}_3$ -SCR reactions. As it is reported in literature, the  $\text{MnO}_x$  reduction could take place in different steps. First, the  $\text{MnO}_2$  is reduced to nonstoichiometrically dispersed  $\text{MnO}_x$  ( $1.5 < x < 2$ , peak at  $T < 200^\circ\text{C}$ ), but it could also be reduced in the  $370\text{--}470^\circ\text{C}$  range, giving rise to two peaks (M-shape curve). Then, the  $\text{MnO}_x$  is reduced to  $\text{Mn}_2\text{O}_3$  (peak at  $200\text{--}350^\circ\text{C}$ ), which is reduced to  $\text{Mn}_3\text{O}_4$  (peak at about  $490^\circ\text{C}$ ) and further reduced to  $\text{MnO}$  (peak at about  $520^\circ\text{C}$ ). This last one is the final reduced state of  $\text{MnO}_x$ . Regarding the Ce, it is reported that the peak at about  $495^\circ\text{C}$  could be assigned to the reduction of surface  $\text{Ce}^{4+}$  to  $\text{Ce}^{3+}$  and the peak at temperatures higher than  $700^\circ\text{C}$  is due to the bulk reduction of ceria [23].

Nevertheless, peaks position is affected by several factors, such as the TPR analysis conditions, samples crystallinity, specific surface area and particle size. These factors could cause a shift in the position of the peaks [31].

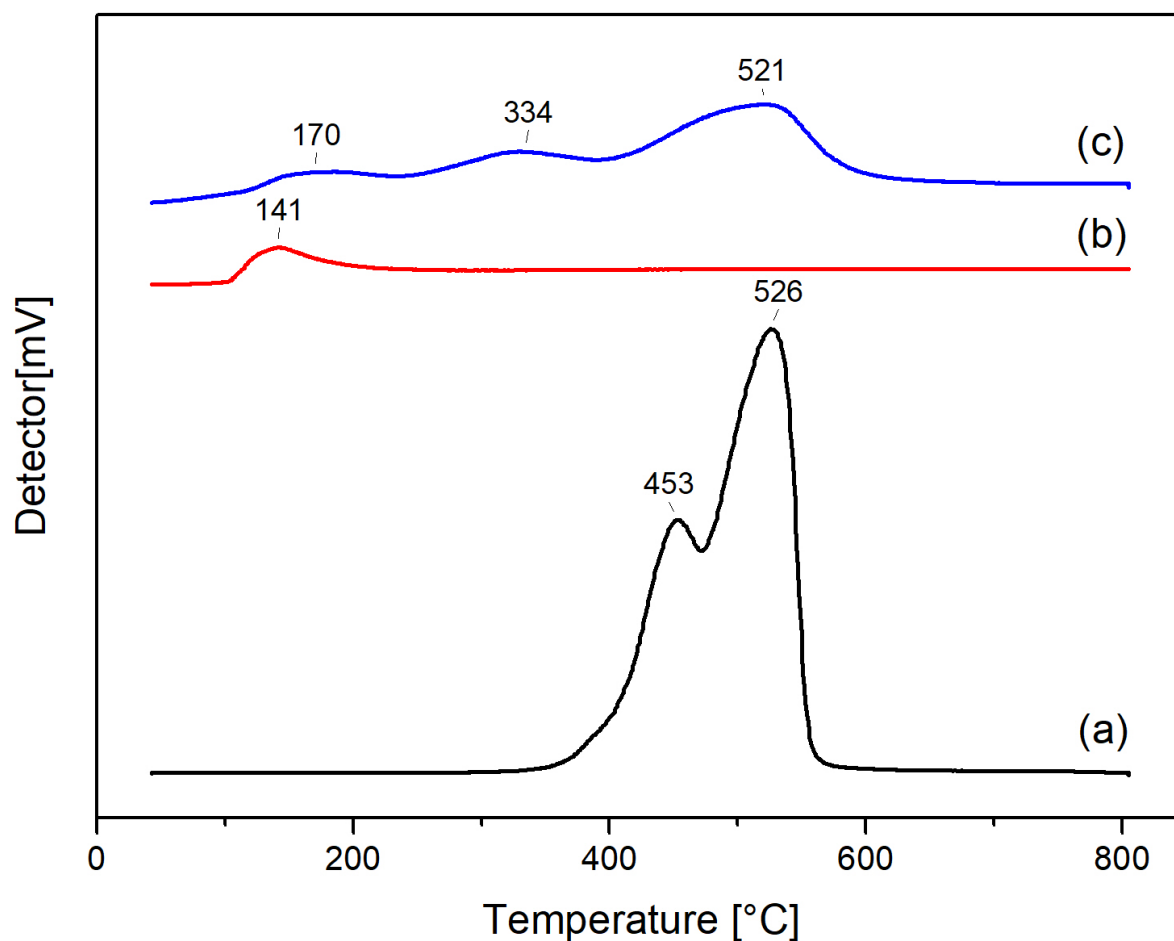


Fig. 3.6 TPR curves of samples  $\text{MnO}_x$  (a),  $\text{Ce}_{0.25}\text{Mn}_{0.75}\text{O}_x$  (b) and  $\text{Ce}_{0.5}\text{Mn}_{0.5}\text{O}_x$  (c).

In the results obtained, it is possible to see that the reduction of the Ce-based catalysts started in the same temperature range, but for the  $\text{Ce}_{0.25}\text{Mn}_{0.75}\text{O}_x$  it was observed just one peak (at  $141^\circ\text{C}$ ) attributed to the reduction of some  $\text{MnO}_2$  amorphous phase. In the case of  $\text{Ce}_{0.5}\text{Mn}_{0.5}\text{O}_x$  were observed three reduction peaks, the first one at low temperature ( $170^\circ\text{C}$ ) corresponding to the reduction of  $\text{MnO}_2$  amorphous phase, the second one at  $334^\circ\text{C}$  is attributed to the reduction of some other  $\text{MnO}_x$  phases present and the third one at  $521^\circ\text{C}$  represents the reduction of  $\text{Mn}_3\text{O}_4$ . On the other hand, the reduction of  $\text{MnO}_x$  started at higher temperatures, two peaks of higher intensity in comparison with the peaks obtained for the Ce-based catalysts were identified. The first one at  $453^\circ\text{C}$  corresponded to the reduction of  $\text{MnO}_2$  and the second one at  $526^\circ\text{C}$  is attributed to the reduction of  $\text{Mn}_3\text{O}_4$ . The shift in the temperature peak was probably due to the lower degree crystallinity of the catalysts in comparison with a pure sample.

Table 3.3 Quantity of  $\text{H}_2$  consumed

Catalyst	$\text{H}_2$ [ $\mu\text{mol/g}$ ]
$\text{MnO}_x$	3891.4
$\text{Ce}_{0.25}\text{Mn}_{0.75}\text{O}_x$	998.57
$\text{Ce}_{0.5}\text{Mn}_{0.5}\text{O}_x$	3231.94

In regard to the quantity of  $H_2$  consumed, reported in Table 3.3, the amount was considerably high in the case of  $MnO_x$  and  $Ce_{0.5}Mn_{0.5}O_x$  in comparison with the catalyst  $Ce_{0.25}Mn_{0.25}O_x$ , indicating that a greater quantity of oxide was reduce for these catalysts and the presence of better redox properties.

### 3.1.6 Temperature Programmed Desorption ( $NH_3$ -TPD)

Through the  $NH_3$ -TPD experiments (Fig.3.7) was possible to study the characteristics of the surface acid sites of the catalysts. These active sites for the  $NH_3$ -adsorption are constituted by surface oxygen species on which the adsorbed  $NH_3$  dissociates and can subsequently generate different products, such as  $N_2$ ,  $NO$ ,  $N_2O$  and  $NO_2$  under certain reaction conditions [51].

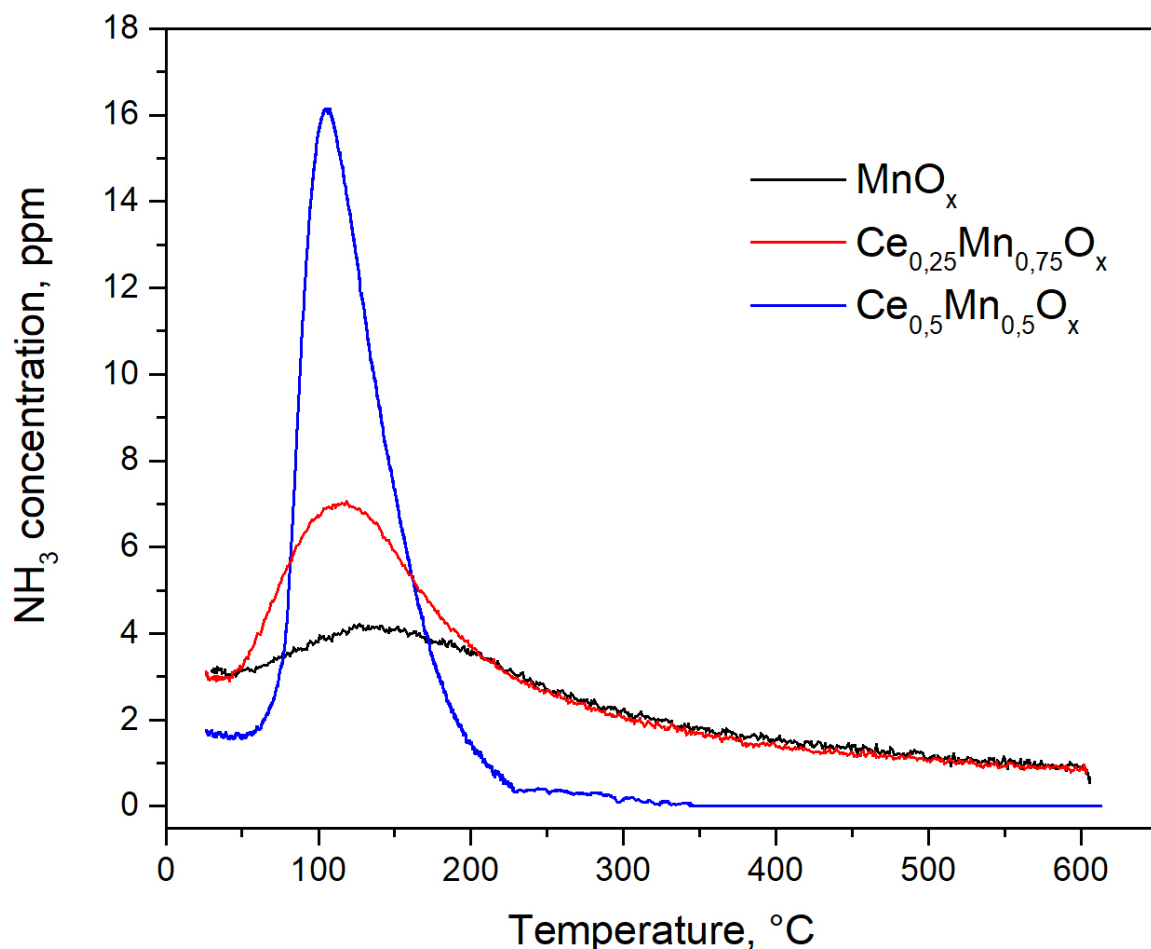


Fig. 3.7  $NH_3$ -TPD curves

All the catalysts presented only one desorption peak more or less at the same temperature, between  $100^\circ C$  and  $200^\circ C$ , which is a temperature range of great interest for the low-temperature SCR applications. Besides, as it is reported in literature, peaks located below  $300^\circ C$  are assigned to molecules adsorbed on Brønsted sites, while peaks at higher temperatures to molecules

coordinated by Lewis sites. Taking this into account, the catalysts acid sites can be classified as Brønsted type.

The intensity of the peak observed for the  $MnO_x$  was very small, indicating the poor adsorption capacity of this catalyst. In the case of  $Ce_{0.25}Mn_{0.75}O_x$ , the desorption started at about  $50^\circ C$ , the desorption peak was observed approximately at  $110^\circ C$  and it was more intense than the  $MnO_x$  peak, but its intensity was still small in comparison with the peak obtained for  $Ce_{0.5}Mn_{0.5}O_x$ , which showed the best acid characteristics.

As shown in Table 3.4 the total amount of ammonia adsorbed by the  $Ce_{0.25}Mn_{0.75}O_x$  and  $MnO_x$  was very similar but represents less than one half of the  $Ce_{0.5}Mn_{0.5}O_x$  adsorption capability. Also, for the three catalysts, the quantity physically adsorbed and consequently easily desorbed at room temperature was higher than the chemically adsorbed.

Table 3.4 Amounts of  $NH_3$  adsorbed

Sample	Total amount of adsorbed $NH_3$ [ $\mu mol/g$ ]	Amount of $NH_3$ adsorbed on weak acid sites [ $\mu mol/g$ ]	Amount of $NH_3$ adsorbed on strong acid sites [ $\mu mol/g$ ]
$MnO_x$	42.28	26.92	15.01
$Ce_{0.25}Mn_{0.75}O_x$	49.58	31.66	17.94
$Ce_{0.5}Mn_{0.5}O_x$	72.22	41.75	30.35

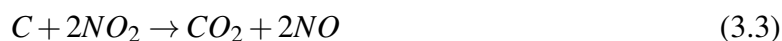
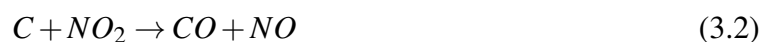
## 3.2 Catalytic activity measurements

### 3.2.1 NO oxidation

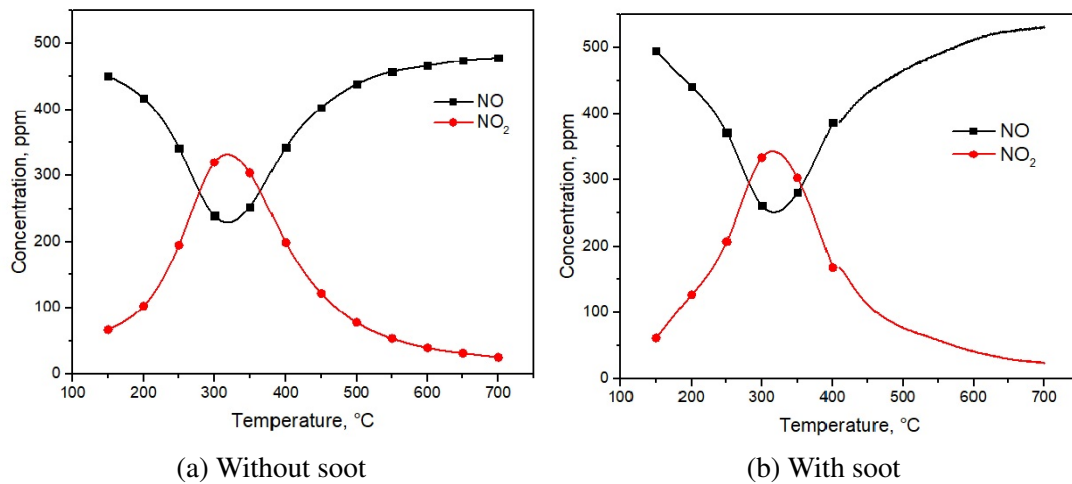
The NO oxidation reaction is described by the equation 3.1:



On the other hand, the reactions involved in  $NO_2$ -mediated soot oxidation are:

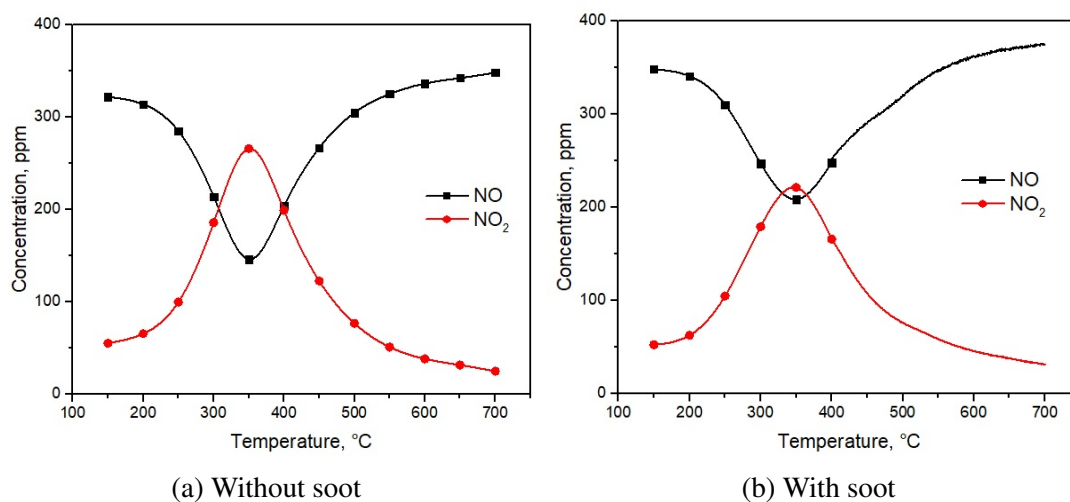


The last two reactions are known as C- $NO_2$ - $O_2$  cooperative reactions [16].

Fig. 3.8 NO oxidation  $\text{MnO}_x$ 

In Fig. 3.8 are reported the results obtained in the NO oxidation test without soot (a) and with soot (b), using  $\text{MnO}_x$  as catalyst. At low temperatures, as described by the equilibrium reaction, the  $\text{NO}_2$  formation is favored, only from 300 °C started the NO formation. In general, both profiles are very similar, but In the case with soot, between 300°C and 400°C the  $\text{NO}_2$  concentration decreased a little bit faster, and since it is reported in literature [52] that below 450°C the soot oxidation is driven by  $\text{NO}_2$ , it is possible that some part of the  $\text{NO}_2$  present was consumed in this reaction. Another indication of this is that the changes in the NO concentration were smaller than the changes of the  $\text{NO}_2$  concentration, not as it was expected from the equilibrium reaction where for each  $\text{NO}_2$  that is consumed one NO is produced, which means that another reaction was taking place. Also, the final concentration of NO was higher than the initial concentration, this due to the fact that an additional amount of NO was produced in the soot combustion.

In the Fig.3.9 is possible to see the results for the test performed with  $\text{Ce}_{0.25}\text{Mn}_{0.75}\text{O}_x$ .

Fig. 3.9 NO oxidation  $\text{Ce}_{0.25}\text{Mn}_{0.75}\text{O}_x$

In this case, the  $\text{NO}_2$  concentration increased until  $350^\circ\text{C}$ , after this temperature the formation of  $\text{NO}$  was favored. The more significant difference between the profile obtained without soot (a) and with its presence (b) was evidenced at  $350^\circ\text{C}$  when the concentration of  $\text{NO}_2$  was bigger when there wasn't soot in the system. This indicates that a part of the  $\text{NO}_2$  was used in the soot oxidation.

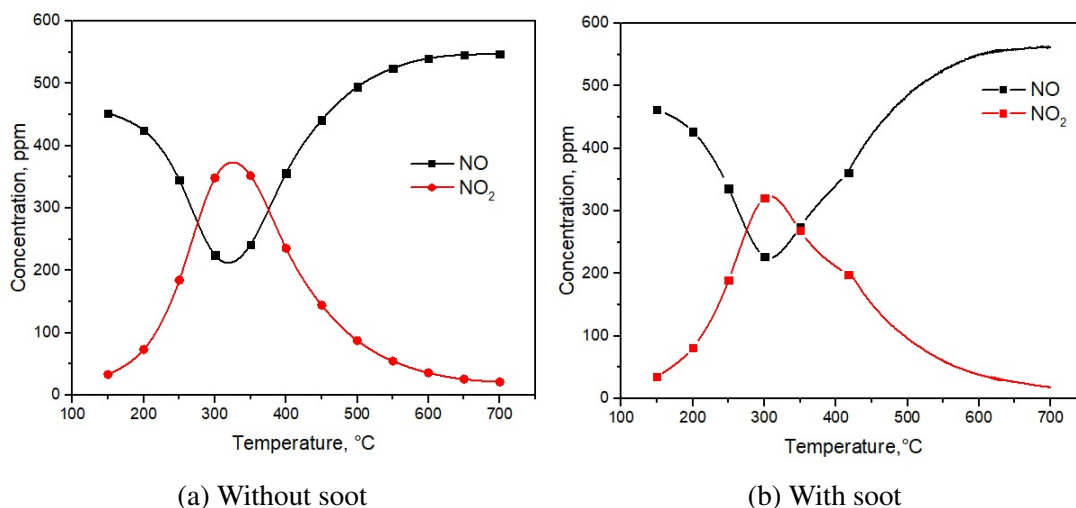


Fig. 3.10 NO oxidation  $\text{Ce}_{0.5}\text{Mn}_{0.5}\text{O}_x$

As can be appreciated in Fig.3.10 with the  $\text{Ce}_{0.5}\text{Mn}_{0.5}\text{O}_x$  catalyst the  $\text{NO}$  was oxidized until  $300^\circ\text{C}$ , after this point the  $\text{NO}_2$  decomposition took place. Also, in the  $300^\circ\text{C}$ - $400^\circ\text{C}$  temperature range the  $\text{NO}_2$  concentration was higher for the case without soot as a part of it was consumed by the soot oxidation reaction. This consumption was more evident between  $300^\circ\text{C}$  and  $350^\circ\text{C}$ , at  $400^\circ\text{C}$  the difference was smaller. After  $400^\circ\text{C}$  due to the similarity of both profiles, the predominant reaction is the  $\text{NO}_2$  decomposition.

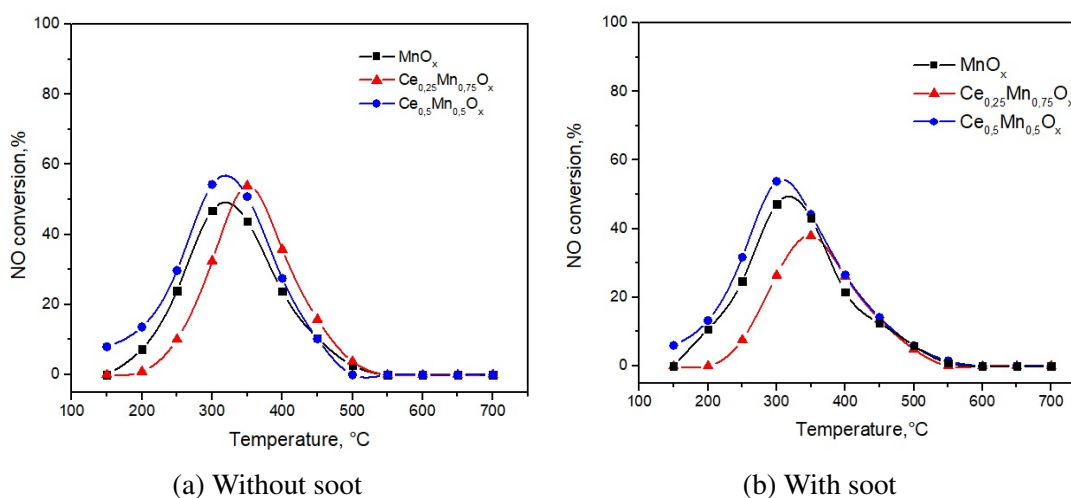


Fig. 3.11 NO conversion

In Fig.3.11 there is a comparison of the NO conversion without and with soot. On the first case, the conversion reached its maximum value (around 60%) at 300°C with the catalysts  $MnO_x$  and  $Ce_{0.5}Mn_{0.5}O_x$ , according to the concentration profiles reported before. The conversion values obtained for both catalysts were very similar in the whole temperature range. With the  $Ce_{0.25}Mn_{0.75}O_x$  the conversion values were lower until 350°C, where the maximum value was reached (approximately 50%), then the conversions were slightly over the values obtained for the other two catalysts. From 500°C the conversion of NO was zero for all the catalysts.

In presence of soot there was a diminution in the conversion values. For  $Ce_{0.5}Mn_{0.5}O_x$  is evidenced a decreased in the conversion at 300°C and 350°C, from 400°C the values were very similar in both cases. For the other two catalysts, the conversion values were smaller from 250°C until 400°C. The diminution in the NO conversion was because its concentration increased as a consequence of the contemporary reaction between the  $NO_2$  and the soot, where NO is a product. Among all the catalysts tested, the  $Ce_{0.25}Mn_{0.75}O_x$  was the one where more  $NO_2$  was also consumed in the soot oxidation reaction, since the NO conversion decreased more than for the other catalysts.

### 3.2.2 $NH_3$ oxidation

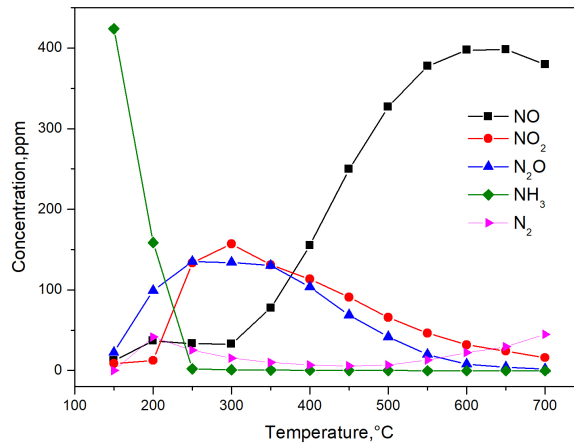
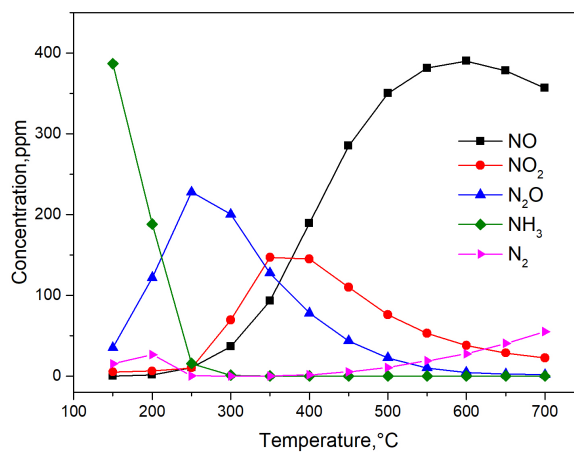
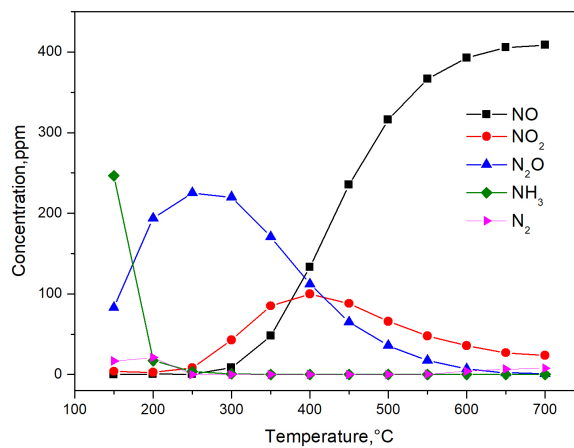
The ammonia oxidation, depending on the operating conditions and the catalyst used, can follow the next reactions:



The reaction described by the equation 3.8 is considered as a potentially approach for the abatement of  $NH_3$  pollution due to conversion of toxic ammonia into nitrogen [53, 54].

If there is formation of NO, it is possible to have also the equilibrium reaction ( equation 3.1) with  $NO_2$ .

The Fig.3.12 shows the results obtain for the  $NH_3$  oxidation using  $MnO_x$  (a),  $Ce_{0.25}Mn_{0.75}O_x$  (b) and  $Ce_{0.5}Mn_{0.5}O_x$  (c).

(a) MnO<sub>x</sub>(b) Ce<sub>0.25</sub>Mn<sub>0.75</sub>O<sub>x</sub>(c) Ce<sub>0.5</sub>Mn<sub>0.5</sub>O<sub>x</sub>Fig. 3.12 NH<sub>3</sub> Oxidation

In the results obtained using MnO<sub>x</sub> as catalyst it is possible to see that the NH<sub>3</sub> concentration decreased rapidly as the temperature increased. From 250 °C all the NH<sub>3</sub> fed was consumed. At 150°C and 200°C the principal product of the NH<sub>3</sub> oxidation was N<sub>2</sub>O, according to the equation 3.7. From 200°C there was a higher production of NO<sub>2</sub>, being one of the main products along with N<sub>2</sub>O. The NO started to be formed at 200°C and from 350°C its concentration increased

considerably, as it was being produced from both the  $\text{NO}_2$  decomposition and the  $\text{NH}_3$  oxidation. Regarding the  $\text{N}_2$ , it was produced in lower quantities in comparison with the other compounds. At  $150^\circ\text{C}$  the concentration reached a maximum, after this temperature the values decreased as the side reactions prevailed, at  $550^\circ\text{C}$  the concentration started to raise again.

For  $\text{Ce}_{0.25}\text{Mn}_{0.75}\text{O}_x$ , the  $\text{NH}_3$  was oxidized at a rate very similar with the one observed for  $\text{MnO}_x$ , but unlike this catalyst a complete conversion was reached at  $300^\circ\text{C}$ . The  $\text{N}_2\text{O}$  was the main product until  $300^\circ\text{C}$ , reaching maximum concentration value of 228 ppm. The  $\text{NO}$  and  $\text{NO}_2$  concentrations started to raise at  $250^\circ\text{C}$ . The quantity of  $\text{NO}$  increased constantly until 390 ppm at  $600^\circ\text{C}$  while the  $\text{NO}_2$  increased just until 147 ppm at  $350^\circ\text{C}$ . The  $\text{N}_2$  concentration increased until  $200^\circ\text{C}$ , after this point the value declined until zero and only at  $500^\circ\text{C}$  started to raise again reaching a value of 50 ppm at  $700^\circ\text{C}$ .

The  $\text{NH}_3$  was consumed faster with  $\text{Ce}_{0.5}\text{Mn}_{0.5}\text{O}_x$  than with the  $\text{MnO}_x$  catalyst until  $200^\circ\text{C}$  but reached a complete conversion at  $300^\circ\text{C}$ . The quantity of  $\text{N}_2\text{O}$  raised until 225 ppm, being the main product of the oxidation reaction until  $350^\circ\text{C}$ , after this temperature the  $\text{NO}$  became the compound present in the highest concentration, whose concentration increased from  $300^\circ\text{C}$  reaching its maximum value, 408 ppm, at  $700^\circ\text{C}$ . The  $\text{NO}_2$  started to be produced from  $250^\circ\text{C}$  and from  $400^\circ\text{C}$  its concentration decreased according to the equilibrium reaction, where the  $\text{NO}$  formation is favored at high temperatures. On the other hand, the  $\text{N}_2$  was only produced at  $150^\circ\text{C}$  and  $200^\circ\text{C}$  in a small quantity.

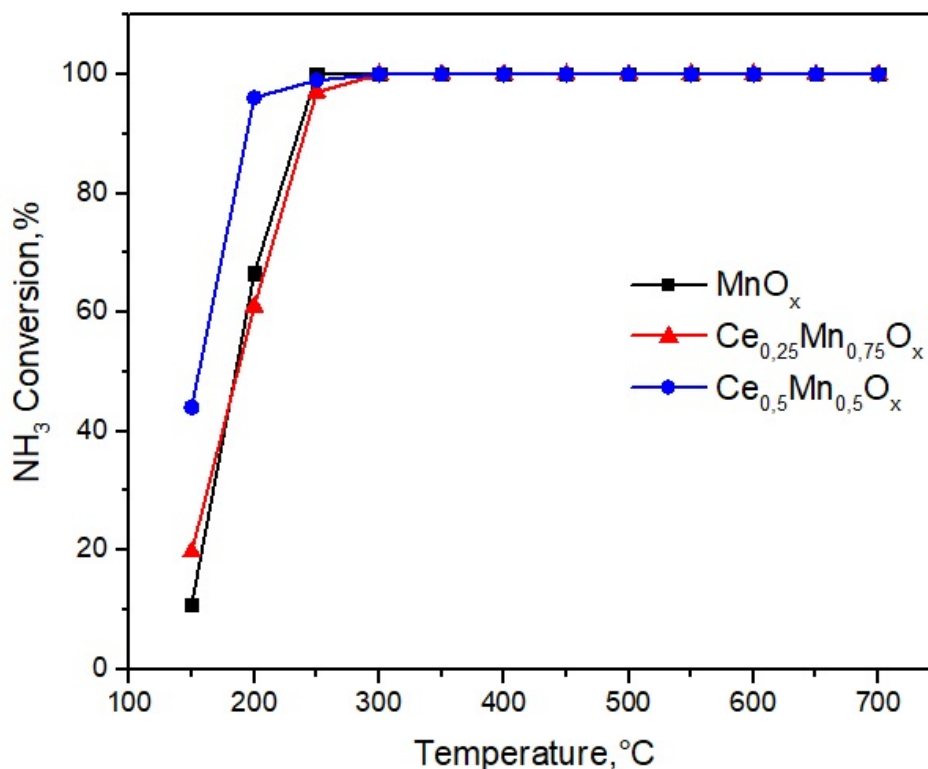


Fig. 3.13  $\text{NH}_3$  conversion

In the Fig. 3.13 is reported the variation of the NH<sub>3</sub> conversion with the temperature. At 150 °C and 200°C the highest conversions were reached with Ce<sub>0.5</sub>Mn<sub>0.5</sub>O<sub>x</sub>, 44% and 96% respectively. For the other two catalysts the conversion values were very similar, as it was expected from the tendency of the concentration values shown before. At 250 °C a conversion of 100% was reached with the MnO<sub>x</sub> catalysts. From 300 °C the conversion was 100% for all the catalysts.

All the catalyst tested showed a high activity in the ammonia oxidation reaction since the light-off temperature was lower than 200 °C and an almost complete conversion was reached at 250°C. However, the activity at lower temperatures was very poor, with conversions of 20% and 10% for the Ce<sub>0.25</sub>Mn<sub>0.75</sub>O<sub>x</sub> and MnO<sub>x</sub> respectively, with the Ce<sub>0.5</sub>Mn<sub>0.5</sub>O<sub>x</sub> catalyst the results were a little better with a conversion over 40

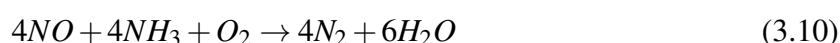
Although high conversions were reached with the catalysts, the selectivity towards the desired reaction (equation 3.8) was very poor, as it could be seen in the concentration profiles, where the concentration values for the N<sub>2</sub> were lower in comparison with the other compounds produced. Also, at high temperatures the production of NO<sub>x</sub> was predominant.

Regarding the by-products, the formation of N<sub>2</sub>O was enhanced by the presence of Ce since for these catalysts the generation of this compound was higher than the one obtained with MnO<sub>x</sub>, even if the conversions were similar. The decrease in the concentration of N<sub>2</sub>O was because at high temperatures it is not very stable, and probably its formation is not favored after certain temperature. The NO<sub>2</sub> was also produced from the NH<sub>3</sub> oxidation, the quantity formed with MnO<sub>x</sub> at low temperatures was higher than with the other catalysts. Finally, for all the catalysts there was a considerable formation of NO, as a result of either the NO<sub>2</sub> decomposition or the NH<sub>3</sub> oxidation (equation 3.6).

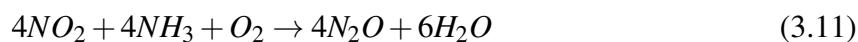
Comparing the results obtained with MnO<sub>x</sub> and Ce<sub>0.25</sub>Mn<sub>0.75</sub>O<sub>x</sub>, the presence of Ce in that proportion did not improve the activity of the catalyst for this specific reaction, instead the quantity of by-products was higher. On the other hand, the use of Mn and Ce in equal proportions enhanced the NH<sub>3</sub> conversion, even if there was a higher formation of N<sub>2</sub>O it was possible to obtain conversions greater than 90% from 200°C while with the other catalysts at this temperature the conversion was slightly over 60%.

### 3.2.3 Standard SCR

The standard SCR is described by the reaction:



Other reaction pathways can occur as well, leading to the formation of undesired products. These reactions may include a partial reduction of NO<sub>x</sub> (equations 3.11-3.13) or the NH<sub>3</sub> oxidation (equations 3.6-3.9).



The Fig.3.14 (a) shows the results obtained for the SCR with  $MnO_x$  as catalyst. At 150°C the conversion was low but with the temperature increase the reaction rate was considerably higher. Between 150°C and 250°C, the consumption of  $NH_3$  was larger than that of NO due to the presence of side reactions, specifically in the 200°C-250°C the small change in the NO concentration indicates that  $N_2O$  and the  $NO_2$  were produced from the ammonia oxidation. From 300°C the  $NO_2$  concentration decreased as the NO quantity raised, according to the equilibrium reaction between these two compounds. Regarding  $N_2$ , the concentration reached a maximum at 200°C (around 200 ppm), after this temperature the value decreased and stabilized at a value close to zero, at 600°C there was a slight increment. At the end of the test the NO was the component in greater quantity.

For the  $Ce_{0.25}Mn_{0.75}O_x$  catalyst, as it is observed in Fig. 3.14 (b), there was no significant formation of  $N_2$  until 450°C, and the quantity formed was very small. The equimolar consumption present between 150°C and 200°C indicates that an incomplete NO reduction was taking place. From this temperature, the  $NH_3$  consumption was larger than the corresponding to the NO as a result of the  $NH_3$  oxidation reactions. The  $NO_2$  concentration rose from 250°C until 400°C, point since where the value decrease. Besides, the NO concentration continuously increased from 250°C, but it reached a lower value in comparison with the other catalysts.

The  $Ce_{0.5}Mn_{0.5}O_x$  catalyst (Fig. 3.14 (c)) was more active at low temperatures, the concentrations of NO and  $NH_3$  at 150 °C were considerably less than those corresponding to the feeding. At 150°C the main product was  $N_2$ , but after this temperature the quantity formed decreased until value very close to zero at 250°C, only after 550°C the concentration rose again. Between 150°C and 200°C there was an equimolar consumption of NO and  $NH_3$ , but since there was a considerable increase in the  $N_2O$  concentration, along with the standard SCR reaction, an incomplete reduction of NO also took place. From 250°C all the ammonia was being consumed, and the NO and  $NO_2$  concentrations started to rise, the first one was continuously produce until reach a maximum value at 650°C while the second one was just produced until 350°C, after this point its concentration decreased until 28 ppm at 750°C.

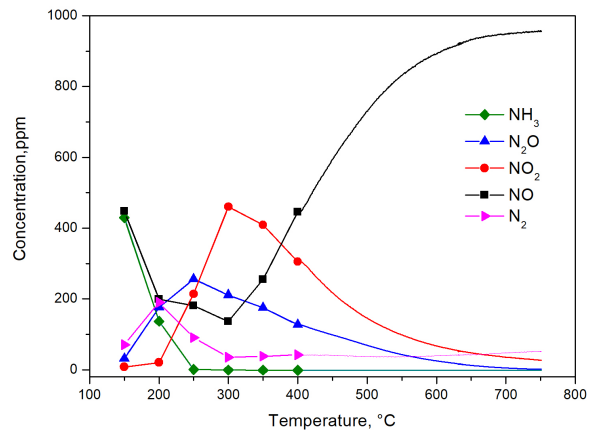
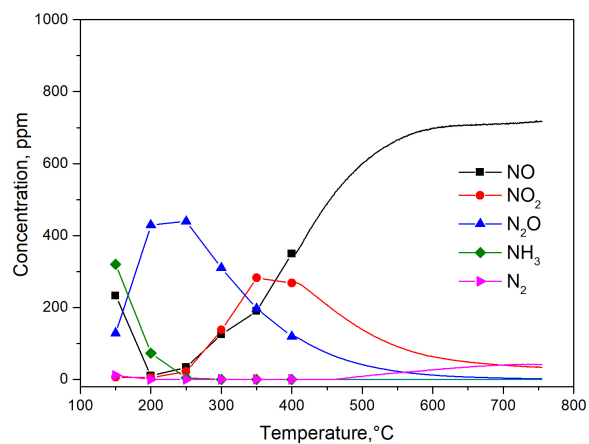
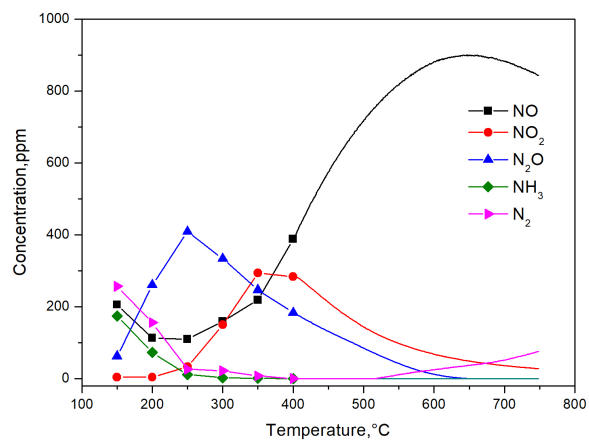
(a) MnO<sub>x</sub>(b) Ce<sub>0.25</sub>Mn<sub>0.75</sub>O<sub>x</sub>(c) Ce<sub>0.5</sub>Mn<sub>0.5</sub>O<sub>x</sub>

Fig. 3.14 Standard SCR

The results showed that the SCR reaction took place at a higher velocity with the Ce<sub>0.5</sub>Mn<sub>0.5</sub>O<sub>x</sub> catalyst. Regarding the N<sub>2</sub>O production, with Ce<sub>0.25</sub>Mn<sub>0.75</sub>O<sub>x</sub> a higher concentration was reached, over 400 ppm, and this added to the fact that there was no formation of N<sub>2</sub> for almost all the temperature range, or the concentration was too low, indicates that the SCR reaction was not taking place, instead the side-reactions, such as an incomplete reduction of NO and the

NH<sub>3</sub> oxidation, were prevalent. Otherwise, with MnO<sub>x</sub> greater quantities of NO and NO<sub>2</sub> were formed.

Since from the concentration profiles was evidenced that a de-NO<sub>x</sub> activity only could take place until 400°C approximately, to do a better comparison of the catalysts performance the N<sub>2</sub> selectivity, the NO<sub>x</sub> and NH<sub>3</sub> conversions were graphed as a function of the temperature, for the 150°C-400°C range.

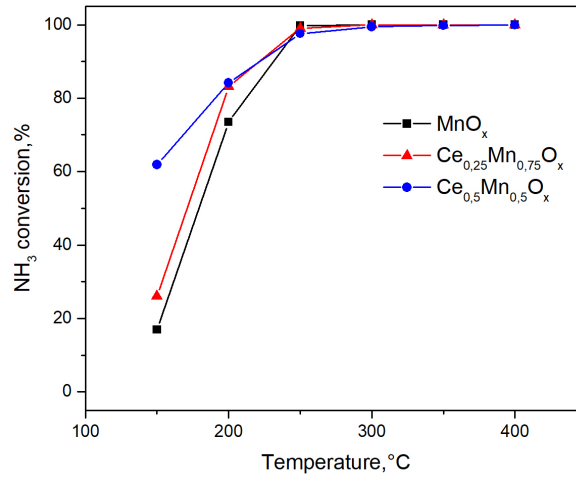
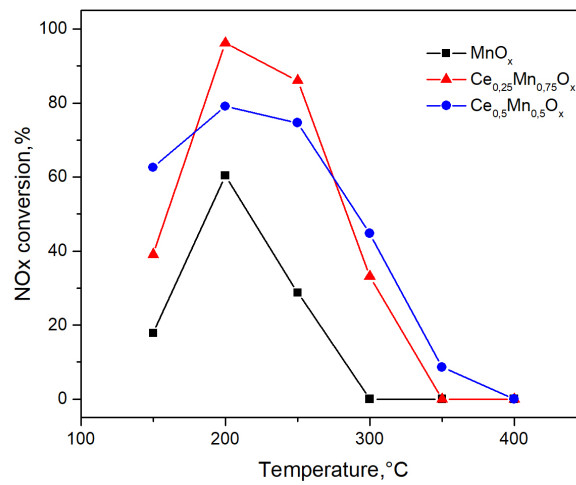
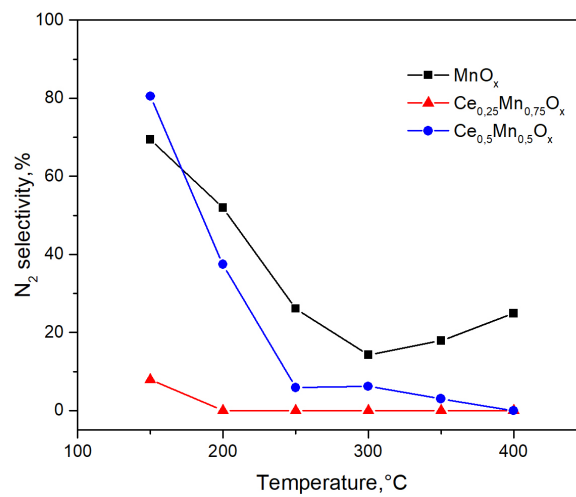
Regarding the NH<sub>3</sub> conversion, reported in the Fig. 3.15 (a), for all the catalysts the conversion was approximately 100% at 250 °C. For MnO<sub>x</sub> the conversion was very low at 150°C but it rose very quickly as the temperature increased, a similar tendency was obtained with Ce<sub>0.25</sub>Mn<sub>0.75</sub>O<sub>x</sub> but the values were slightly higher. Instead, with Ce<sub>0.5</sub>Mn<sub>0.5</sub>O<sub>x</sub> greater conversions were reached at low temperatures.

The highest NO<sub>x</sub> conversions (Fig.3.15 (b)) were reached with Ce<sub>0.25</sub>Mn<sub>0.75</sub>O<sub>x</sub>, 96% at 200°C and 86% at 250°C, while the MnO<sub>x</sub> was the catalyst with the least activity. At 200 °C the conversion for all the three catalysts reached the maximum value, after this temperature the conversion fell, decreasing in a more pronounced way for the MnO<sub>x</sub>, reaching a conversion of zero already at 300°C, instead, the Ce<sub>0.25</sub>Mn<sub>0.75</sub>O<sub>x</sub> catalyst was able to convert the NO<sub>x</sub> until 350 °C and Ce<sub>0.5</sub>Mn<sub>0.5</sub>O<sub>x</sub> until 400°C, being the catalyst with the wider conversion range.

As shown in Fig.3.15 (c) , the catalysts did not show a high selectivity towards the formation of N<sub>2</sub>, as was expected from the considerable formation of by-products evidenced in the concentration profiles. In general the MnO<sub>x</sub> catalyst was the most selective one. The Ce<sub>0.25</sub>Mn<sub>0.75</sub>O<sub>x</sub> catalyst only had a selectivity value different from zero at 150°C, an even at this temperature the value was very low. Ce<sub>0.5</sub>Mn<sub>0.5</sub>O<sub>x</sub> had a maximum value at 150°C, 81%, after this temperature the selectivity rapidly decreased until 250 °C then it declined in a more gradually way up to 0 at 400°C.

From the results obtained with the three catalysts it is possible to say the SCR reaction was not the principal reaction, side-reactions as the incomplete NO reduction and the NH<sub>3</sub> oxidation played an important role and after 200°C became predominant. Also, the NO<sub>x</sub> conversions showed that the greatest values were reached with Ce<sub>0.25</sub>Mn<sub>0.75</sub>O<sub>x</sub> but its poor selectivity allowed to conclude that the presence of Ce in that proportion does not represent an improvement compared with the manganese oxide, even if the catalyst was more active.

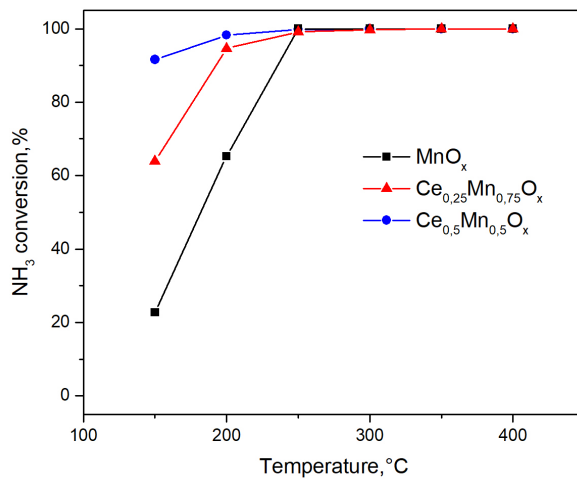
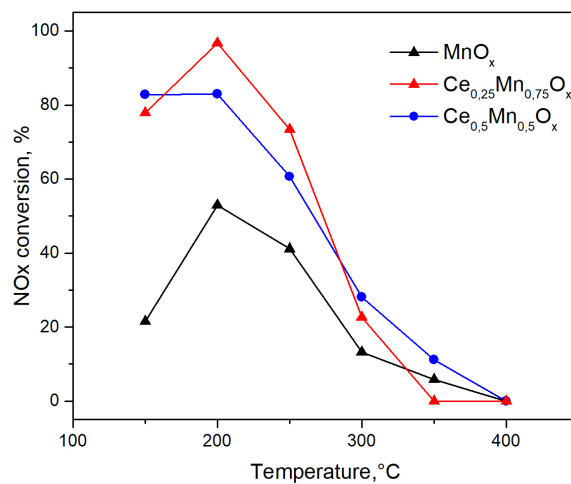
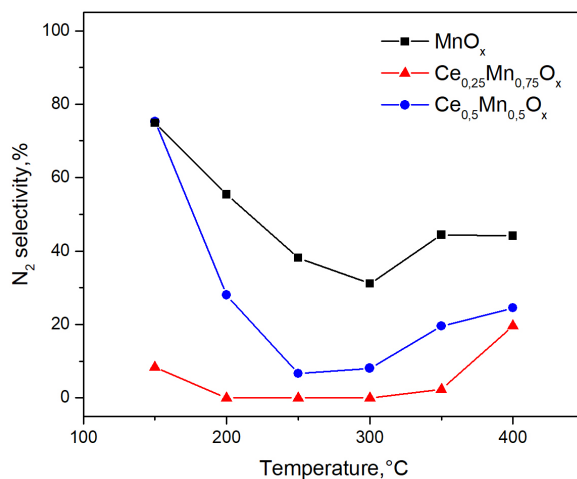
Finally, even if the catalysts did not show the best performance for the SCR, since they were too oxidative, the best between them was the Ce<sub>0.5</sub>Mn<sub>0.5</sub>O<sub>x</sub> , this means that maybe better performances could be reached with a higher Ce content, it is necessary though to improve the selectivity.

(a)  $\text{NH}_3$  conversion(b)  $\text{NO}_x$  conversion(c)  $\text{N}_2$  selectivityFig. 3.15 Standard SCR:  $\text{NH}_3$  and  $\text{NO}_x$  conversion,  $\text{N}_2$  selectivity

### 3.2.4 Standard SCR in soot presence

In presence of soot, the catalyst that showed a higher conversion of ammonia (Fig.3.16 (a)) was the  $Ce_{0.5}Mn_{0.5}O_x$  reaching a value of 90% at 150°, followed by  $Ce_{0.25}Mn_{0.75}O_x$  and  $MnO_x$  whose performances improved considerably as the temperature raised. For the  $NO_x$  conversion (results in Fig.3.16 (b)), at 150°C the catalysts with the highest activity were  $Ce_{0.25}Mn_{0.75}O_x$  and  $Ce_{0.5}Mn_{0.5}O_x$  with conversions around 80%, for  $MnO_x$  the conversion at this temperature was about 20%. At 200°C the conversion increased for  $MnO_x$  and  $Ce_{0.25}Mn_{0.75}O_x$ , being almost 100% for the latter, while the value remained equal for the other catalyst. After this temperature the conversion started to decrease for all the catalysts until a value of zero was reached at 350°C for  $Ce_{0.25}Mn_{0.75}O_x$  and at 400°C for the other two. Regarding the  $N_2$  selectivity (Fig.3.16 (c)), the results obtained showed a poor selectivity, mainly after 150°C, from where there was a diminution in the value, after 300°C the selectivity increased but the value remained small.

Considering the results obtained, the presence of Ce clearly increased the catalytic activity mainly in the 150°C-200°C temperature range, but for the case of the  $Ce_{0.25}Mn_{0.75}O_x$  catalyst this rise led to a notable decrease in the selectivity. The use of Ce in the same percentage as the Mn represents an improvement in comparison with the other two catalysts. Moreover, the low values of selectivity indicated that from 200°C the presence of competitive reactions was significant. Also, for the three catalysts the temperature range where there was  $DeNO_x$  activity was very small and as consequence there was a considerable  $NO_x$  generation, as indicates the conversion of 0%.

(a) NH<sub>3</sub> conversion(b) NO<sub>x</sub> conversion(c) N<sub>2</sub> selectivityFig. 3.16 Standard SCR + soot: NH<sub>3</sub> and NO<sub>x</sub> conversion, N<sub>2</sub> selectivity

In order to understand better the influence of the soot presence on the SCR reaction, a comparison between the performance with and without soot was made for each catalyst.

• MnO<sub>x</sub> catalyst:

In the Fig.3.17 are reported the results obtained for the SCR run with (a) and without soot (b) in the 150°C-400°C range. As it can be seen, for both cases the NH<sub>3</sub> was consumed at higher rate than the NO, indicating the presence of side-reactions. Between 150°C and 200°C, due to the almost equimolar consumption of NH<sub>3</sub> and NO, and the higher values of N<sub>2</sub> concentration in comparison with the N<sub>2</sub>O, it is clear that the SCR reaction was dominant, but after 200°C the low changes in the NO concentration make evident the presence of other competitive reactions. Also, there was a NO<sub>x</sub> abatement until 200°C, after this point their concentration increased constantly either by the generation of NO<sub>2</sub> or NO.

For both cases, the N<sub>2</sub>O generation was very similar but the amount of N<sub>2</sub> produced was higher in the whole temperature range when the soot was present in the system. The latter could have been produced either by the SCR reaction or the NH<sub>3</sub> oxidation, the lower consume of NO especially after 200°C and the similar N<sub>2</sub>O concentration values suggest that the increase in the N<sub>2</sub> production was due to the NH<sub>3</sub> oxidation (equation 3.8) and not because the standard SCR was more dominant in this temperature range.

Regarding the NO, it was consumed at a higher rate until 300 °C in both cases. Particularly, between 250°C and 300°C the change in the concentration was smaller for the case with soot. After 300°C the quantity started to increase, at 400°C the concentrations values were very similar for the run with and without soot. On the other hand, the NO<sub>2</sub> reached a higher concentration when the SCR was performed without soot, this because the NO<sub>2</sub> was reacting with the NH<sub>3</sub> according to the fast SCR reaction, producing N<sub>2</sub>. Also, a part could have been consumed in the soot oxidation.

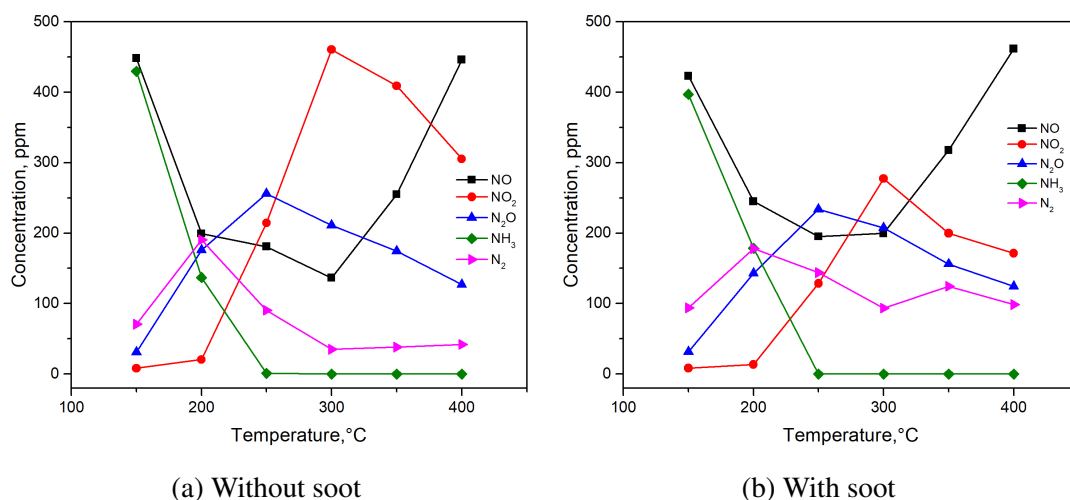


Fig. 3.17 Standard SCR MnO<sub>x</sub> catalyst

The N<sub>2</sub> selectivity and the NH<sub>3</sub> and NO<sub>x</sub> conversion were compared too. The Fig. 3.18 (a) shows that for activity test made with soot the selectivity was always higher due to the more quantity of N<sub>2</sub> formed. The NO<sub>x</sub> and NH<sub>3</sub> conversion are reported in Fig.3.18 (b) Only at

150°C the NH<sub>3</sub> conversion was higher for the case with soot, for the other temperatures the amount of NH<sub>3</sub> consumed was greater when there was not soot present, but for both cases a 100% conversion was reached at 250°C. For the NO<sub>x</sub> conversion the value was slightly higher at 150°C when there was soot, then the value increased for both cases but only until 200°C, being higher at this temperature for the case without soot (almost 60%), after it decreased as the NO and NO<sub>2</sub> formation raised, but the conversion values were higher in the presence of soot. The NO<sub>x</sub> conversion became 0 at 300°C when there was not soot present while for the other case it reached that value at 400°C.

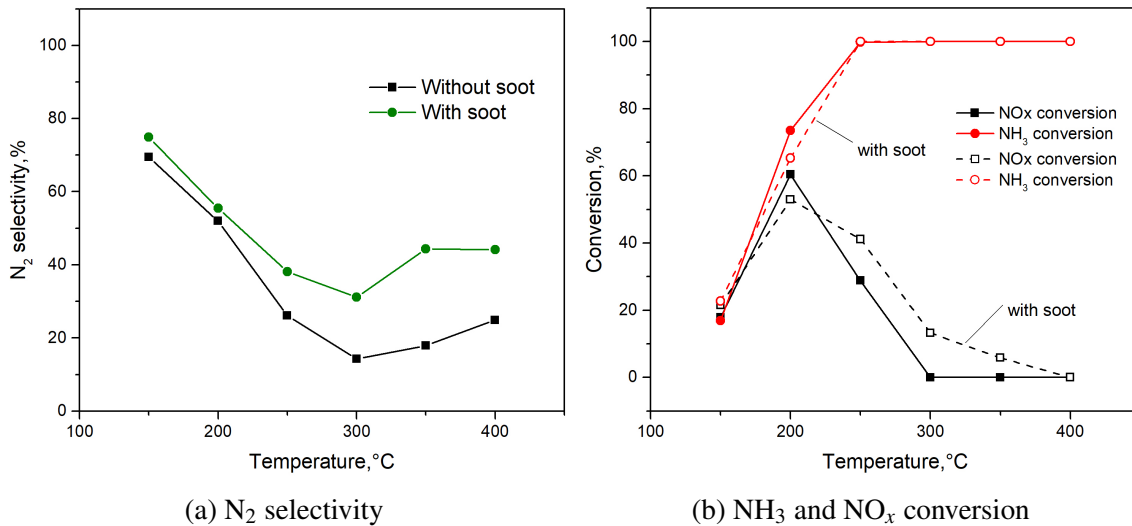
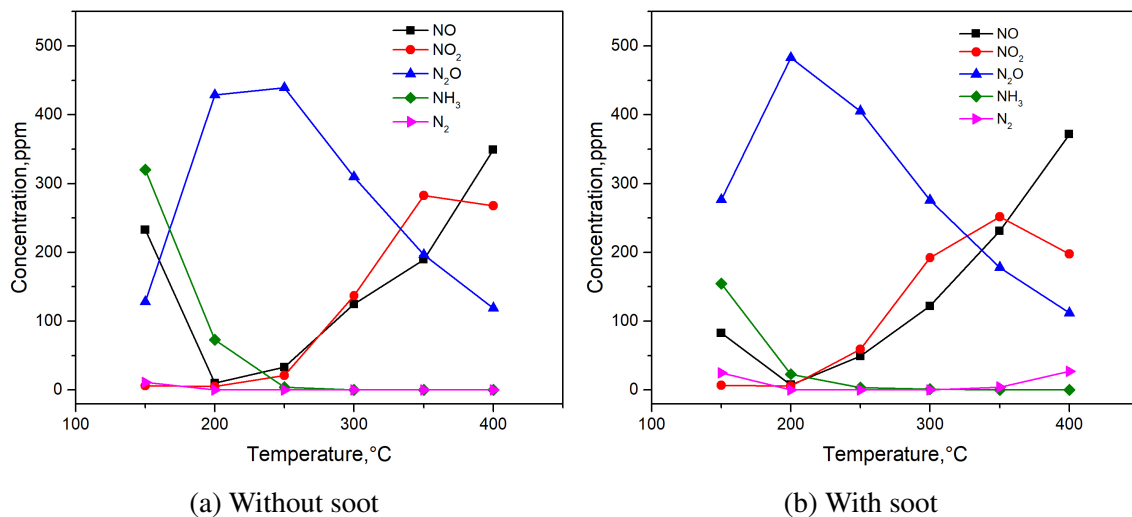


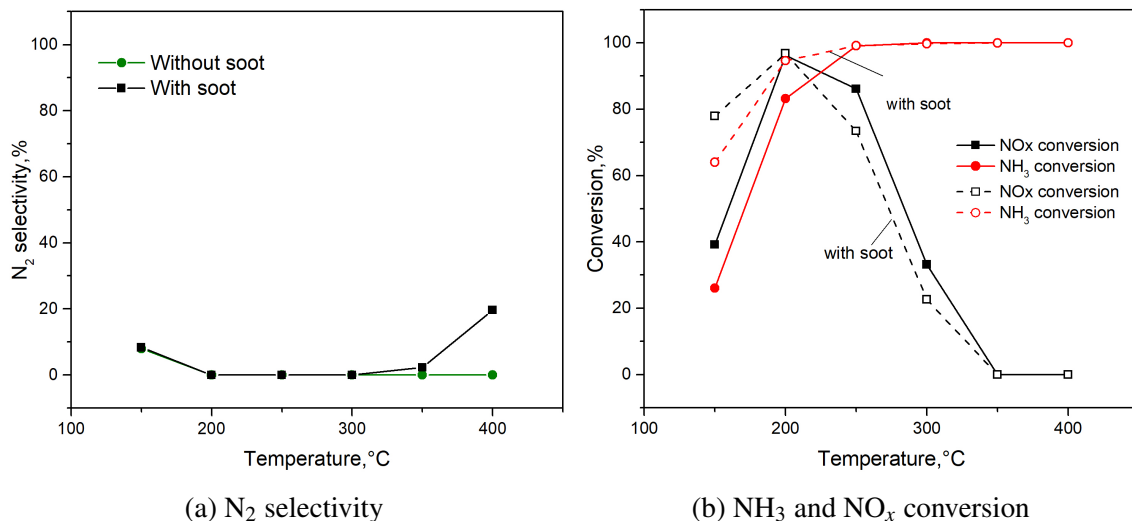
Fig. 3.18 Standard SCR MnO<sub>x</sub> catalyst with and without soot: (a) N<sub>2</sub> selectivity, (b) NH<sub>3</sub> and NO<sub>x</sub> conversion.

#### • Ce<sub>0.25</sub>Mn<sub>0.75</sub>O<sub>x</sub> catalyst:

For this catalyst, as it can be seen in Fig.3.19, there was a higher activity at low temperatures when the soot was present but a considerable amount of the reagents was consumed in side reactions, as indicates the greater quantity of N<sub>2</sub>O formed and the small concentration of N<sub>2</sub>. For the case without soot the NO<sub>2</sub> concentration reached a slightly over the corresponding for the case with soot, but the NO concentration was very similar for both, which indicates that more NH<sub>3</sub> was oxidized to N<sub>2</sub>O. Between 250°C and 300°C, in the case with soot, the quantity produced of NO<sub>2</sub> was higher as well as in the 350°C-400°C temperature range its consumption was higher for this case too. Because the NO concentration was similar in both cases, the increase in the amount of NO<sub>2</sub> was because more NH<sub>3</sub> was oxidized to NO<sub>2</sub>. On the other hand, the diminution in the concentration was due to the fact that part of NO<sub>2</sub> was used in the soot oxidation, as also indicated by the higher value of NO present in comparison with the case with no soot.

Fig. 3.19 Standard SCR  $\text{Ce}_{0.25}\text{Mn}_{0.75}\text{O}_x$  catalyst

Regarding the values obtained for the  $\text{N}_2$  selectivity, shown in Fig.3.20 (a), the results are very similar for both cases. On the other hand, in both cases a conversion of almost 100% was reached at the same temperature but the presence of soot improved the conversion of  $\text{NO}_x$  (results shown in Fig.3.20 (b)) at 150 °C. After 200 °C the  $\text{NO}_x$  was produced in larger quantities as the temperature increased when the soot was present. For both cases the  $\text{NO}_x$  conversion became zero at 300 °C. For the  $\text{NH}_3$  conversion, reported in Fig.3.20 (b), it was observed that ammonia was consumed faster when the soot was present reaching an almost complete conversion at 200 °C. However, for both cases a conversion of 100% was reached at the same temperature, 250 °C.

Fig. 3.20 Standard SCR  $\text{Ce}_{0.25}\text{Mn}_{0.75}\text{O}_x$  catalyst with and without soot: (a)  $\text{N}_2$  selectivity, (b)  $\text{NH}_3$  and  $\text{NO}_x$  conversion.

•  $\text{Ce}_{0.5}\text{Mn}_{0.5}\text{O}_x$  catalyst:

The results obtained with  $\text{Ce}_{0.5}\text{Mn}_{0.5}\text{O}_x$  are reported in Fig.3.21. At  $150^\circ\text{C}$  the catalytic activity was higher when soot was present. Also, even if the  $\text{N}_2\text{O}$  concentration was greater there was more production of  $\text{N}_2$ , this indicates that the reagents were consumed more in the standard SCR reaction than in the side reactions. Between  $150^\circ\text{C}$  and  $200^\circ\text{C}$ , when there was soot, an almost complete  $\text{NH}_3$  conversion was reached and the  $\text{N}_2\text{O}$  concentration increased considerably possibly due to an incomplete  $\text{NO}$  reduction. At  $250^\circ\text{C}$  the  $\text{N}_2\text{O}$  concentration reached its maximum value for both cases but the value was higher when there was not soot, then the concentration decreased as it decomposed with the temperature raises. Regarding the  $\text{NO}_x$ , there was only a growth in the  $\text{DeNO}_x$  activity up to  $200^\circ\text{C}$  for both cases, after this temperature the concentration decreased constantly. The  $\text{NO}_2$  was produced in a larger quantity from  $150^\circ\text{C}$  until  $300^\circ\text{C}$  in the activity test with soot, although the maximum concentration value reached was lower than the corresponding to the case without soot. After  $200^\circ\text{C}$  the  $\text{NO}$  concentration was almost the same for both cases.

Regarding the  $\text{N}_2$  concentration, its production was higher with the soot presence, mainly at low temperatures. As it was mentioned before,  $\text{N}_2$  is a product of both the standard SCR and the  $\text{NH}_3$  oxidation. Because after certain temperature value, the  $\text{NO}$  consumption started to decrease and the  $\text{N}_2\text{O}$  production was lower, it is possible that a considerable part of the increase in the  $\text{N}_2$  concentration was due to the  $\text{NH}_3$  oxidation. Besides, the decrease in the  $\text{NO}_2$  concentration evinced after  $300^\circ\text{C}$  could have been because it was being consumed in the fast SCR, producing  $\text{N}_2$  as well.

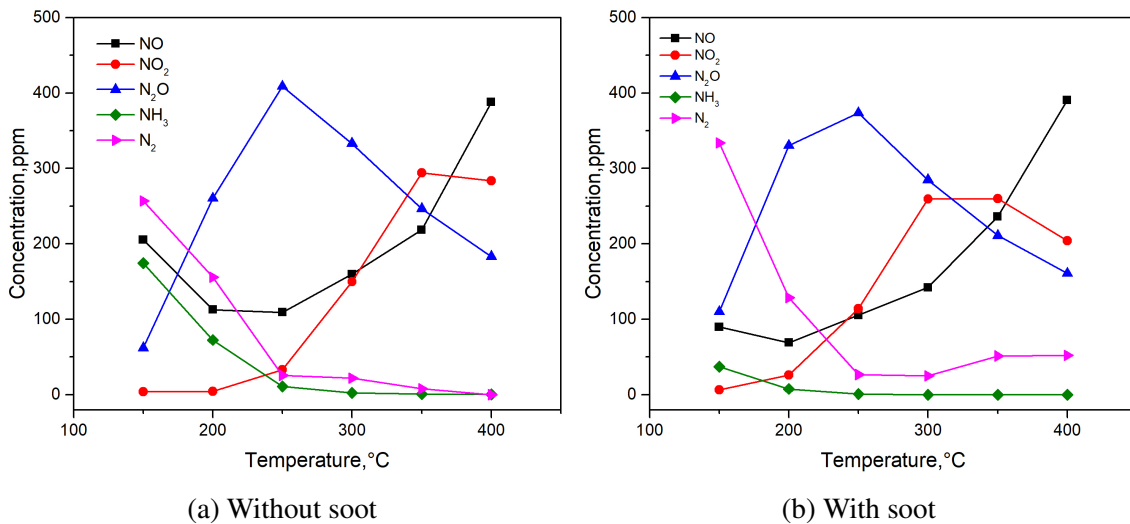


Fig. 3.21 Standard SCR  $\text{Ce}_{0.5}\text{Mn}_{0.5}\text{O}_x$  catalyst

The results for the  $\text{N}_2$  selectivity are shown in Fig.3.22 (a), up to  $300^\circ\text{C}$  the values for the case without soot were slightly higher. After this temperature, the values for the case with soot increased while the corresponding to the case without soot showed a little diminution.

In the Fig.3.22 (b) are reported the  $\text{NH}_3$  and  $\text{NO}_x$  conversions. It is possible to see that there was a higher conversion of  $\text{NH}_3$  with the presence of soot, a value very close to 100% was

reached even at 200 °C. For the  $\text{NO}_x$  conversion, up to 200°C there was also a better performance when there was soot but then the rate of conversion decreased faster than for the case with no soot, as expected from the values obtained for the concentration as a function of the temperature.

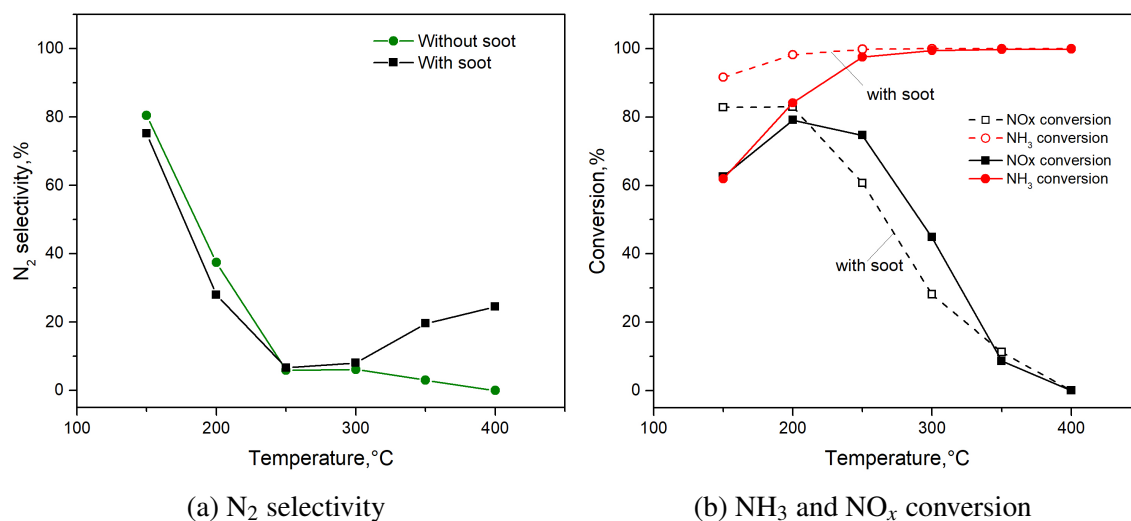


Fig. 3.22 Standard SCR  $\text{Ce}_{0.5}\text{Mn}_{0.5}\text{O}_x$  catalyst with and without soot: (a)  $\text{N}_2$  selectivity, (b)  $\text{NH}_3$  and  $\text{NO}_x$  conversion.

As it could be seen in the results, for the  $\text{Ce}_{0.25}\text{Mn}_{0.75}\text{O}_x$  catalyst the activity at low temperatures increased as it can be seen in the higher values of  $\text{NH}_3$  and  $\text{NO}_x$  conversion obtained for the case in presence of soot. In particular, at 150°C the quantity of  $\text{N}_2$  formed was higher but so was the amount of  $\text{N}_2\text{O}$  and in a bigger proportion, which means that this increase in the conversion values was probably because the  $\text{NO}$  and ammonia were consumed in side reaction, such as  $\text{NH}_3$  oxidation and the incomplete  $\text{NO}$  reduction, and not in the standard SCR reaction. Also, after 200°C the catalyst suffered from the presence of soot, as indicates the loss of  $\text{DeNO}_x$  performance.

On the other hand, in the case of  $\text{Ce}_{0.5}\text{Mn}_{0.5}\text{O}_x$  the improvement in the SCR performance was considerably higher, mainly at 150°C where there was an increase of approximately 80 ppm in the quantity of  $\text{N}_2$  produced while for the  $\text{N}_2\text{O}$  was just of about 50 ppm with respect to the case when there wasn't soot present, which shows that the SCR reaction was prevalent over the other side reactions. However, the decrease in the  $\text{DeNO}_x$  performance from 250°C, indicates that the SCR activity suffered in some way from the soot presence. In addition, because the maximum concentration of  $\text{NO}_2$  (corresponding to 350°C) was lower when the soot was present part of it was probably consumed in the soot oxidation reaction or in the fast SCR reaction, increasing in this way the  $\text{N}_2$  concentration as well.

For the  $\text{MnO}_x$  catalyst, unlike the other catalysts, in the presence of soot there was an increase in the  $\text{NH}_3$  and  $\text{NO}_x$  conversions after 200°C. In particular the higher values of  $\text{NO}_x$  conversion could be because the  $\text{NO}_2$  was also being consumed in the fast SCR, which explain the increase in the  $\text{N}_2$  concentration. Besides, mainly in the temperature range from 300°C until 400°C, it is

possible that just a small part of the  $\text{NO}_2$  participated at the soot combustion reaction, producing a less quantity of  $\text{NO}$  and in this way reducing the  $\text{NO}_x$  generation.

For both  $\text{MnO}_x$  and  $\text{Ce}_{0.5}\text{Mn}_{0.5}\text{O}_x$  it was evidenced an increase in the  $\text{N}_2$  concentration with the presence of soot in the whole temperature range. From the concentration profiles it is possible to say that this increase was more likely to be due to an increase in the oxidation of ammonia to  $\text{N}_2$ , which could have been enhanced by the soot presence, as it is reported in literature [8].

Finally, even if there was an increase in the conversions, the presence of soot did not have any influence in the temperature range where there was an actual  $\text{NO}_x$  abatement and an enhancement in the SCR reaction was only evident at low temperatures.

### 3.2.5 Soot oxidation

In Fig. 3.23 is reported the variation of  $\text{CO}$  and  $\text{CO}_2$  concentration as a function of the temperature during soot oxidation.

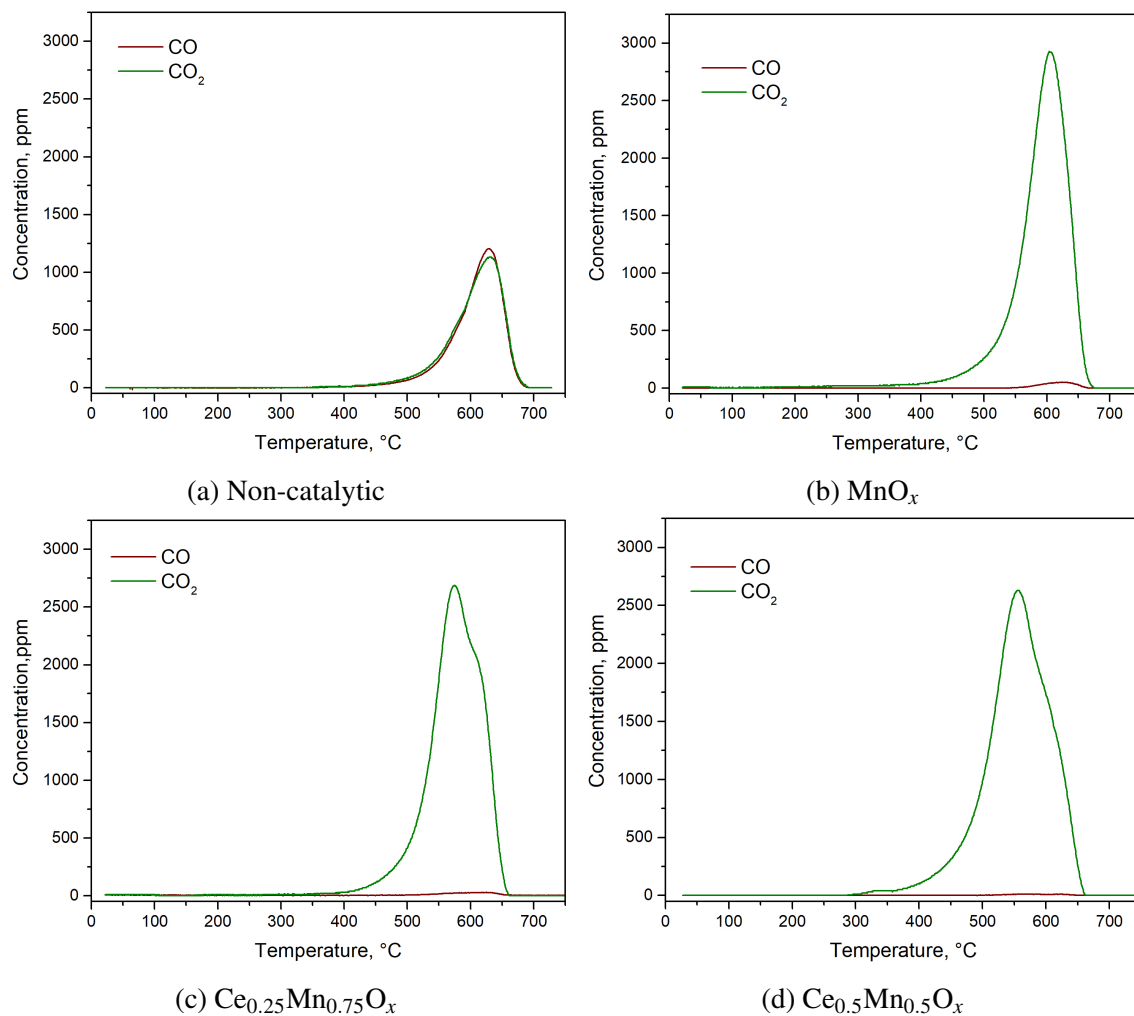


Fig. 3.23 Soot Oxidation

In the non-catalytic test, a considerable part of the soot was consumed in an incomplete combustion, as indicated by the high values of CO concentration. Also, the low values of CO<sub>2</sub> produced in comparison with the results obtained for the soot oxidation catalyzed, shows that the incomplete combustion was predominant. On the other hand, in the graphic is possible to see that the soot oxidation started at around 500°C and the temperature of the CO<sub>2</sub> peak was approximately 640°C.

When Ce<sub>0.5</sub>Mn<sub>0.5</sub>O<sub>x</sub> was used as catalyst, the CO<sub>2</sub> started to be produced first, at around 400°C, and for a wider temperature range, while with the other two catalysts the production started after 450°C and finished more or less at the same temperature value, approximately 660°C and 670 °C for Ce<sub>0.25</sub>Mn<sub>0.75</sub>O<sub>x</sub> and MnO<sub>x</sub>, respectively. With this last catalyst the CO<sub>2</sub> reached a peak at a higher concentration (0.29%) but a higher temperature too (approximately 600°C). With the Ce-containing catalysts the CO<sub>2</sub> peak was reached at a concentration and temperature very similar, for Ce<sub>0.25</sub>Mn<sub>0.75</sub>O<sub>x</sub> a 0.27% peak was obtained at 570°C and for the Ce<sub>0.5</sub>Mn<sub>0.5</sub>O<sub>x</sub> a 0.26% peak was present at 550°C. Also, in the profile obtained Ce<sub>0.25</sub>Mn<sub>0.75</sub>O<sub>x</sub> it is present a shoulder at higher temperatures, probably due to the non catalyzed reaction.

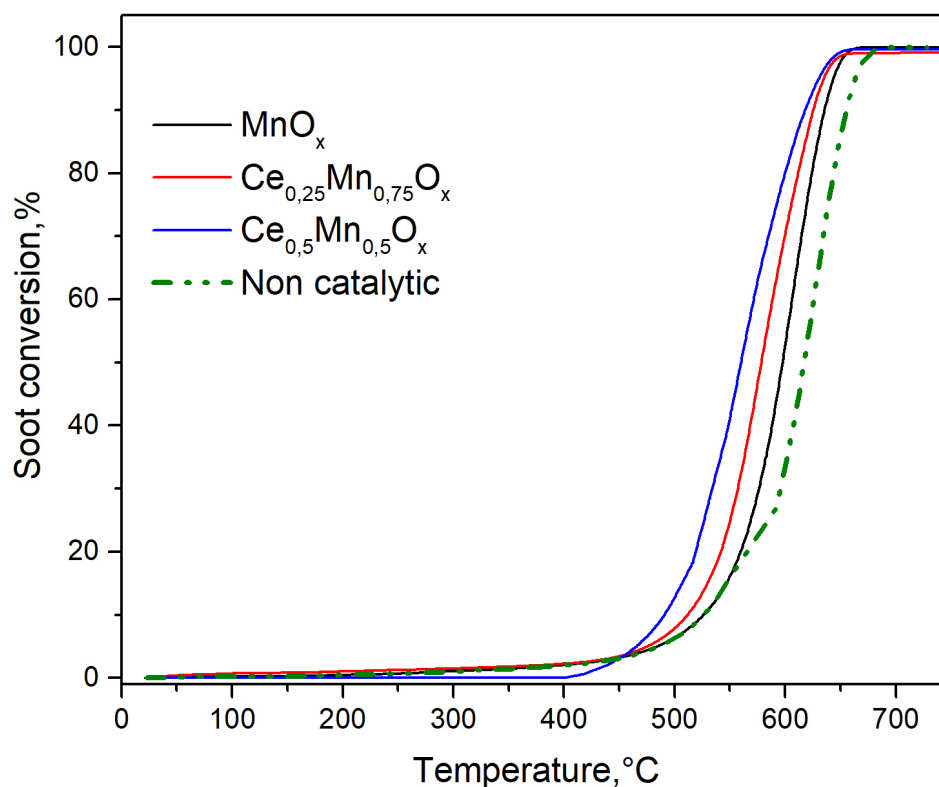


Fig. 3.24 Soot conversion

As it can be seen in the soot conversion (Fig.3.24) a complete conversion was reached within few degrees of difference for all the catalysts. For the Ce-containing catalysts a 100% conversion was obtained at approximately the same temperature (around 660°C). With MnO<sub>x</sub> the entire soot conversion was obtained within a temperature range of 100°C, and as the concentration profile showed, the CO<sub>2</sub> reached a bigger value, but it is required to reach a higher temperature to start

to have any conversion. Besides, the soot was converted at a higher rate with the  $\text{Ce}_{0.5}\text{Mn}_{0.5}\text{O}_x$  catalyst, followed by  $\text{Ce}_{0.25}\text{Mn}_{0.75}\text{O}_x$  and  $\text{MnO}_x$ , as it can be seen in the corresponding light-off temperature values: 550°C, 570°C and 600°C, respectively. In the non-catalytic test the light-off temperature was at around 640°C and the complete conversion was reached a few degrees later than for the tests conducted with a catalyst.

In general, the results obtained with the Ce-based catalysts were very similar, both the intensity and the temperature of the peak had very close values. In comparison with the  $\text{MnO}_x$  catalyst, with the presence of Ce there was a shift toward lower temperatures for the  $\text{CO}_2$  peak, also the combustion started first, in the case of  $\text{Ce}_{0.5}\text{Mn}_{0.5}\text{O}_x$ , and took place at a higher rate, while with  $\text{MnO}_x$  a complete conversion was obtained in a narrow temperature range and as it was mentioned before, the intensity of the peak was higher but also the temperature. With the Ce-based there was a lower production of  $\text{CO}_2$  and the temperature range required to complete the reaction was wider.

Taking into account the results obtained in the non-catalytic test, it is clear that the diminution in the temperature of the  $\text{CO}_2$  peak was not that representative with the use of catalysts, but it was possible to obtain a remarkable selectivity to the  $\text{CO}_2$ , due to the very small quantities of CO produced.

In Fig.3.25 it is possible to see the reaction rate as a function of the temperature for the different kind of test performed with soot. In general, a shift towards lower values in the temperature at which the reaction rate was maximum it observed in presence of  $\text{NO}_x$  and  $\text{NH}_3$ . Also, the soot was consumed at a lower rate when these compounds were present in the system, this due to the fact that different reactions occur in parallel and compete for the  $\text{O}_2$  usage.

For the  $\text{MnO}_x$ , the soot oxidation in presence of  $\text{NO}_x$  started at a temperature lower, almost 200°C, than the base case (soot oxidation with only the presence of oxygen), and reached a maximum value at approximately 500°C, temperature at which the soot oxidation initiated for the  $\text{O}_2$ -assisted reaction. At about 600°C in the curve it is present another small peak, that correspond to the soot oxidation driven by  $\text{O}_2$ . In the case of the SCR, the soot oxidation initiated at the same temperature than for the NO oxidation case, but the reaction rate was lower, due to this the temperature of the maximum rate was higher. This decrease in the reaction rate was because a part of the  $\text{NO}_2$  available for the  $\text{NO}_2$ -assisted soot combustion was being used in the fast SCR reaction.

For  $\text{Ce}_{0.25}\text{Mn}_{0.75}\text{O}_x$ , unlike for the other catalysts, the soot oxidation started and reached a maximum reaction rate at temperature lower in the SCR + soot test (at about 450°C), meaning that most of the  $\text{NO}_2$  available was used for the  $\text{NO}_2$ -assisted soot oxidation and not in the fast SCR reaction. In the NO oxidation + soot test, the soot oxidation initiated at around 300°C, as for the other catalysts, the maximum in the reaction rate was reached at approximately 500°C and its value was very similar to the peak of the SCR test. In both cases, it is observed a shoulder at about 570°C, corresponding to the  $\text{O}_2$ -assisted soot oxidation.

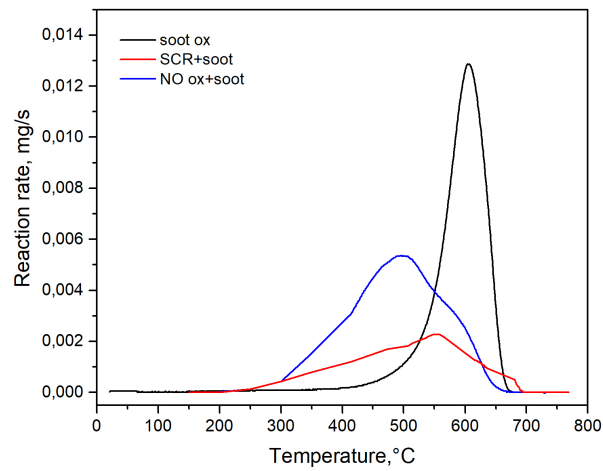
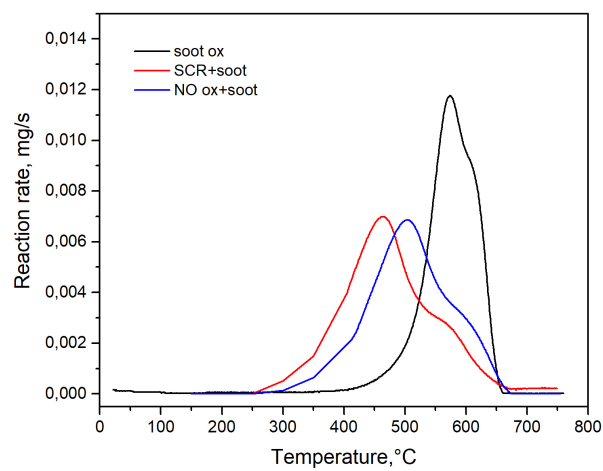
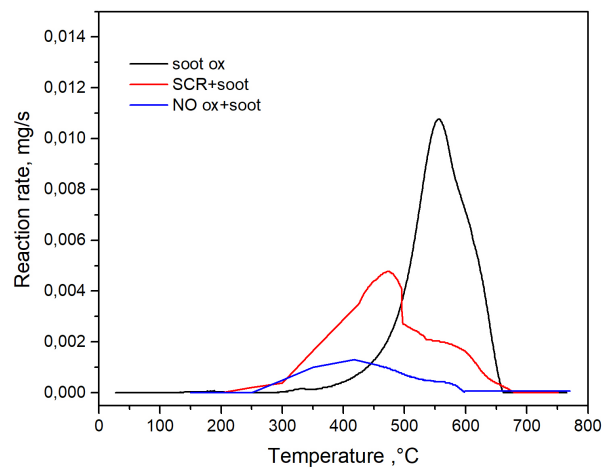
(a)  $\text{MnO}_x$ (b)  $\text{Ce}_{0.25}\text{Mn}_{0.75}\text{O}_x$ (c)  $\text{Ce}_{0.5}\text{Mn}_{0.5}\text{O}_x$ 

Fig. 3.25 Soot reaction rate

In the case of the  $\text{Ce}_{0.5}\text{Mn}_{0.5}\text{O}_x$  catalyst, the reaction in presence of  $\text{NO}_x$  occurred at the lowest rate, which indicates that the soot oxidation was in some way inhibited and the preferred reaction path of the  $\text{NO}_2$  was the one given by the equilibrium with the  $\text{NO}$ . Despite this, the soot oxidation started at a lower temperature and the reaction rate reached a maximum faster than the

base case. It is possible to appreciate also a shoulder around 600°C due to O<sub>2</sub>-assisted reaction. On the other hand, in the SCR test performed in presence of soot, the reaction rates were higher than for the case of NO oxidation but were still smaller in comparison to the base case. The soot oxidation started almost 150°C before and the maximum soot consumption was evinced at about 470°C.

# Chapter 4

## Conclusions

The main objective of this thesis was to develop catalysts to SCR<sub>o</sub>F applications. In order to accomplish this, three different catalysts were synthesized by SCS. After being synthesized, these catalysts were characterized using different techniques with the purpose of achieve a better understanding of some of their physical and chemical properties and how they could affect their performance in the reactions of interest. Subsequently, a series of test were carried out to have a better understanding of all the reactions that could be involved in the SCR<sub>o</sub>F and to determine how adequate were the catalysts for this kind of application.

All the catalysts showed a high activity in the ammonia oxidation reaction, reaching an almost complete conversion at 250°C. However, the selectivity towards the formation of nitrogen was very poor and therefore a high quantity of by-products was formed, specifically the presence of Ce enhanced the formation of N<sub>2</sub>O while for the MnO<sub>x</sub> catalyst there was an appreciable quantity of NO<sub>2</sub> formed. In the NO oxidation, in comparison with the ammonia oxidation, the activity was lower with a maximum conversion of 60%. Among all the catalysts, MnO<sub>x</sub> was the one with the less activity. Also, it was evinced that from 300°C, for the case of the MnO<sub>x</sub> and Ce<sub>0.5</sub>Mn<sub>0.5</sub>O<sub>x</sub> catalysts, and from 350°C for Ce<sub>0.25</sub>Mn<sub>0.75</sub>O<sub>x</sub>, the equilibrium favored the NO formation.

Regarding the SCR reaction, the catalysts did not show the best performance because even if high ammonia conversions were reached, the catalysts showed a poor selectivity, as reflected in the high quantity of by-products formed. Besides, only at low temperatures was possible to obtain a high DeNO<sub>x</sub> activity, with NO<sub>x</sub> conversions up to 96%, but after 200°C the values decreased constantly until reach a value of zero in the temperature range between 300°C and 400°C.

In the soot oxidation, although with the use of catalysts the diminution in the temperature of the CO<sub>2</sub> peak was not that representative in comparison with the non-catalytic test, it was possible to obtain a notable selectivity towards the formation of CO<sub>2</sub>.

With the presence of soot in the reaction system, it was observed a diminution in the  $\text{NO}_2$  concentration in the temperature range between  $300^\circ\text{C}$  and  $400^\circ\text{C}$ , which indicates that a part of the  $\text{NO}_2$  was used in the soot oxidation reaction, this was effectively confirmed in the results obtained for the reaction rate of the soot as a function of the temperature, where was evidenced soot combustion activity at lower temperatures than in the  $\text{O}_2$ -assisted soot oxidation test. For the  $\text{MnO}_x$  catalyst, the reaction rate was very low in the case of the SCR test meaning that the  $\text{NO}_2$  was preferably consumed in the fast-SCR reaction, while for the  $\text{Ce}_{0.5}\text{Mn}_{0.5}\text{O}_x$  the lowest reaction rate values were obtained for the NO oxidation test, indicating in this case that the preferred reaction path of the  $\text{NO}_2$  was that of its decomposition. On the contrary, for the  $\text{Ce}_{0.25}\text{Mn}_{0.75}\text{O}_x$  the highest reaction rates were obtained for both the SCR and NO oxidation tests, showing a high consumption of  $\text{NO}_2$  in the  $\text{NO}_2$ -assisted oxidation.

The presence of soot had some influence in the SCR performance as well. There was an increase in the catalytic activity, as reflected in the higher values of  $\text{NH}_3$  and  $\text{NO}_x$  conversion obtained. However, in the case of the Ce-based catalysts, after  $200^\circ\text{C}$  there was a lost in the  $\text{DeNO}_x$  performance. An increase in the  $\text{N}_2$  selectivity was also observed, as the quantity of  $\text{N}_2$  produced increased while the  $\text{NO}_2$  production decreased, but from the concentration profiles it is possible to say that this increase in the concentration of  $\text{N}_2$  was probably due to a rise in the quantity of ammonia oxidize to  $\text{N}_2$ , enhanced in some way by the soot presence.

Among the three catalysts synthesized and tested the  $\text{Ce}_{0.5}\text{Mn}_{0.5}\text{O}_x$  was the catalyst with the highest catalytic activity even at low temperatures. This was attributed to the surface composition, characterized by a higher amount of surface labile oxygen and a considerable amount of  $\text{Mn}^{4+}$  species. To the latter the large adsorbent capacity of ammonia evidenced is ascribed. Also, its specific surface area was considerably higher in comparison with the other catalysts.

In addition, some of the physical-chemical properties of the  $\text{MnO}_x$  and  $\text{Ce}_{0.25}\text{Mn}_{0.75}\text{O}_x$  catalysts were similar due to the high content of Mn in the latter. However the presence of Ce and the different surface composition, led to a rise in the catalytic activity, but in some cases this growth resulted in a considerable decrease in the selectivity.

# References

- [1] C. Guerreiro, A. Ortiz, F. de Leeuw, M. Viana, and J. Horálek, *Air quality in Europe — 2016 report*. 01 2016.
- [2] G. S. Madia, “Measures to enhance the NO<sub>x</sub> conversion in urea-SCR systems for automotive applications,” 2002.
- [3] M. Nahavandi, “Selective catalytic reduction (SCR) of NO by ammonia over V<sub>2</sub>O<sub>5</sub>/TiO<sub>2</sub> catalyst in catalytic filter medium and honeycomb reactor: a kinetic modeling study,” *Brazilian Journal of Chemical Engineering*, vol. 32, pp. 875 – 893, 12 2015.
- [4] I. O. IEA, “Energy and air pollution: World energy outlook special report 2016,” 2016.
- [5] İ. A. Reşitoğlu, K. Altinişik, and A. Keskin, “The pollutant emissions from diesel-engine vehicles and exhaust aftertreatment systems,” *Clean Technologies and Environmental Policy*, vol. 17, no. 1, pp. 15–27, 2015.
- [6] M. Piumetti, S. Bensaid, D. Fino, and N. Russo, “Catalysis in diesel engine NO<sub>x</sub> aftertreatment: a review,” *Catalysis, Structure & Reactivity*, vol. 1, no. 4, pp. 155–173, 2015.
- [7] S. Wagloehner, M. Nitzer-Noski, and S. Kureti, “Oxidation of soot on manganese oxide catalysts,” *Chemical Engineering Journal*, vol. 259, pp. 492–504, 2015.
- [8] F. Marchitti, I. Nova, and E. Tronconi, “Experimental study of the interaction between soot combustion and NH<sub>3</sub>-SCR reactivity over a Cu-zeolite SDPF catalyst,” *Catalysis Today*, vol. 267, pp. 110–118, 2016.
- [9] B. Pereda-Ayo and J. R. González-Velasco, “NO<sub>x</sub> storage and reduction for diesel engine exhaust aftertreatment,” in *Diesel Engine-Combustion, Emissions and Condition Monitoring*, InTech, 2013.
- [10] L. Shuang, W. Xiaodong, W. Duan, and R. Rui, “Ceria-based catalysts for soot oxidation: a review,” *Journal of Rare Earths*, vol. 33, no. 6, pp. 567–590, 2015.
- [11] D. Fino, S. Bensaid, M. Piumetti, and N. Russo, “A review on the catalytic combustion of soot in diesel particulate filters for automotive applications: from powder catalysts to structured reactors,” *Applied Catalysis A: General*, vol. 509, pp. 75–96, 2016.
- [12] A.-M. Stamatellou and A. Stamatelos, “Overview of diesel particulate filter systems sizing approaches,” *Applied Thermal Engineering*, 2017.
- [13] G. M. Assist, “Diesel particulate filters,” 2013.
- [14] U.S. Environmental Protection Agency, “Diesel Particulate Filter General Information,” 2010.

- [15] J. Fang, Z. Meng, J. Li, Y. Pu, Y. Du, J. Li, Z. Jin, C. Chen, and G. G. Chase, "The influence of ash on soot deposition and regeneration processes in diesel particulate filter," *Applied Thermal Engineering*, 2017.
- [16] H. Zhang, S. Yuan, J. Wang, M. Gong, and Y. Chen, "Effects of contact model and NO<sub>x</sub> on soot oxidation activity over Pt/MnO<sub>x</sub>-CeO<sub>2</sub> and the reaction mechanisms," *Chemical Engineering Journal*, 2017.
- [17] Y. Deng, W. Zheng, E. Jiaqiang, B. Zhang, X. Zhao, Q. Zuo, Z. Zhang, and D. Han, "Influence of geometric characteristics of a diesel particulate filter on its behavior in equilibrium state," *Applied Thermal Engineering*, vol. 123, pp. 61–73, 2017.
- [18] I. Atribak, A. Bueno-López, and A. García-García, "Uncatalysed and catalysed soot combustion under NO<sub>x</sub>+O<sub>2</sub>: Real diesel versus model soots," *Combustion and Flame*, vol. 157, no. 11, pp. 2086 – 2094, 2010.
- [19] L. Yang, V. Franco, A. Campestrini, J. German, and P. Mock, "NO<sub>x</sub> control technologies for Euro 6 diesel passenger cars. Market penetration and experimental performance assessment," 09 2015.
- [20] W. Kang, B. Choi, S. Jung, and S. Park, "PM and NO<sub>x</sub> Reduction Characteristics of LNT/DPF + SCR/DPF Hybrid System," *Energy*, 2017.
- [21] M. Iwasaki and H. Shinjoh, "A comparative study of "standard", "fast" and "NO<sub>2</sub>" SCR reactions over Fe/zeolite catalyst," *Applied Catalysis A: General*, vol. 390, no. 1, pp. 71–77, 2010.
- [22] F. Millo, M. Rafigh, D. Fino, and P. Miceli, "Application of a global kinetic model on an SCR coated on Filter (SCR-F) catalyst for automotive applications," *Fuel*, vol. 198, pp. 183–192, 2017.
- [23] Q. Liu, Z. Fu, L. Ma, H. Niu, C. Liu, J. Li, and Z. Zhang, "MnO<sub>x</sub>-CeO<sub>2</sub> supported on Cu-SSZ-13: A novel SCR catalyst in a wide temperature range," *APPLIED CATALYSIS A-GENERAL*, vol. 547, pp. 146–154, 2017.
- [24] K. Harth, "Compact catalytic converter system for future diesel emissions standards," *MTZ worldwide*, vol. 73, no. 9, pp. 10–14, 2012.
- [25] I. Nova and E. Tronconi, *Urea-SCR technology for deNO<sub>x</sub> after treatment of diesel exhausts*. Springer, 2014.
- [26] D. Karamitros and G. Koltsakis, "Model-based optimization of catalyst zoning on SCR-coated particulate filters," *Chemical Engineering Science*, vol. 173, pp. 514–524, 2017.
- [27] S. Bensaid, V. Balakotaiah, and D. Luss, "Simulation of NO<sub>x</sub> and soot abatement with Cu-Cha and Fe-ZSM5 catalysts," *AIChE Journal*, vol. 63, no. 1, pp. 238–248, 2017.
- [28] M. Purfürst, S. Naumov, K.-J. Langeheinecke, and R. Gläser, "Influence of Soot on Ammonia Adsorption and Catalytic DeNO<sub>x</sub>-Properties of Diesel Particulate Filters Coated with SCR-Catalysts," vol. 168, 05 2017.
- [29] A. K. Alves, C. P. Bergmann, and F. A. Berutti, *Novel synthesis and characterization of nanostructured materials*. Springer, 2013.
- [30] A. Civera, M. Pavese, G. Saracco, and V. Specchia, "Combustion synthesis of perovskite-type catalysts for natural gas combustion," *Catalysis Today*, vol. 83, no. 1, pp. 199–211, 2003.

- [31] F. A. Deorsola, S. Andreoli, M. Armandi, B. Bonelli, and R. Pirone, “Unsupported nanostructured Mn oxides obtained by Solution Combustion Synthesis: Textural and surface properties, and catalytic performance in NO<sub>x</sub> SCR at low temperature,” *Applied Catalysis A: General*, vol. 522, pp. 120–129, 2016.
- [32] N. Leddy, “Surface area and porosity-CMA analytical workshop,” 2012.
- [33] M. Lawrence and Y. Jiang, *Porosity, Pore Size Distribution, Micro-structure*, pp. 39–71. Dordrecht: Springer Netherlands, 2017.
- [34] B. Nie, X. Liu, L. Yang, J. Meng, and X. Li, “Pore structure characterization of different rank coals using gas adsorption and scanning electron microscopy,” *Fuel*, vol. 158, no. Supplement C, pp. 908 – 917, 2015.
- [35] Z. Allothman, “A review: Fundamental aspects of silicate mesoporous materials,” vol. 5, pp. 2874–2902, 12 2012.
- [36] Ulm University, “Derivation of the BET and Langmuir Isotherms.” [http://www.uni-ulm.de/fileadmin/website\\_uni\\_ulm/nawi.inst.251/Lehre/PC3-SS14/BET.pdf](http://www.uni-ulm.de/fileadmin/website_uni_ulm/nawi.inst.251/Lehre/PC3-SS14/BET.pdf), 2011. Online; accessed 16 November 2017.
- [37] Carbon Group , “Field Emission SEM.” [https://areeweb.polito.it/ricerca/carbongroup/fac\\_fesem.html](https://areeweb.polito.it/ricerca/carbongroup/fac_fesem.html). Online; accessed 16 November 2017.
- [38] Radboud University Nijmegen, “Information on the FESEM (Field-emission Scanning Electron Microscope) .” [http://www.vcbio.science.ru.nl/public/pdf/fesem\\_info\\_eng.pdf](http://www.vcbio.science.ru.nl/public/pdf/fesem_info_eng.pdf). Online; accessed 16 November 2017.
- [39] ACMAL eTraining, “Hitachi S-4700 FE-SEM.” [http://mceff.mtu.edu/acmal/electronmicroscopy/FE\\_Form\\_Function.htm](http://mceff.mtu.edu/acmal/electronmicroscopy/FE_Form_Function.htm), 2014. Online; accessed 16 November 2017.
- [40] Dutrow, Barbara L. and Clark, Christine M., “X-ray Powder Diffraction (XRD).” [https://serc.carleton.edu/research\\_education/geochemsheets/techniques/XRD.html](https://serc.carleton.edu/research_education/geochemsheets/techniques/XRD.html). Online; accessed 16 November 2017.
- [41] M. J. Flohr, “X-ray powder diffraction,” tech. rep., U.S. Dept. of the Interior, U.S. Geological Survey, 1997.
- [42] Department of Physics-Montana State University, “X-Ray Powder Diffraction.” <http://www.physics.montana.edu/ical/instrumentation/xrd.html>. Online; accessed 16 November 2017.
- [43] Yale University, “X-ray Photoelectron Spectroscopy (XPS).” <http://ywcmatsci.yale.edu/xps>. Online; accessed 26 November 2017.
- [44] J. Qu and H. M. Meyer, *X-Ray Photoelectron Spectroscopy (XPS)*, pp. 4133–4138. Boston, MA: Springer US, 2013.
- [45] Micromeritics, “Application note 120: Temperature-Programmed Reduction Using the AutoChem ,” 1999.
- [46] A. Rawaz Abdulrahman, “Temperature Programmed Reduction of Ni monometallic and Ni bimetallic catalysts supported on SBA-15,” *Kurdistan Academics Journal (KAJ)*, vol. 12, p. Part A, July 2016.
- [47] M. Fadoni and L. Lucarelli, “Temperature programmed desorption, reduction, oxidation and flow chemisorption for the characterisation of heterogeneous catalysts. theoretical aspects, instrumentation and applications,” *Studies in Surface Science and Catalysis*, vol. 120, pp. 177–225, 1999.

- [48] S. Kouva *et al.*, “Temperature-programmed methods for probing surface interactions on catalytic oxide materials,” 2015.
- [49] Micromeritics, “Temperature-Programmed Desorption (TPD) For Characterizing The Acid Sites On Oxide Surfaces.” <https://www.azonano.com/article.aspx?ArticleID=1475>. Online; accessed 26 November 2017.
- [50] F. Lónyi and J. Valyon, “On the interpretation of the NH<sub>3</sub>-TPD patterns of H-ZSM5 and H-mordenite,” *Microporous and Mesoporous Materials*, vol. 47, no. 2, pp. 293–301, 2001.
- [51] S. Andreoli, F. A. Deorsola, C. Galletti, and R. Pirone, “Nanostructured MnOx catalysts for low-temperature NOx SCR,” *Chemical Engineering Journal*, vol. 278, pp. 174–182, 2015.
- [52] O. Mihai, M. Stenfeldt, and L. Olsson, “The effect of changing the gas composition on soot oxidation over DPF and SCR-coated filters,” *Catalysis Today*, 2017.
- [53] P. Bera and M. Hegde, “Oxidation and decomposition of NH<sub>3</sub> over combustion synthesized Al<sub>2</sub>O<sub>3</sub> and CeO<sub>2</sub> supported Pt, Pd and Ag catalysts,” 2002.
- [54] M. Jabłońska, L. Chmielarz, and A. Węgrzyn, “Selective catalytic oxidation (SCO) of ammonia into nitrogen and water vapour over hydrotalcite originated mixed metal oxides: a short review,” *Chemik*, vol. 67, no. 8, 2013.